

Yordan Kyosev *Editor*

Recent Developments in Braiding and Narrow Weaving

 Springer

Recent Developments in Braiding and Narrow Weaving

Yordan Kyosev
Editor

Recent Developments in Braiding and Narrow Weaving

 Springer

Editor
Yordan Kyosev
Faculty of Textile and Clothing Technology
Hochschule Niederrhein
Mönchengladbach
Germany

ISBN 978-3-319-29931-0 ISBN 978-3-319-29932-7 (eBook)
DOI 10.1007/978-3-319-29932-7

Library of Congress Control Number: 2016932866

© Springer International Publishing Switzerland 2016

This work is subject to copyright. All rights are reserved by the Publisher, whether the whole or part of the material is concerned, specifically the rights of translation, reprinting, reuse of illustrations, recitation, broadcasting, reproduction on microfilms or in any other physical way, and transmission or information storage and retrieval, electronic adaptation, computer software, or by similar or dissimilar methodology now known or hereafter developed.

The use of general descriptive names, registered names, trademarks, service marks, etc. in this publication does not imply, even in the absence of a specific statement, that such names are exempt from the relevant protective laws and regulations and therefore free for general use.

The publisher, the authors and the editors are safe to assume that the advice and information in this book are believed to be true and accurate at the date of publication. Neither the publisher nor the authors or the editors give a warranty, express or implied, with respect to the material contained herein or for any errors or omissions that may have been made.

Printed on acid-free paper

This Springer imprint is published by Springer Nature
The registered company is Springer International Publishing AG Switzerland

Preface

“Recent Developments in Braiding and Narrow Weaving” presents selected works on recent developments in the area of braiding, narrow weaving and related technology topics, presented during the “International Week of Narrow Fabrics” in March 2016 at the Hochschule Niederrhein—University of Applied Sciences in Mönchengladbach, Germany.

The faculty of Textile and Clothing Technology at the Hochschule Niederrhein has a unique position in the area of education and research of narrow fabrics, having professorship and several regular classes at the bachelor and master levels, covering machines, technologies, and applications of narrow woven and braided fabrics. The international week of narrow fabrics hosted two conferences—the “2nd Mönchengladbach braiding colloquium” and the “1st Mönchengladbach narrow weaving colloquium”, where leading industries, researchers and students met and discussed the recent topics intensively.

The chapters are grouped into four parts, where the first part covers two new machines. Daniel Denninger’s new method and machine for covering profiles creates triaxial woven-like structures, similar to the braided structure, although it is a winding structure interlaced as a woven one. Multibifurkation branches produced on the Herzog variation braiding machine is the topic of the second chapter in this part.

The part “modelling and testing” comprises two papers on experimental investigations of linen double-braided ropes and two papers on prediction of the geometry and properties of braids with modern software. The last chapter in this part presents the possibilities of application of the Wisetex software for modelling dense technical tapes.

The part “technical applications” includes chapters on end fasteners and new applications of woven tapes as narrow woven conveyors and batteries. The other three chapters cover experimental investigations of different parameters of the braiding process for composites.

The part “materials and modifications” includes competitive price-performance analysis of Chinese HMPE fibres in textile semi-finished parts, followed by a chapter on surface modifications of narrow fabrics and concludes with an overview of the sustainable materials for composites.

I hope you will enjoy this work and will get several new useful ideas and information for your praxis.

Mönchengladbach
January 2016

Yordan Kyosev

Contents

Part I New Machines

Over-braiding or Overweaving—An Alternative Covering Process . . .	3
Daniel Denninger	
Multi Bifurcation Branch Braided Structures on a Herzog Variation Braiding Machine	15
Roxana Miksch and Frank Ficker	

Part II Modelling and Testing

Geometrical Modelling of Tubular and Flat Braids Within the Jamming Limits—Verification and Limitations	23
Yordan Kyosev and Alena Cordes	
Geometrical Modeling of Tubular Braided Structures Overbraiding Polygonal Prism Based on the Intersection of Surfaces	33
Ning Fanggang and Yu Weidong	
Investigation of the Bending Rigidity of Double Braided Ropes	47
Lawrence R. Msalilwa, Yordan Kyosev, Amit Rawal and Uttam Kumar	
Tensile Properties of Double Braided Flax Fiber Ropes	59
Lawrence R. Msalilwa, Yordan Kyosev, Amit Rawal and Uttam Kumar	
The Numerical Prediction of the Tensile Behaviour of Multilayer Woven Tapes Made by Multifilament Yarns	69
Yordan Kyosev, Stepan Lomov and Katalin Küster	

Part III Technical Applications

End Fasteners of High Performance Fibre Ropes 83
Markus Michael, David Holschemacher and Peter Streubel

**Influence of Braid Carrier Tension on Carbon Fibre Braided
Preforms** 91
Sree Shankhachur Roy, Wentao Zou and Prasad Potluri

**Sensor Integration in Carbon Fiber Reinforced Plastics
(CFRP) to Detect Tension Differences** 103
Jens Schäfer, Cristin Konkart and Thomas Gries

**Investigation of the Relations Between the Parameters
in the Radial Braiding Process.** 111
Viktor Reimer, Su Alptekin and Thomas Gries

Narrow Woven Fabrics Applied for Conveyor Facilities 121
I. Berbig, D. Holschemacher, C. Kern and M. Michael

Multilayer Textile-Based Woven Batteries 129
Marina Normann, Yordan Kyosev, Andrea Ehrmann
and Anne Schwarz-Pfeiffer

Part IV Materials and Modifications

**Chinese HMPE Fibers in Textile Semi-finished
Parts—A Competitive Price–Performance Analysis** 139
Jens Mammitzsch, David Häser and Andreas Kretschmer

**Natural Materials for Surface Modification of Cellulosic Narrow
Woven Fabrics—Strides Towards Fully Bio-based Composites** 149
Thomas Grethe, Hajo Haase and Boris Mahltig

**Overview of the Sustainable Materials for Composites
and Their Industrial Adaptability** 155
Taraneh Khademi

**Erratum to: Influence of Braid Carrier Tension on Carbon Fibre
Braided Preforms** E1
Sree Shankhachur Roy, Wentao Zou and Prasad Potluri

Part I
New Machines

Over-braiding or Overweaving—An Alternative Covering Process

Daniel Denninger

Abstract The following study deals with the synthesis of a specialized drive technology to generate an innovative shifting motion as an alternative covering process. Advantages of the system “Horn” versus the horn gear motion system lie in a gentle and parallel processing of the braiding materials. Simultaneously an increase in the speed of braiding, due to the machine design with a mirror-inverted rotary movement of two rotors, is of great benefit for an economical mass production. The challenge in extrapolating the potential of the system “Horn” for the production of preforms by over-braiding in a circular drive concept with a large opening is to integrate a third yarn system into a laying technique that is gentle to the fibres and technically feasible for processing a triaxial braided structure. For the synthesis of the drive technology and to guarantee an optimal kinematic and parallel transfer of threads, a process-oriented synthesizing method, based on a technology synthesis, was elaborated.

Introduction

Braiding technology provides outstanding conditions for the gentle processing of carbon and reinforcement fibres as well as for the economically efficient serial production of near-net shaped semi-finished products or for preforms. The layer-by-layer over-braiding of formative cores ideally combines the relatively high storage rate of fibres, in connection with braiding technology that equally has a large range of products for a geometrically flexible design. In particular, the weaving-like bonding structure of the braiding material leads to unique structural and mechanical characteristics with a high damage tolerance [1]. To realize a fibre orientation which is reproducible and suitable for the flow of forces, three yarn systems usually are processed to one triaxial, unidirectional braid.

D. Denninger (✉)
Technische Universität Chemnitz, Chemnitz, Germany
e-mail: daniel.denninger@mb.tu-chemnitz.de

Essence of the conventional manufacturing processes are common Maypole braiding machines or radial braiding machines, based on the horn gear motion system, with mechanical forced operation to generate the shifting motion of the yarn and a fixed track. Rotor (Wardwellian) braiding machines—particularly lever arm braiders adapted from the system “Horn”—are not used in this connection. Advantages of the system “Horn” versus the horn gear motion system lie in the bobbin arrangement, which is ideal for taking of the fibres and also shows a steady alignment, together with a distinctive shifting of the yarn accompanied by a gentle and parallel processing of the braiding materials. Simultaneously an increase in the speed of braiding, due to the machine design with a mirror-inverted rotary movement of two rotors, is of great benefit for an economical mass production [2].

Objective of this study is to extrapolate the potential of the system “Horn” for the production of semi-finished products or preforms by over-braiding in a circular drive with a large opening. The challenge was to integrate a third yarn system into a laying technique that is gentle to the fibres and technically feasible for processing a triaxial braided structure. For the synthesis of the drive technology and to guarantee an optimal kinematic and parallel transfer of threads, a process-oriented synthesizing method, based on a technology synthesis, was elaborated. The methodology’s initial point was a synthesizing method with a direct coupling to a kinematic process simulation to design the transfer of yarns. The synchronization and optimization of the transfer of threads was carried out by an iterative synthesis of mechanisms in close connection with the kinematic analysis of the suggested drive concept. In a structural design, the physical feasibility of the innovative drive concept, as well as the non-destructive transfer of yarns, was established. As a result, the drive concept of the new rotor braiding machine “**D-3F**” (Denninger-3Faden), for producing a weaving-like bonding structure as a combination of laying and braiding or weaving, came into being: “**D-3FG**” (Denninger-3Faden Geflecht) [1].

“Prozessorientierte Synthesemethodik” Based on the Technological Synthesis

With growing demands towards the manufacturing of composites, the demands for the used textile semi-finished products or preforms are also increasing and therefore the demands for their production or manufacturing processes are also increasing. By manufacturing these technical textiles, the technological challenge lies in the creation of a reproducible and flux-oriented fibre orientation and a gentle handling of reinforcement fibres by simultaneously using variable process parameters that allow a geometrically flexible design of the end product. From these extensive technological specifications and from the required output quantity for the realization of an economic mass production result the specifications for the development of a textile manufacturing process and, as a consequence thereof, the installation engineering. When implementing these requirements into a system, that is, in accordance with the specifications of the systems engineering, the engineers of textile machines or plant

manufacturers usually refer to familiar and controllable drive engineering from conventional manufacturing processes. Due to the mostly demanding kinematic specifications for the processing and the handling of threads, mechanical drive solutions are predominantly used for textile machines to generate movement.

To overcome the discrepancy between the existing drive engineering and the technological specifications, the synthesis of these drive solutions takes an important role in the development and engineering process. As a general rule, the method of choice is the adaption of conventional production processes by partially optimizing or expanding the conventional production processes through integrating additional drive components and features (see also [3, 6]). This approach allows a minimization of development risk and an adaption of conventional production techniques as well as textile machines to the requirements of the processing of reinforcing materials. Due to limited possibilities in the context of a partial optimization, a solution which is optimal for the procedure and practicable concerning the drive engineering is rarely possible. Furthermore, this only allows a small range of possible inventions of new textile products with innovative bonding structures and novel production processes. The execution of such specialized manufacturing processes requires fundamental but partly non-existent knowledge of the process sequences for a defined description of the kinematic requirements and the immediate consideration of the feasibility during the invention process concerning the drive engineering. As a consequence of lack of references and unknown process parameters, practical value often provides the starting point of an innovation that is implemented with the characteristic instruments and algorithms of the construction methodology as well as the synthesis of mechanisms. Even the new technological requirements are only partly suitable for the unification of the demanded output quantity and the economical serial production after adaption. With an increasing degree of novelty, the number of iteration loops and the overall development risk increases.

In the design's innovation process of fibre composites for lightweight construction applications and their automated series production, special textile products and optimized manufacturing processes have to be developed. Such textiles are bound to a wide range of technological product specifications due to their special application; these specifications need to be taken into consideration during manufacturing with regard to the necessary orientation according to the flux and the gentle handling of reinforcement fibres. The implementation of these requirements into a manufacturing process rests on, with all possible consequences, the textile machinery and plant manufacturers. While doing so, design engineers are stretched to the limits of feasibility concerning the drive technology and structure with the common tools, namely the synthesis of mechanisms to adapt a conventional drive solution through partial optimization. Likewise, the holistic approach of the gearbox design, with rigidly predetermined technological requirements (movement task), can often lead to a subjective ideal result. Especially when following a strict orientation of consisting production techniques and known bonding structures, a relatively low grade of invention is established.

The decisive approach to develop a process-oriented synthesis, based on the synthesis of technology, was to expand the process of innovation by designing ideal

textile products and directly taking the technical realization of the drive into account. The aim is to develop new bonding structures through a superficial synthesis of the drive technology that is essential for production. By using a combination of the demands which are ideal for the gear and are technologically necessary, this synthesis process is made. The method's starting points are technologically necessary requirements of a textile product and its intended usage. To gain creative freedom for the technological synthesis, the fixed requirements need to be loosened and to be analysed according to their usage. This approach offers the possibility to provide an innovative and an alternative product with equivalent or optimized features considering the drive's technical efficiency. With that, the process-oriented synthesizing method, based on the technology synthesis, represents a target-oriented and purposeful approach in the innovation process of novel textile semi-finished products. Provided that a loosening in certain areas is accepted under strict conditions, this approach is equivalently adaptable to other fields of innovation.

In the available example, technology synthesis is conceived as the kinematic synthesis of the innovative laying technique “**D-3F**” for over-braiding with three thread systems, directly considering the necessary technological or permitted requirements and the essential drive engineering. The fundamental study and demand analysis of the textile process chain to manufacture fibre composites represent the minimal requirement towards this innovation technology. This foundation delivers existential preconditions for a synthesis in the form of a pool of ideas and the required competence of assessment. Especially the known manufacturing processes of conventional textile semi-finished products and their technological basis as well as the realization of the drive engineering offer various reference points and kinematic solution concepts. Furthermore, it is only possible to validly question and equally replace technological requirements with the basic knowledge of interdisciplinary correlations in the textile process chain which are needed to construct and produce fibre compound plastics and components. Moreover, it is made possible to design new bonding structures with an ideal realization of actually necessary demands in terms of the functionalization potential, Fig. 1.

The holistic and process-oriented synthesis' starting point was, contrary to a classical approach, to critically study and analyse the statement of requirements which were defined initially. Aim of this analysis is the isolation of reinforcement features that are independent of the bonding structure and their evaluation concerning the kinematic handling requirements towards the reinforcement fibres. Often, the actual required bonding structures and product characteristics allow a loosening up of known bonding structures and the compartmentation and structuring of the demanded movement task associated with that. With the technological synthesis, as a new combination of technological requirements in a novel bonding structure, it is possible to directly design the kinematic demands qualitatively concerning their physical practicality. The fundamental technological analysis of related or originally given manufacturing processes is suitable for the drive technology's synthesis. In doing so, the goal is the identification of parameters of gear technology-related and constructional indicators and the evaluation of these, with regard to the suitability of deriving the novel bonding structure. In turn, this

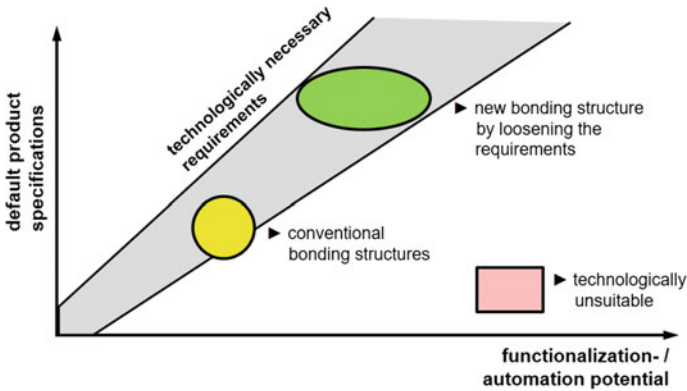


Fig. 1 Innovative potential by technological synthesis

identification of parameter serves a target-oriented new combination of known gear structures in direct consideration of their inherent properties and their potential constructive itemization. The process-oriented synthesis represents an extension of the holistic gear’s synthesis with a target-oriented application of CAD- and MKS functionalities, Fig. 2. A kinematic process simulation was chosen for the laying

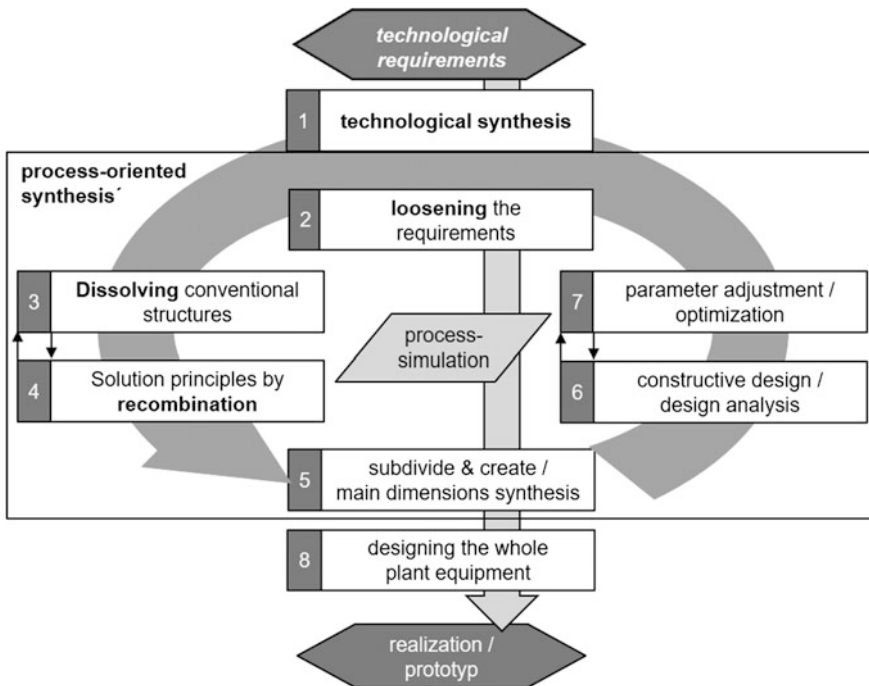


Fig. 2 Process-oriented synthesizing method, based on the technological synthesis

technique's synthesis and applied to the ongoing adjustment of parameters of the technological, kinematic, structural and constructional requirements. This synthesis method can therefore be designated as an interdisciplinary method of the innovation process with direct linking of the technological and drive technology-related realization.

Laying of Threads During Braiding in the System “D-3F”

The technological synthesis for integrating a third yarn system leads to a novel and technological textile manufacturing process with a new weaving-like bonding structure as a combination of laying and braiding or weaving “D-3FG” (see Fig. 3). Along with that, the drive concept of the new rotor braiding machine “D-3F” is in the process of patent application (file reference 102014016832.8) with the title “*Flechtvorrichtung und Flechtverfahren zum Überflechten eines Flechtkerns*” (*Device and technology for braiding to over-braid a braided core*). The property rights that were investigated within the scope of the patent application and the writing of this paper were confirmed by the “*Sächsische PatentVerwertungsAgentur*” by means of an independent enquiry. Therefore, the patent claim which is to be registered is not characterized in any of the consulted property

The result of the logical interpretation of the new laying technique in a rotary braider system, based on the system “Horn”, is shown in the following Fig. 4. The rotary braiding system “D-3F” matches a targeted combination of all characteristics typical for braiding in a system concept that is suitable for producing preforms with a tangential alignment of bobbins and parallel laying of threads. Thus, the preforms are produced by “over-braiding” with the new weaving-like bonding structure. According to the patent claim, the drive-related functionalization of the novel laying technique in a circular drive concept is solved as follows:

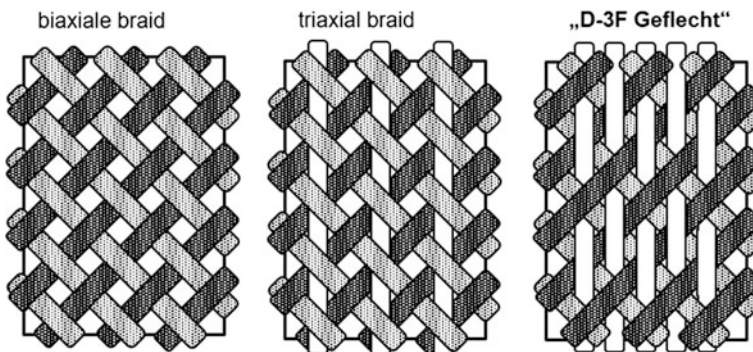


Fig. 3 Biaxial, triaxial and new “D-3F Geflecht” (“D-3F braid”)

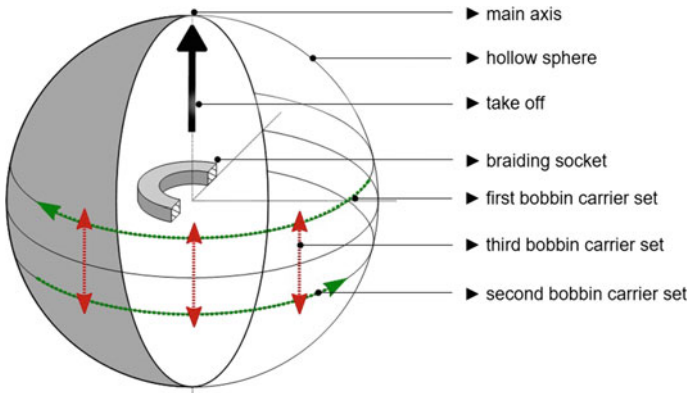


Fig. 4 Rotary braiding system “D-3F”

- “At least one first bobbin carrier set and at least one second bobbin carrier set, where at least one of the two bobbin carrier sets can be moved along a circular path, where between the two bobbin carrier sets when over-braiding the braided core a relative movement can be executed and where by the relative movement, each of the bobbin carriers of the two bobbin carrier sets drawn yarns can be stored as intersecting weft yarns to the braiding.”
- “At least one third, stationary arranged bobbin carrier set, and”
- “At least one actuating element, where the yarns that are unwound throughout the process of over-braiding the braided core from the bobbin carrier of the third bobbin carrier set by at least one adjusting element in an oscillating upward and downward movement are displaceable and thereby are laid as warp yarns to form a binding alternating above and below the crossing points of the weft yarns.”

Recombination of Sub-functions and Sub-function Carriers

The ZIM-cooperation project “*design of a novel laying device for yarns in Wardwellian braiding machines*” of the company **Kabelflechter Alfeld**, has to be mentioned as part of the executed investigations to develop the potential and accumulating ideas. Aim of the cooperation project was to achieve an increase of the braiding’s output up to 50 % as against the conventional lever arm braiding machines and an extreme reduction of the braid’s contamination with lubricants. Especially the reduction of lubricants was successfully projected towards a potential processing of high-performance/reinforcement fibres. The method of choice was the partial optimization of the technical and technological limited sub-function carriers in the innovative rotary system, namely, “Kabelflechter”. Therefore, the cooperation project’s crucial task consisted, on the one hand, in the synthesis and integration of a

novel mechanism to kinematically and optimally lay warps as a replacement of the thread lever; on the other hand, it was to replace the approved sliding guide with a roller conveyor guide that is mounted in anti-friction bearing to reduce the released particles of the lubricant.

To develop performance-enhanced textile machines or textile machines with new requirements, the preferred approach is a partial optimization in the first step. With that, it is possible, as in the case at hand, to maintain existing basic principles and technological boundary conditions as far as possible and to minimize development risks. According to that, the equivalent replacement of sub-function carriers becomes less expensive than a complete redevelopment. Likewise, the chosen approaches to a solution in the cooperation project to optimize sub-function carriers were able to verify their theoretical functionality in separate testings. However, the obvious constructive weaknesses in the originated prototype, on the basis of a conventionalized set-up, finally led to a non-fulfilment of the desired braiding output. Besides the weaknesses minimizing the output, based on the concept limitations became apparent with decisive importance for the technological requirements towards the over-braiding of shaping cores in the production of preforms. Particularly the realization of a large opening in a circular braiding device is not expedient with the current approach of a coupled rotary gear and cannot be solved solely by partial optimization. The known options of integrating stationary threads to produce a conventional triaxial braiding structure are also not convenient.

Nevertheless, these weaknesses and the concept-based limitations of the “Kabelflechter” illustrated the necessity of a combined approach to design and synthesize the laying of threads for braiding as well as their drive technology. As a logical consequence of this, a new methodology for a process-oriented synthesis, based on the technological synthesis, was developed and integrated in the holistic approach of the gear synthesis. Starting point of the technological synthesis is the fundamental study and demand analysis of the textile process chain that produces fibre-composite components with reinforcement fibres that are reproducible and possess an orientation that is aligned with the flux in the inserted textile semi-finished products. The unrestrained consideration of all conditions needed for an economical serial production of preforms that are suitable for the required load by over-braiding shaping cores layer by layer provided further reference points. The qualitative and kinematic analyses of the braiding systems suitable for over-braiding made it possible to isolate parameters in relation to their drive technology and construction. This specific approach was both accompanied by the resolving of kinematic, structural and constructive standards of the known braiding systems and the target-aimed recombination of required sub-functions, which are needed to manufacture the best possible and ideal bonding structure. In doing so, it is necessary to optimally integrate the gained experiences as well as the suitable results of the cooperation project into the synthesis process.

Production processes for manufacturing strand-shaped profiles, without changing the cross section, with a combination of laying and braiding are already to be seen as state of the art, likewise research (see also [4, 5]). Due to unavailable cross connections from the braiding to the laying, the probability of wrinkle formation or

Table 1 Recombination of the sub-functions and sub-function carriers

Horn gear motion system	<i>System “Horn”</i>	<i>System “Kabelflechter”</i>
Parameters concerning production technology and process description, combination of materials, thread guide elements, etc.		
Production process and peripheral installation engineering to handle the braiding cores		
Form-fit and non-slipping motion transmission to generate the laying movement (constrained)		
Circular construction with a large opening	Arrangement in a hollow sphere	
	Steady orientation of the bobbin arrangement, tangentially to the machine’s rotational axis (parallel shifting of braiding yarns)	
	Construction of bobbin carriers	
		Roller conveyor guide of the weft thread system, mounted in anti-friction bearing
Mechanically passive facility for compensating the length of weft threads at the weft thread’s bobbin carriers		
		Guided actuator of threads for a constrained laying of warp threads
		Active facility to compensate the length of warp threads

shifting of reinforcement fibres rises during the over-braiding of the shaping cores. A reproducible and flux-aligned orientation of the reinforcement fibres is therefore hardly feasible. Hence, the novel bonding structure offers, with the logical application of the process-oriented synthesis method, a target-oriented constrained drive solution for the design of a manufacturing process of preforms, suitable for the given load. The following Table 1 lists all the essential sub-functions and sub-function carriers of the recombination:

Synthesis Model and Synchronization

To synchronize the movement of the chaining threads (see Fig. 5); the synthesis model was implemented in Creo 3.0[®] based on the defined arrangement sketches and fundamental kinematic requirements. The parametric structure allowed an iterative procedure when it came to concretize the synthesis model’s main components and, according to this, also allowed a fluent transition to the draft design. The dimensions of the components that interact with each other had to be gradually

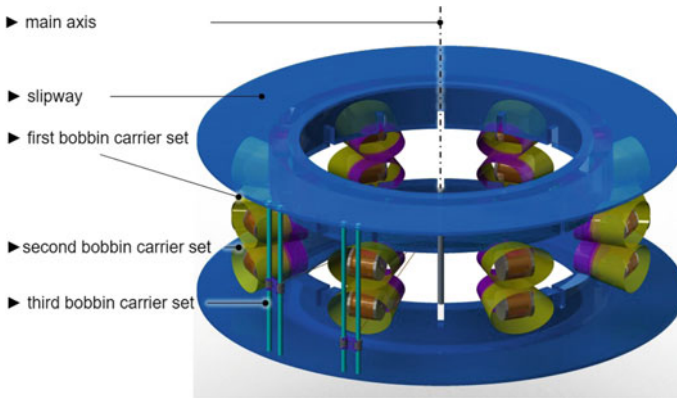


Fig. 5 Synthesis model for the synchronization of the chaining threads

adjusted and kinematically synchronized in the synthesis model. For instance, a modification of the slipway's radius, in addition to a modification of the remaining radii, entails a change of the bobbin carrier's representative. Thus, the required slot depth and, as a consequence thereof, the geometry of the slipway is altered.

The synthesis model was expanded by a kinematic process simulation to directly illustrate and evaluate the essential functionalities of the process. To take a variable length of the braiding thread during the shifting motion into consideration, each braiding thread was assembled out of three beam elements. The beam elements were integrated by means of the release definitions from the thread-take-off-point via the braiding ring up to the braiding point, respectively the tangent conditions while incoming and departing the deflectors, the braided core as well as when storing on the core. Conditions of parallelism, to regard the overlapping of the track guide of motions that is changing, do not apply due to the system. Due to the mirror-inverted rotary movement of the weft thread's system, linked to the steady removal of the braiding core, it was possible to depict the storing of the weft threads, idealized in the form of paths of the braiding threads, with the aid of tangent conditions. To save calculating time, symmetries were applied and the minimal necessary number of braiding threads was inserted to evaluate the relocation.

Goal of the process-oriented synthesis was the design of a non-destructive and kinematically ideal shifting motion of warps to avoid vibration stimulations of the warp threads. Therefore, a depiction of the friction-afflicted sliding processes on the contact points during the braid's contraction as well as during the storing on the braiding core was neglected. Initial point for the design of the kinematic shifting motion of warp threads was the fundamental synchronization of both the shifting motion of warp and weft threads to prevent a direct collision of the warp threads with the moving representatives of the bobbin carriers or the static machine elements. Decisive premises of a non-destructive creation of sheds were the exact synchronization of the mirror-inverted rotary motion of both weft systems and their

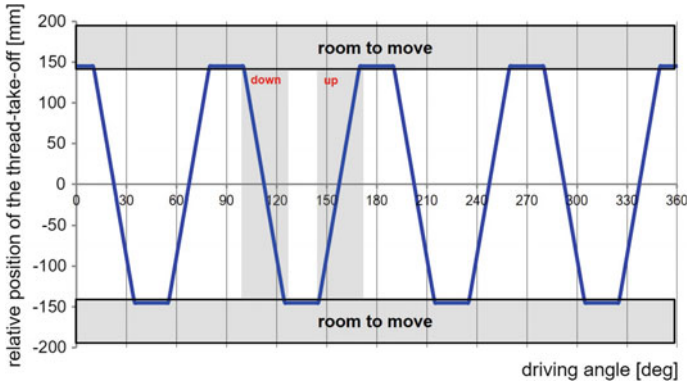


Fig. 6 Motion chart of a synchronized warp thread

positioning regarding the slits on the respective slipway. The warp thread's relative movement to open and close a shed takes place in those time frames where the carriages are as symmetrical as possible between the two slits of the particular slipway and are aligned symmetrically to the opposite carrier. Aim of this synchronization task was the kinematic description of the movement task, in relation to technology, in a motion chart. Static position specifications were implemented as a drive of the thread's actuators to fundamentally synchronize the warp thread's shifting motion which resulted from investigated process points. The aim for the influence of the position specifications led to a motion chart of an actuator of threads, see Fig. 6.

Conclusions

In this paper, the synthesis and the synthesis model for a new circular drive concept to generate an innovative shifting motion as an alternative covering process were shown. This alternative covering process is a result of the recombination of the required sub-functions which are needed to manufacture the best possible and the ideal bonding structure. The technological synthesis for integrating a third yarn system led into the novel and technological textile manufacturing process with a new weaving-like bonding structure as a combination of laying and braiding or weaving. For an extensive validation, under consistent continuation of the process-oriented synthesis methodology a rotor braiding machine, based on the novel laying technology, needs to be developed and the "D-3FGeflecht" has to be manufactured. This project is, as a result of the raised variety of issues and considered topics, only in conjunction with specialized partners feasible.

References

1. D. Denninger, Prozessorientierte Synthesemethodik am Beispiel der neuartigen Verlegetechnik "D-3D" zum Überflechten mit drei Fadensystemen, Dissertation (Draft) for Technischen Universität Chemnitz
2. W.A. Douglass, *Braiding and Braiding Machinery* (Cleaver-Hume-Press Ltd., London, 1964)
3. T. Meyer, M. Gabler, T. Nguyen-Dang, D. Denninger, M. Berger, *Mechanismenentwicklung einer Antriebsbaugruppe zur Integration von Festkörpern in ein technisches Textil*. 17. VDI Getriebetagung—Bewegungstechnik, Nürtingen 2014-09-24
4. M. Milwich, *Flechtpultrusion & Flechtentwicklungen am ITV Denkendorf*. 1. Mönchengladbacher Flecht-Kolloquium, Mönchengladbach 2014-11-7
5. J. Schäfer, T. Gries, *Kontinuierliche Herstellung von faserverstärkten Profilen mittels Flechtpultrusion*. 1. Mönchengladbacher Flecht-Kolloquium, Mönchengladbach 2014-11-7
6. R. Wallasch, *Entwicklung eines kontinuierlich arbeitenden Antriebskonzeptes zur Herstellung einer neuartigen Faserverbundkonstruktion*. Diplomarbeit (unveröffentlicht) Technische Universität Chemnitz—Professur Montage- und Handhabungstechnik, Chemnitz 2013

Multi Bifurcation Branch Braided Structures on a Herzog Variation Braiding Machine

Roxana Miksch and Frank Ficker

Abstract A project about multi bifurcated branch braided structures for lashing straps and cables was carried out in the Institute for Materials Science at Hof University. For this work three manufacturing processes were used. The braidings were produced on a Herzog variation braider and the woven structures on shuttle and needle looms. The aim was to create bifurcated structures without sewing several woven or braided fabrics together. The woven fabrics had only two branches, but with the Herzog variation braiding machine structures with two and up to six branches have been produced. The two branched fabrics were tested for their tensile strength. The main result is that the structures with less elongation have better tensile strength.

Introduction

The limbs and the roots of a tree are splitting into branched structures to increase its stability and to ensure sufficient nutrition. The natural bifurcation of the roots braces the tree securely in the ground and improves its resistance against external influences like rain, snow and wind. In nature and in technical science, bifurcations are essential. Therefore the Institute for Materials Science at Hof University has been working to transfer the biomimetic properties of natural bifurcations into braided and woven lashing straps, cables and other applications. The target of this project was to produce versatile interlaces of bifurcated branches and to analyze and compare the resulting technical properties, especially their tensile strength. The bifurcated branches should be manufactured in a continuous production process excluding any

R. Miksch · F. Ficker (✉)
Hochschule Hof—University of Applied Sciences, Alfons-Goppel-Platz 1,
95028 Hof, Germany
e-mail: frank.ficker@hof-university.de

R. Miksch
e-mail: roxana.miksch@hof-university.de

manual sewing processes. Those additional time consuming steps shall be avoided and an increased stability is expected, caused by a higher integrity of the structure.

To realize the project and to compare different production processes, a Herzog variation braiding machine, a Univall-Jacquard loom with shuttle weft insertion and a needle loom have been used. The bifurcation characteristics of the resulting products have been tested and compared to assess their suitability for industry applications. Beside the tie-down segment, a possible application field for branched structures is the medical sector, e.g. as artificial multi-bifurcated vessels and veins.

Implementation

Braiding requires a minimum of three threads, while the maximum number of threads is only limited by the chosen machine. A conventional braiding machine features a circular setup, in which the bobbins are handled by horn gears, crossing each other on counter-rotating, pseudo-sinusoidal tracks. The necessary thread stock for the entire braid is pooled on these bobbins. Through the movement of the bobbins, the threads cross each other and produce the braid.

The advanced setup of a variation braiding machine allows producing much more complex braids if the number of threads exceeds the minimum amount of three threads. The setup of the Herzog variation braiding machine for example consists of a 4×4 arrangement of horn gears. Between the transfer points of the horn gears, the traveling tracks for the bobbins are equipped with pneumatically triggered crossings. Instead of just counter-rotating pseudo-sinusoidal tracks, it is possible to change the track plate pattern individually and to allocate each bobbin separately on different tracks. Provoked by intensive research, there is a huge number of possibilities to produce undivided braids using the tracking plate of variation braiding machines [1, 2].

To produce a single braid (basic braid) all tracks need to cross each other. If the tracks are separated correctly, for example if the tracking plate is split in two areas, a bifurcated branch will be produced. Using this technique, it is possible to produce basic braids, splitting up in multi bifurcated braids and consolidating back into a basic braid, using only one braiding machine, just by changing the pattern of the track plate.

For this project, several variations of basic braids have been produced; each one equipped with a different branched braid with two ends. One example is shown in Fig. 1.

The potential of the variation braiding machine in optimizing the bobbin setup is multifarious, the track setup and the crossing setup are widely used for splitting and reuniting the tracking plate. Because of the crossing options, the variation braider is able to produce a huge amount of different basic and bifurcated two end branches.

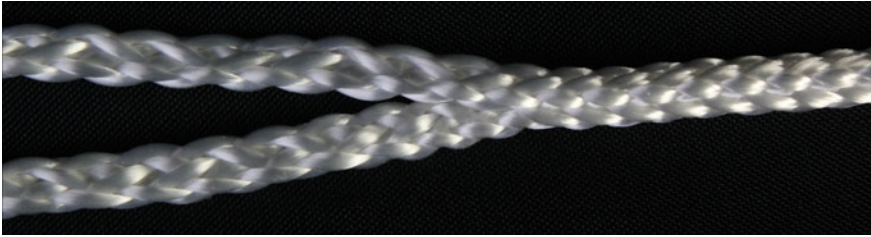


Fig. 1 Picture of a bifurcated braid

A big number of different combined braids have been produced, using this technique, although the total possibilities of the variation braiding machine are not close to exhausted, because of the freely programmable controllers. The combination of basic braid and bifurcated two end braid is realized with changing the crossings and might take some horn gear rotations. Depending on the braid, the time for track changing may vary from one to several horn gear rotations and might require complex combined setups of crossings and tracks. The changing should be as short as possible, because otherwise unwanted effects such as thread twisting or loosening up of the existing braids might occur. Additionally, existing braids can de-braid because of unfavourable setups. Such behavior should be avoided, because it is equal to destroying the braid. Furthermore an eye should be kept on the lay length and the pulling speed of the takeoff disk, because it varies between the different setups and has to match the situation. The lay length has to be adapted by the control engineering. It could happen that during the setup change, the disk has to stop, to guarantee a clean transition between the different braids.

Contrary to braiding, which crosses the threads at an angle of approximately $\pm 45^\circ$, for weaving the crossing angle is usually $0/90^\circ$. Therefore the threads are separated into vertical warp threads and horizontal weft threads. The weave pattern is developed by rhythmic lifting and lowering of the warp, while the weft secures every change by crossing the warp.

To produce a multilayer weaving structure, it is mandatory to use one weft thread for each layer [3]. A bifurcated structure with two threads is a woven multilayer structure with two layers.

There are different ways to transport the weft through the shed. In this work two possibilities have been used: shuttle weft insertion and needle weft insertion. Only these two have been considered because they are the only systems with a continuous weft thread. Other weft insertion systems include cutting the weft thread, which is not useful for this project.

A needle loom has been used as a reference machine to the Univall-Jacquard loom machine with shuttle weft insertion. The differences between simple bifurcated woven structures produced using the two different machine types should be analyzed.



Fig. 2 Picture of a bifurcated shuttle loom woven product

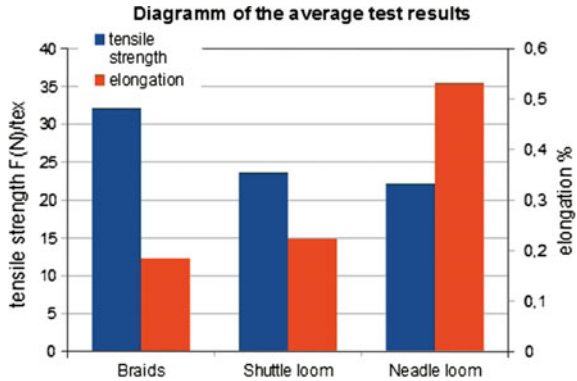
On the Univall-Jacquard loom with shuttle weft insertion, the whole weft thread stock is traveling through the warp. After the shuttle has reached the end of the warp, the warp changes position and the shuttle returns to its starting point. The Univall-Jacquard loom has four independent shuttles, which allow producing a multilayer structure with four unconnected layers. The Univall-Jacquard loom lifts or lowers every thread independently by an electric powered drive. Advanced control systems allow individual positioning of every thread in the weft, which means that the weft movement of every single thread is individually manageable. Therefore it is possible to configure several sheds, while having low harm and stress for each warp thread. This facilitates a high variability of the warp threads position in z-direction. Furthermore, it provides the possibility to produce 3-dimensional structures, as seen in Fig. 2.

The weft insertion of the needle loom is carried out, as already stated by the name, by a needle. The needle inserts the weft as double layered thread with a loop. At the end of the shed the loop of the weft thread is trapped by a second needle and intermeshed with the loop of the previous weft thread. The needle loom has two independent needles, which are both needed, to create the two layered structures analyzed in this work.

Results

Every produced structure was made from the same material, with the identical thread thickness. The bifurcation structures were tested in terms of their tensile strength and elongation, especially in the bifurcation area. Eleven different bifurcation braids with two ends were compared to fifteen shuttle loom—and six needle loom bifurcation fabrics. The potential of every single bifurcation production process, which affect the maximum strength of load restrain assemblies, could be evaluated. The gathered test data was used to calculate the average tensile strength of every bifurcation production process. The same comparative calculation has been done for the resulting average structural lay length. Both values are shown in Fig. 3.

Fig. 3 Diagramm of the average tensile test results



The diagram shows that the bifurcated shuttle loom fabrics have a higher tensile strength than the bifurcated needle loom fabrics. Also it is clearly visible that even the bifurcated shuttle loom fabrics cannot compete with the bifurcated braidings. Furthermore, it shows that the lay length of the bifurcated weavings is in both cases higher than the lay length of the braided bifurcations, with the needle loom fabrics having the highest lay length. This is owed to the different processes of braiding and weaving with different insertion systems. Because of the correlation between tensile strength and lay length, the hypothesis that a high lay length decreases the tensile strength, can be confirmed.

In the course of this study, only pieces of the big picture could be considered. The possibilities are not yet exhausted and with modern machines the limitations of pattern variations are widely conceived, which still leaves much room for innovation.

Conclusion

Summarizing the results, the braided structures with two ends showed better abilities in case of tensile strength as woven structures. Furthermore, the Herzog variation braiding system allows to design different bifurcations fitting the needs for lashing straps, cables and other applications, even if the load is split differently between bifurcations.

As stated above, for this work only bifurcation braids with two ends were developed. The possibility of producing complex bifurcated braided structures, with more than two ends, is also given with variation braiding machines. Mostly a basic braid is only split in bifurcated structures with two branches, but it is also possible to produce braids that are bifurcated in three or four ends from one basic braid.

Beyond this, the Institute for Materials Science at Hof University has developed a basic braid which is split in a bifurcation with six branches. Each one of the six bifurcation braids is an evenly flat braid. The braid shows a structure like a normal

Fig. 4 Picture of a bifurcated braid as net structure



three strained hair braid. In addition it is possible to connect the six bifurcated braids to a net shaped structure. This net shaped structure can be a plane or tubular structure, as seen on Fig. 4.

It is conceivable that the Herzog variation braiding machine allows producing a bifurcated braiding with eight branches, starting in one basic braid. This shows the high potential of the research on multi bifurcated braiding structures and their production. This area of research is very promising.

References

1. Y. Kyosev, *Braiding Technology for Textiles* (Woodhead Publishing, 2014)
2. L. Muller, M. Milwich, A. Gruhl, H. Bohm, M. Gude, T. Haushahn, Biomimetisch optimierte verzweigte Faserverbundstrukturen mit hoher Tragfähigkeit. Melliand Textilberichte Nr. 02 Part: Band- und Flechtindustrie, p. 088, 7 June 2013
3. E. Essig, *Nadelbandwebtechnik* (Jakob Müller Institute of Narrow Fabrics, Frick, 2005)

Part II

Modelling and Testing

Geometrical Modelling of Tubular and Flat Braids Within the Jamming Limits—Verification and Limitations

Yordan Kyosev and Alena Cordes

Abstract Designing and developing braids requires specific knowledge about the structure, properties of the yarn, settings of the machine and other parameters. There are several works in the scientific literature that provide a large number of equations to calculate unknown braid parameters if some of the other values are known. Most of these works are useful for a scientific approach, but are often not practical for the everyday use in an industrial workspace environment. It would simply take too much time and effort for an engineer in a braiding company, to solve integrals in order to find the mass of a braid or another parameter. This paper presents an evaluation of the software *TexMind Braider*, which implements the above-mentioned scientific equations and performs several calculations automatically for the user. The benchmark has the goal to check and identify possible applications of this software, to find errors in the implementation or in the theories behind the equations and to state the general limitations of using geometrical models for modelling. The comparison will include a tubular braid with a monofilament yarn, a tubular braid with a multifilament yarn and a flat braid with a monofilament yarn.

Introduction

Braided products are used for ropes, reinforcement of hoses and pipes, medical catheters, composite profiles and many other applications. During their live cycle, the braids perform large numbers of loaded cycles between axial tension, relaxation and in some cases even compression (Fig. 1). The knowledge about the changes of the braiding angle and the diameter during these cycles is important to understand the behaviour of overbraided products, and whether the core and the sheet interact under these conditions or not.

Y. Kyosev (✉) · A. Cordes
Hochschule Niederrhein—University of Applied Sciences,
41065 Monchengladbach, Germany
e-mail: yordan.kyosev@hs-niederrhein.de

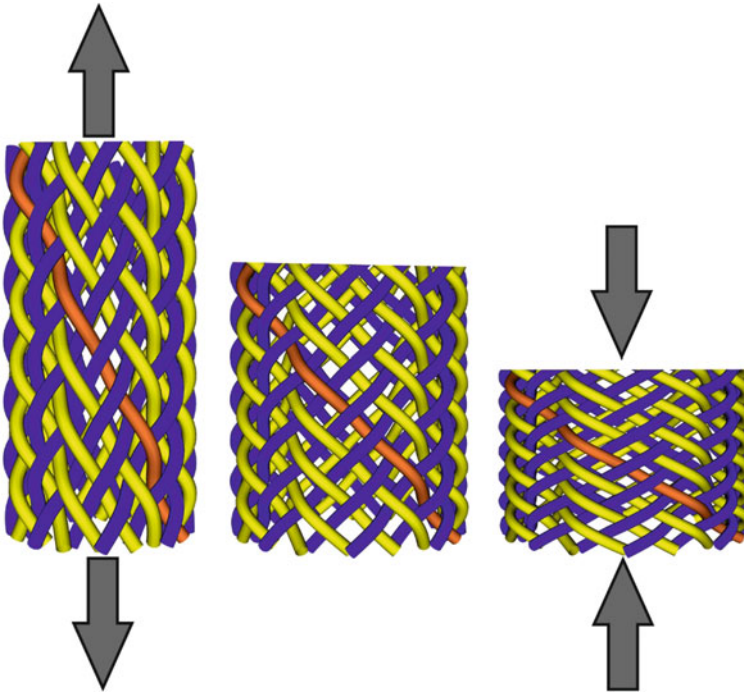


Fig. 1 A tubular braid under axial tension, relaxed state and compression

The behaviour of the braid and its properties depend on the used yarns, the type of the interlacement and machine settings. There are several works describing properties of braids; for instance, the pioneering work of Brunnschweiler [1], and following titles [2–4, 8, 9] and many more. In several of the models, described in these works, the yarn axis is assumed to be known and defined with some periodic functions. They, however, do not cover the generation of the geometry of the yarn axis for braids with arbitrary floating length and yarns in a group. Using the rules for interlacement of the yarns during the braiding, described in Kyosev [6] is a generalized geometrical model for braided structures, which is implemented in Software Braider [5]. This work provides verification of the simulated results from the software with practical measurements.

Geometry

The 3D geometry of the braids is created based on pure geometrical models as described in Kyosev [6]. The algorithm calculates the yarn axis coordinates for the given braid, if the pattern, braid diameter, yarn diameter and the braiding angle are

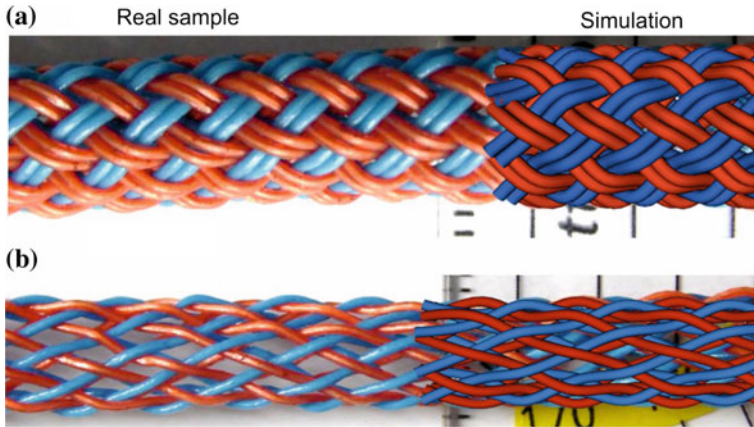


Fig. 2 Comparison between the simulation and reality. a 1:1–2. b 1:1–1

specified by the user. As the yarns are presented with a circular cross section, a monofilament yarn was used for the comparison between the real braid and the simulation. Figure 2 presents a picture of two braids where the structure is continued in a simulation: Both braids with a floating length of one, but once with two yarns in a group (Fig. 2a) and once with one yarn in a group (Fig. 2b).

In order to illustrate the compression states, the simulations for one tubular and one flat braid are compared with the data of real samples. Compared are the geometrical data for the jamming states and the values between these two limits.

Flexibility and Jamming States for Tubular Braid

As described in [1, 4] the jamming conditions for the braids depend on the number of the yarns, their lateral compression properties and the diameter of the braid. The simplified equations based on kinematical frame theory do not consider the yarn compression [10] and can be used as good initial approximations for the calculation of the jamming conditions of braids with less data, as described in Kyosev and Aurich [7]—because during the design process of braids engineers do not consider the material properties at the first step.

As described in Kyosev and Aurich [7], one of the jamming angles for a braid can be calculated using the following equation

$$\alpha_1 = \frac{1}{2} \cdot \arcsin \frac{2 \cdot N \cdot (w + d) \cdot \sin \alpha_0}{\pi \cdot D_0} \tag{1}$$

And the second is

$$\alpha_2 = \frac{\pi}{2} - \alpha_1 \quad (2)$$

where N is the number of the unit cells in one braid, which corresponds to the half of the carrier numbers for tubular braids, w is the width of the yarn, d is the thickness of the yarn and D_0 is the initial diameter of the braid, this is the diameter of the braid on the braiding machine.

The equation is valid only until the relation

$$\frac{2 \cdot N \cdot (w + d) \cdot \sin \alpha_0}{\pi \cdot D_0} \leq 1 \quad (3)$$

Which means, for open braids—there the yarns do not cover the complete circumference of the braids:

$$2 \cdot N \cdot (w + d) \cdot \sin \alpha_0 \leq \pi \cdot D_0 \quad (4)$$

In all other cases, the braid is closed and dense enough, so that geometrically it cannot be deformed in the axial direction.

In the practical case, some deformation is still possible because of the compressibility of the yarns.

Once the braid changes its geometry because of stretching or compression, the braid changes as well its diameter. The current braid diameter depends on the initial one (during the braiding) and on the braiding angle during braiding.

$$D = D_0 \cdot \frac{\sin \alpha}{\sin \alpha_0} \quad (5)$$

Figure 3e presents an original braid compared to its simulation. On the left and right side the calculated jamming states for this braid are given, which correspond to tension and compression states, respectively. In the first row, three scans of the original braid are shown, deformed manually to its maximal tension and compressional state. The word scan was used intentionally here, because during scanning the braids were pressed and on the image their pressed width is visible and does not show their optical diameter. This method was preferred over a contact measurement of the diameter, using a calliper rule, as the applied pressure would influence the real diameter. Optical methods for the measurement of the diameter are connected with errors from the perspective, which depends on the measured diameter itself and the use of more expensive optical devices could lead to more precise results.

The calculated and measured diameters and braiding angles are presented in Fig. 4. The figure demonstrates that the geometric algorithm computes almost exactly the jamming angle under tension (the smallest one) but the calculated maximal braiding angle under compression is about 15° larger compared to the one

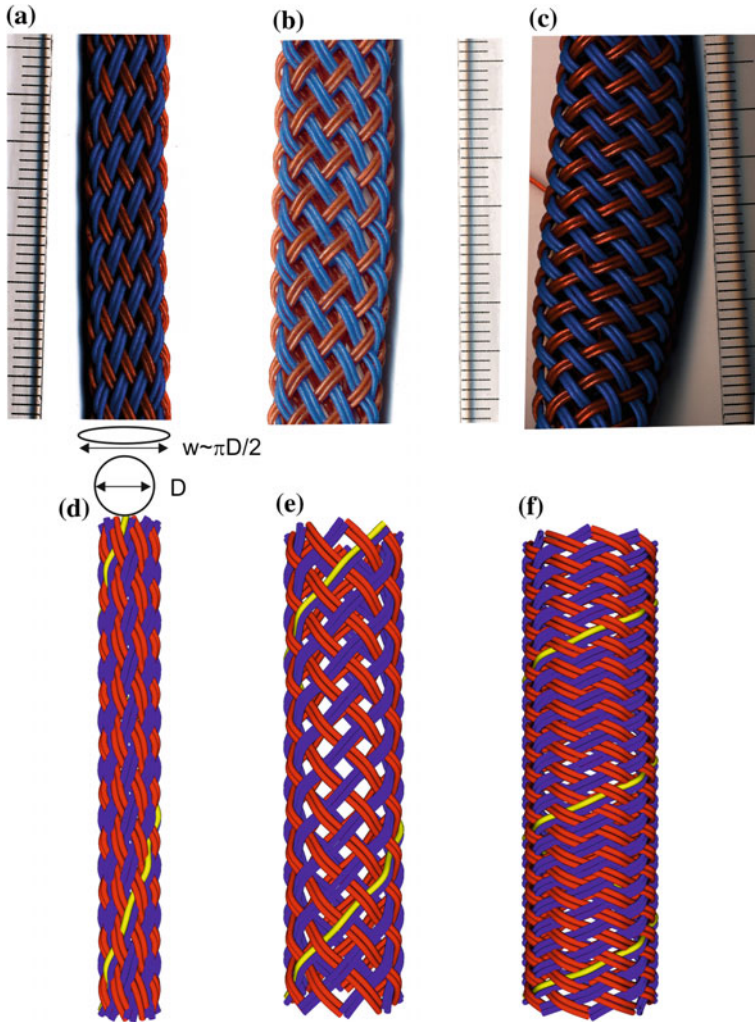


Fig. 3 Initial state of the braid (b and e), its jammed state under tension (a, d) and under axial compression (c and f), real sample versus simulation

of the manual state. A reason for this could be the method of the measurement—the braided structures were pressed manually due to the scanner wherefore the maximal pressed state could not be reached, as if such a test is performed on a tensile testing machine.

The trend of both lines simulated and measured are identical, the small difference of about one millimetre can be explained with the measuring error, which is larger for the braids with smaller diameter.

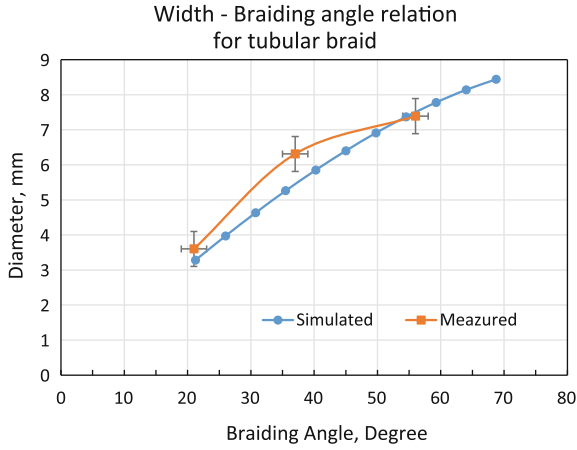


Fig. 4 Comparison between the simulated and measured diameter and angle of the investigated braid. Used was braid with 16 groups of coated glass fibre with PVC, pattern 1:1–2, each yarn with 0.4 mm diameter

Flexibility and Jamming States for Flat Braid

For flat braids, the relation (1) changes slightly—instead of the circumference of the braid, the braid width and the number of the unit cells in the width is equal to the half of the total number of the yarns:

$$\alpha_1 = \frac{1}{2} \cdot \arcsin \frac{(N_{yarns}/2) \cdot (w + d) \cdot \sin \alpha_0}{width_0} \tag{6}$$

The remaining equations have to be adjusted accordingly.

Figure 5 shows an optical comparison between the simulated geometry and the real geometry of a braid of 33 flax yarns with a diameter of 3 mm. This yarn was

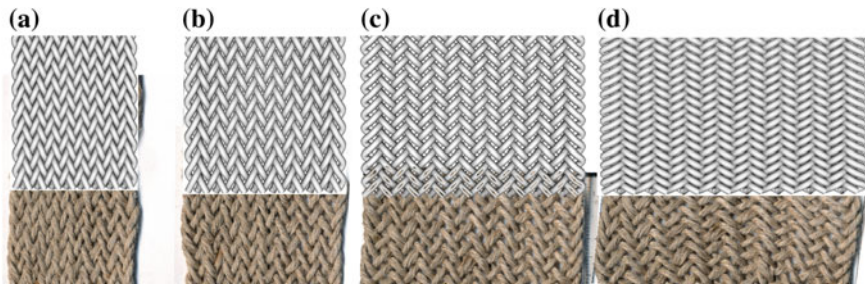
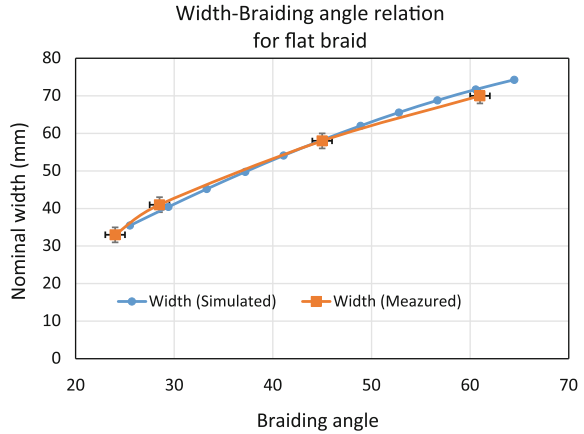


Fig. 5 Simulated geometry versus real geometry for a flat braid with 33 flax yarns with 2 mm diameter, pattern 2:2–1. Braiding angles **a** jamming state under tension at braiding angle 24°, **b** 28°, **c** 45°, **d** practical jamming state under axial compression 61°

Fig. 6 Comparison between the measured and simulated width at different braiding angles within the jamming limits of the flat braid from Fig. 5



used in order to check the accuracy of the model for conditions, which satisfy the assumptions of the ideal braid during the creation of the mathematical model—yarns with circular cross section.

Figure 6 presents the data from this optical comparison in a diagram, where the model again overestimates the jamming angle under compression, but the simulated results are very close to the measured ones. The better correlation in this case is positively influenced by two factors—the size of the braid and the method of the measurement. As the braid has a larger size, the measuring error from the estimation of the width has the same absolute value, but in relation to the measured dimension this error remains with negligible relative value. Additionally, the width of a flat braid can be scanned and estimated more exact than the width of a pressed tubular braid, which do not completely flatten during pressing.

Further Applications

This first validation of the mathematical models and their implementation in the TexMind Braider software show that the geometry of the structure is well represented during the simulation, while the structures with less number of yarns have larger deviations and the larger braids are more precisely modelled.

Based on the modelled geometry and the linear density of the yarn, the weight per meter for the braids can be calculated, and for monofilament yarns and wires it can be expected, that the simulated values will be very close to the reality. Validations of the weight per unit length and of the theoretical strength were not performed for the structures presented in Figs. 3 and 5. This validation is in progress now for larger sets of multifilament yarns, which are more important for the practical applications. However modelling braids with multifilament yarns is more complicated than modelling yarns with circular cross section.

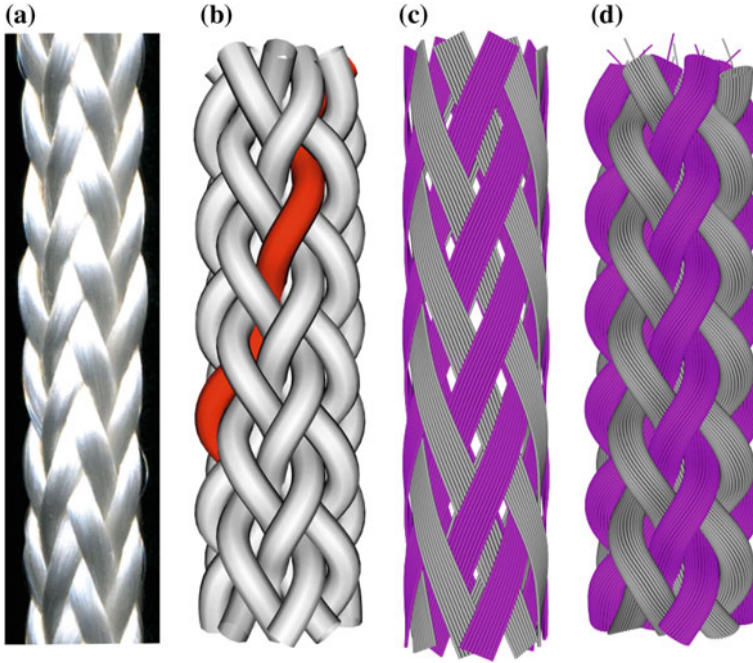


Fig. 7 Tubular braid produced of multifilament yarns with negligible twist **a** original, **b** model where each yarn is modelled as a single tube, **c** each yarn is presented as 10 filaments arranged as flat cross section, **d** each yarn is presented as a multifilament structure, the last layer has 30 filaments

Limitations of the Geometrical Models

One of the main limitations of geometrical models is that they are based on parametrical relations for given number of points of the yarns. Such relations become significantly complex if the yarns are consisting of several (thousand) multifilaments (Fig. 7a). In such a case, the simulated geometry (Fig. 7b) presents the architecture of the braid only in a simplified way, but the density of the braid cannot be exactly reproduced. If the yarn is presented as a set of single filaments, arranged in a flat cross section, the appearance is completely different—this is common geometry for over braiding of hydraulic hoses and pipes, but not for ropes (Fig. 7c). Using complete fillings of the yarns with single filaments, the appearance is more close to the reality (Fig. 7d), but the single filaments are still placed in some ideal positions. Such geometry can be used as initial configuration for calculations; for instance, with Finite Element Software, but in their current form do not give any advantage over the usage of a monofilament model.

Conclusions

This work presents a comparison between the real geometry of tubular and flat braids in different deformed states and the simulated values for these braids. The comparison demonstrates that the geometrical models are able to predict the limits of the deformation of tubular and flat braids and their geometrical parameters (diameter of the tubular braid or width of the flat braid) well. The overestimated jamming state under compression in the geometrical models is caused by the measurement method. While scanning the applied force during the axial compression of the braid can be insufficient because it is performed manually and not on a tensile testing machine. This successful validation closes the current development step of the implementation of geometrical models in the software TexMind Braider and confirms that these can be used as a basis for the development of more complex, refined models of braids or during the calculations of the parameters for double-layered braids.

References

1. D. Brunnschweiler, 5—The structure and tensile properties of braids. *J. Text. Inst. Trans.* **45**(1), T55 (1954). doi:[10.1080/19447025408662631](https://doi.org/10.1080/19447025408662631)
2. Du Gw, P. Popper, Analysis of a circular braiding process for complex shapes. *J. Text. Inst.* **85**(3), 316–337 (1994). doi:[10.1080/00405009408631277](https://doi.org/10.1080/00405009408631277)
3. R.H. Hopper, J. Wallace Grant, P. Popper, Mechanics of a hybrid circular braid with an elastic core. *Text. Res. J.* **65**(12), 709–722 (1995)
4. F.K. Ko, C.M. Pastore, A.A. Head, *Handbook of industrial braiding* (Atkins & Peirce, 1989)
5. Y.K. Kyosev (2012) TexMind Braider, Mönchengladbach, www.texmind.com
6. Y.K. Kyosev, Generalized geometric modelling of tubular and flat braided structures with arbitrary floating length and multiple filaments. *Text. Res. J.* (2015) (accepted)
7. Y.K. Kyosev, M. Aurich, Investigations about the braiding angle and the cover factor of the braided fabrics using Image Processing and Symbolic Math Toolbox of Matlab, in *Advances in Braiding Technology: Specialized Techniques and Applications*, ed. by Y.K. Kyosev (Woodhead Publishing Limited, 2016)
8. R. McConnel, P. Popper, Complex shaped braided structures (1988) (4719837)
9. P. Popper, Braiding, in *Handbook of Composite Reinforcements*, ed. by S.M. Lee (John Wiley & Sons, Hoboken, 1992), pp. 24–40
10. M.E. Yuksekkaya, S. Adanur, Analysis of Polymeric braided tubular structures intended for medical applications. *Text. Res. J.* **79**(2), 99–109 (2009)

Geometrical Modeling of Tubular Braided Structures Overbraiding Polygonal Prism Based on the Intersection of Surfaces

Ning Fangggang and Yu Weidong

Abstract This paper presents a geometrical modeling method for braided structures overbraiding polygonal prism based on the intersection of helical surface and braiding surface. These two kinds of surfaces are abstracted based on the decomposition and re-composition of strand motions. The braiding surface is the composition of axial motion and radial motion and represents the outline of the braided structures. The axial motion and the circumferential motion could compose the helical surfaces, which defines the braiding angle and strand position. The braiding strand could be obtained by the intersection of braiding surface and helical surface. Using the braiding surface transformed from the surface with polygonal prism, the detailed modeling process for braided structures overbraiding regular polygonal prism and the combined structures is introduced based on the SolidWorks® 2013.

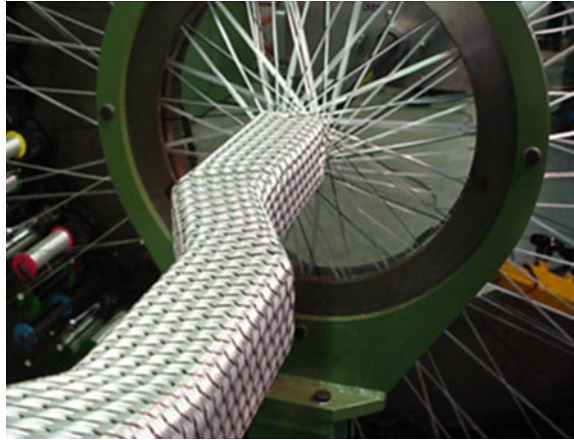
Keywords Braided structures · Geometrical modeling · Polygonal prism · Intersection of surfaces

Introduction

Braided structures are realized by interlacing strands in two directions according to certain patterns; for ropes, there are no mandrels within the core of this braiding strand. If adding specific mandrels in the core of braided structures, the net-shaped braided structures could be obtained with the profile of the mandrels. Among these, the braided structures overbraiding polygonal prism are widely used in practice, as shown in Fig. 1. As the development of textile composites, especially the application of advanced fiber, this kind of technique is widely used to produce the enforcement of composites with complex outline. Braiding over a mandrel can potentially have number of advantages [1], including the ability to precisely align

N. Fangggang (✉) · Y. Weidong
Engineering Research Center of Technical Textiles, Textile College,
Donghua University, 201620 Shanghai, China
e-mail: edward1654@163.com

Fig. 1 Manufacturing process of braided structure overbraiding polygon prism [12]



the constituent strands and to build the desired number of layers to obtain the required level of thickness along with the possibility of forming near-net shapes [2]. Due to these unique advantages, these kinds of structures have attracted lots of researches as follows.

The work by Brunnschweiler [3] in the 1950s is almost the early research on braided structures; he analyzed in detail the structure of diamond braid, and its geometry is developed, based on assumptions similar to those of Peirce and described a practical method of testing tubular braids to find their tensile properties, while the structures discussed are common braids not the braids overbraiding mandrels. Du and Popper [4] are the early scholars to discuss the braids over complex mandrels. They developed a detailed model of the braiding process, which related the shape of the braid to the machine speeds, and a number of other machine settings and this model also could be used to predict the local micro-geometry. Then Kessels and Akkerman [5] introduced a model to predict the fiber angles on complex biaxially braided preforms based on a mathematical method. Potluri et al. [2] introduced a computer-controlled braiding machine to manufacture triaxial tubular braids and the braided structure had been simulated using virtual reality modeling language. Rawal et al. [6, 7] focused on producing three-dimensional shapes by braiding over contoured mandrels, which included circular cylinder, circular cone, elliptical cone, square prism, and square pyramid. However, in order to simplify the geometrical models, these investigations did not consider the crimp of strands. In 2012, Alpyildiz [8] studied geometrical modeling for tubular braids and proposed a simple three-dimensional model after considering the crimp of the braiding yarn. 3D drawings of the model for diamond, regular, and triaxial braids were given with the aid of Visual Basic and 3DSMax Studio. Based on Alpyildiz's mathematical model, Rawal [1] used VRML to visualize the models of strand trajectory on the surface of cylindrical and conical mandrels and simulated these complicated structures. Recently, Kyosev [9, 10] gave a generalized geometrical approach for modeling flat and tubular braided structures with arbitrary floating

length and filaments in the yarn based on the braiding machine. Based on this modeling method, CAD software for braiding named Texmind Braider [11] was developed.

Previous work above mainly focused on the relationship of structures and manufacturers and provided the directions for manufacturers. While as the base of modeling manufacturers, the development of geometrical models of braids especially the braids overbraiding complex mandrels is lack of the development of its usage. The only relevant work was conducted by Rawal who mainly introduced the modeling method for complicated braid with revolving cross section. As to the braids of polygonal prism, no relevant literatures reported. This may be due to that the strand is difficult to be described by mathematical method. While as the development of computer techniques, especially the CAD techniques, the strand models could be obtained by the relationships of braiding elements instead of mathematical expressions. Based on this thought, this paper raises a geometrical modeling method for braided structures overbraiding polygonal prisms based on the analysis of braiding process.

Motion Analysis of Braiding Process

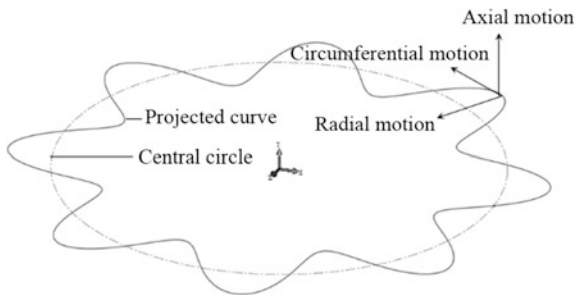
For a traditional braiding process, the carriers with strands run along two interlacing tracks in clockwise and anticlockwise, respectively, and pass the points of intersection one by one to form the braided structures. At the same time, the braided strands are drawn out by take-up roller continuously to form braided structures.

The interlacing patterns of tracks on braiding machines define the interlacing pattern of braided structures. Due to the soft properties, these strands or tapes may adjust themselves to adapt the braiding force, while the braiding pattern will not be changed at all; therefore, different braiding tracks on braiding machines will produce different braided structures.

Decomposition of Strand Motions

On the braiding plane, carriers run the following closed tracks. When carriers run along these tracks, on one hand, the carriers will run along a central circle and meanwhile oscillate around this circle, which form interlacing with the carriers in another direction. According to the motion of carriers, it would be reasonable to decompose the motion of carriers into two sub-motions, one is circumferential motion along the central circle and the other is the radial motion, as shown in Fig. 2. These two sub-motions have different meanings for the formation of braided structures. The circumferential motion is a kind of driving motion which ensures the strands run along the central circle and make the braiding process run smoothly, while the radial motion is the characteristic motion which realizes the braiding

Fig. 2 Decomposition of strand motion



process. For different braided structures with different braiding patterns, the frequency of radial motion is different.

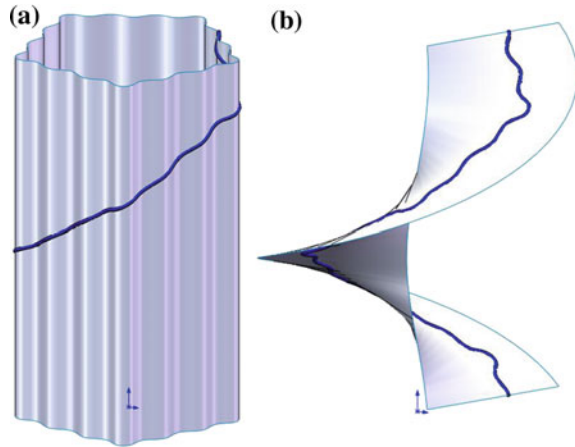
During the braiding process, the take-up roller continuously draws out the braided structures from the braiding zone to form the braided structures. The movement of take-up roller provides an axial motion to the braiding strands. The speed of axial motion depends on the speed of take-up roller and determines the pitch of braided structures.

Re-composition of Sub-motions and Two Kinds of Surfaces

The above analysis is based on the motions of carriers and take-up roller in braiding process; the braided structures are formed by the regular motion of these two parts. In another word, the strands are the record of these motions. The projection of braided strand on the cross section of braids is similar to the track. The pith of braids is defined by the speed of carriers and take-up rollers. Therefore, the motions during braiding process would be employed to describe the modeling process.

Based on the analysis of decomposition of motions, the motion of strands is the composition of motion of carriers and take-up roller; therefore, the motion of strands could also be decomposed into circumferential motion, radial motion, and axial motion. According to the position of these three sub-motions, they could be divided into motions in braiding plane including radial motion and circumferential motion and axial motion. The motions in the braiding plane are independent with each other. Both of them are simultaneous with the axial motion and thus they could compose with axial motion. The radial motion and the axial motion could compose a motion which always lie on a surface formed by sweeping the projected curve along the braiding axis; this surface is named braiding surface, as shown in Fig. 3a. The circumferential motion and the axial motion could compose a motion which always lies on a surface formed by helically sweeping a radius along the braiding axis, as shown in Fig. 3b. This surface is named helical surface. The braiding surface and the helical surface include all motions of strand, so the strand could be obtained by the intersection of these two surfaces.

Fig. 3 Two kinds of surfaces
a braiding surface **b** helical
 surface



For braided structures overbraiding the polygonal prism, the path of the strands could be affected by the mandrel, and the braiding surface will become a special surface which is similar with the outline of the mandrels. The helical surface is not affected by the outline of mandrels. So the strands of braided structures overbraiding a polygonal prism could be obtained by the intersection of modified braiding surface and the helical surface.

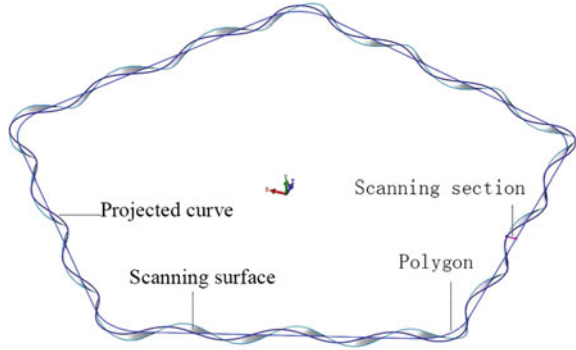
Geometrical Modeling of Braided Structures of Regular Polygonal Tube

Based on these two surfaces and their intersection, it would be available for geometrical modeling of braided structures overbraiding polygonal prism using CAD software. Lots of CAD software could be employed to realize the modeling process based on the modeling method mentioned here, for example, the CATIA[®], UG[®], etc. In this paper, the SolidWorks[®] 2013 is employed to complete the whole modeling process.

From the analysis mentioned above, the modeling process, in fact, is also the process of the generation of two kinds of surfaces. As to these two surfaces, the braiding surface is the key points for the whole modeling process and it is generated by sweeping a special curve, which is the projection of strand on the braiding cross section, along the braiding axis. So the realization of the projected curve would become the controlling point for this modeling process.

As shown in Fig. 4, the polygon is similar with cross section of mandrel and is corner-rounded which would be more reasonable for braided structures and also for the realization of sweeping process. This polygon could be the center of the modeled structure. A scanning surface could be obtained by helically sweeping a section along the rounded polygon. This process could be realized using the “swept

Fig. 4 Realization of projected curve



surface” tool taking the polygon as the path, the scanning section as the profile, and setting the option as “twist along path”. The number of turn would be the integral multiple of the number of the polygon sides. The length of the scanning section would be the wave amplitude of the braiding strand in braids and would depend on the diameter of strands. The projected curve is the projection of the outside of the helical surface and could be obtained by “convert entity” tool. The projected curve could be obtained taking outside of the helical surface as the entity to convert the plane of cross section. There are also some other methods to realize the projected curve, for example, using the spline to connect relevant points of polygons.

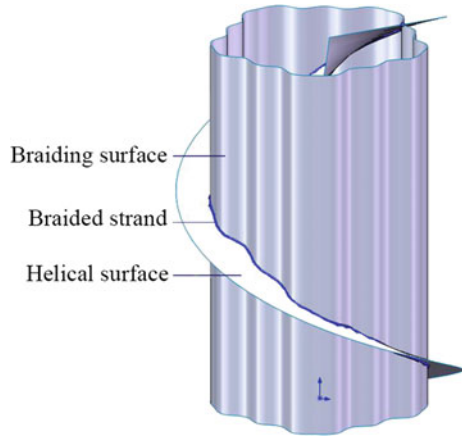
The projected curve is the basic element for the braiding surface and the key controlling factor. Once obtaining the projected curve, the braiding surface could be easily obtained by sweeping the projected curve along the braiding axis, as shown in Fig. 3a. The helical surface is the composition of circumferential motion and the axial motion and could be obtained by helically sweeping the radius along the axial, as shown in Fig. 3b; here, the length of the radius could be a little longer than the radius of the braided structures so that the helical surface could intersect with the braiding surface. The helical angle could be the same with the braiding angle. The position of the sweeping radius determines the position of the strands.

Because the braided strand is the composition of axial motion, circumferential motion, and the axial motion and these three motions could compose two kinds of surfaces including all information of braiding process, thus, the central line of the braiding strand could be obtained by the intersection of braiding surface and helical surface. In SolidWorks[®], the intersection could be realized by “intersection curve” tool by taking the braiding surface and the helical surface as the interlacing entities, as shown as Fig. 5.

Once obtaining the central line of strands, the braided strand could be obtained by sweeping the cross section of the strand along the braiding curve. The braided structures modeled by this method are not confined by the cross section; any closed shape could be taken as the cross section of the strand including circle, ellipse, and polygon.

All strands in the same direction lie on the same braiding surface, while on different helical surfaces, the position of the helical surfaces depends on the position

Fig. 5 The intersection of braiding surface and helical surface



of strands. For braided structures overbraiding polygonal prism, the strands in the same direction, taking clockwise as example, are of a phase difference among adjacent strands. For polygon of M side with N wave along each side, the phase difference would be $2\pi/MN$. Based on this phase difference, N strands on one side could be generated by changing the initial position of helical surfaces, as shown in Fig. 6a. The strands on the other side could be obtained by circle pattern tool.

For strand in different directions, besides the helical direction, the projected curve is also different. The phase of projected curve of strands between clockwise and anticlockwise is opposite, which means that there are π phase differences. So once the projected curve in clockwise is obtained, the projected curve in anticlockwise could be obtained by adjusting the phase, as shown in Fig. 6b. The diamond braid is the simple and widely used structure and is formed by interlacing strands in clockwise and anticlockwise with one-up and one-down pattern. Figure 7a shows the braided structure overbraiding a quadrilateral cylinder.

Fig. 6 Strands on one edge
a strands on anticlockwise
b strands on clockwise

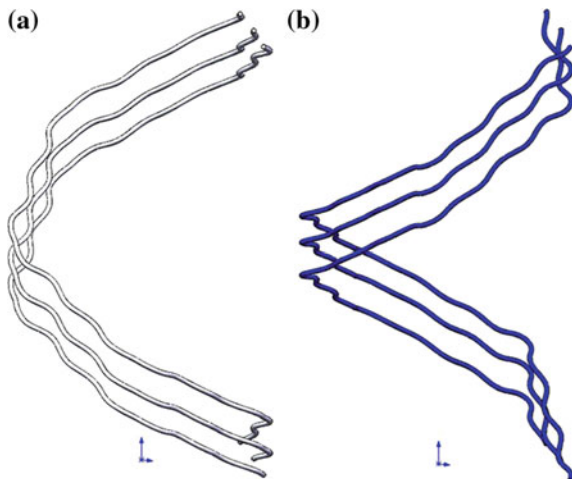
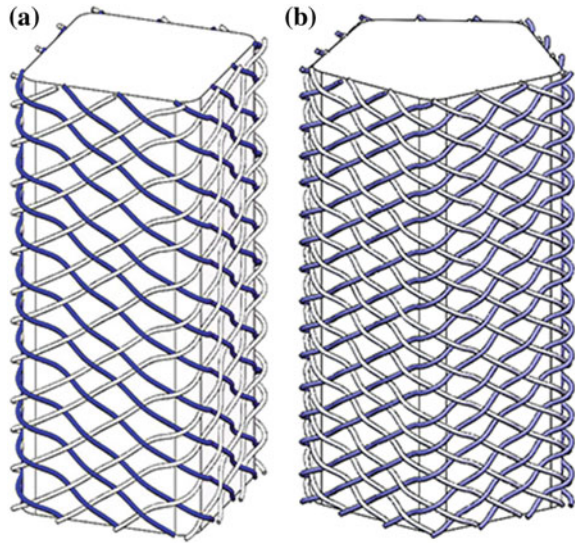


Fig. 7 Braided structure with polygon prism **a** quadrilateral cylinder; **b** Pentagonal cylinder



The quadrilateral braided structure could also be simulated following the modeling process mentioned above. The main difference lies on the braiding surface. For quadrilateral braided structure, the braiding surface is a kind of quadrilateral surface with waves and is similar with the quadrilateral cylinder. In manufacturers, the mandrel with quadrilateral cylinder could be used to manufacture this kind of structure. Figure 7b shows the braided structure overbraiding pentagonal cylinder. From these two braided structures simulated by this modeling method, it would be observed that the modeled structures are of good interlacing structures and the modeling method could reflect the braiding pattern.

Geometrical Modeling of Braided Structures of Combined Polygonal Tube

From the modeling process of braided structure overbraiding regular polygonal prism, it could be concluded that the two kinds of surfaces have different meanings for the modeled structures. The helical surface defines the position of the strands and the braiding angle. The braiding surfaces determine the outline of the braided structures, and it could be reasonable to treat the braiding surface as a kind of transformation of surface of the polygonal prim or aimed structures, as shown in Fig. 8. The characteristic of this kind of transformation is adding a series of waves along the sides of polygon. This kind of wave would form a series of rising and falling on the surface which make it possible for strands in another direction to pass without overlapping with each other. The braided strands lie on this surface to form the interlacing structure with strands in another direction. So the braiding surface is

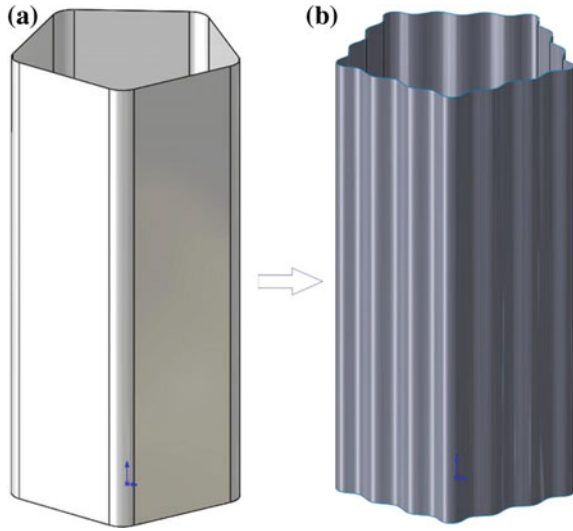


Fig. 8 Surface transformation from pentagonal cylinder (a) to braiding surface (b)

a kind of transformation of surface of mandrels and is the key step for geometrical modeling.

From the analysis above, it could be observed that the outline for the braided structures totally depends on the profile of braiding surfaces. Therefore, the braiding surface could be treated as a kind of transformation of aimed structures. In this case, other braided structures overbraiding polygonal prism could be realized if the corresponding braiding surface could be obtained by a certain transformation.

Figure 9a shows a kind of combination of polygonal prism with different sizes, which are widely used in practice. The modeling process would be similar with that

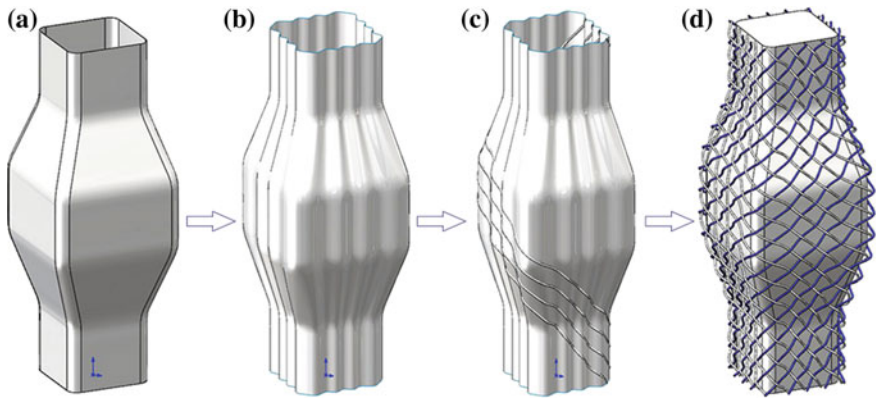
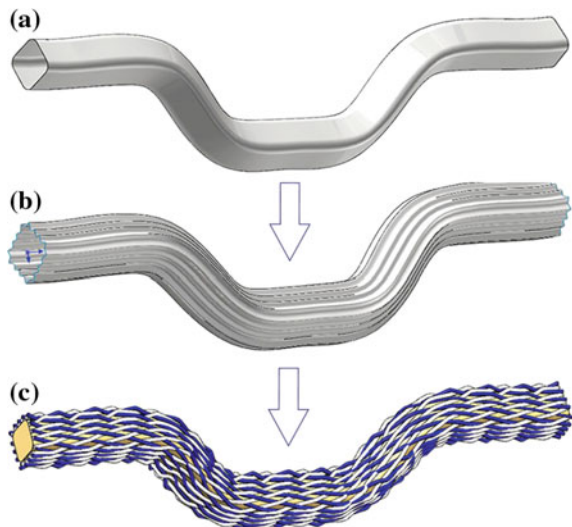


Fig. 9 Modeling process **a** combined polygonal surface **b** braiding surface **c** the realization of responding strands **d** the completed combined polygonal braided structure

of braided structures overbraiding regular polygonal prism. At first, the braiding surface would be obtained based on the aimed surface. Compared with the braiding of regular polygonal prism, the cross section of braiding surface of combined braided structure would be changed along the braiding axis, which means that the projected curve would be changed during the sweeping process. In order to make this, two guide lines would be needed. These two guide lines could be obtained by the intersection of aimed surface with two vertical surfaces and at the same time, these two guide lines have the intersection points with the projected curve on the cross section of braided structures. Based on these two guide lines, the “swept surface” tool could be employed to realize the braiding surface by taking the projected curve as the sweeping profile and the braiding axis as the path, as shown in Fig. 9b. The strands could be realized by the intersection of the braiding surface and the helical surface. Following the similar steps, the whole braided structures overbraiding a combined polygonal prism could be obtained, as shown in Fig. 9c, d. For the modeling process of this kind of structure, the guide lines which are employed to ensure the projected curve change with the outline of aimed surface are the key points.

Besides the combined polygonal prism, the non-axisymmetric braided structures are also widely used in practice. For this kind of structure, it would also be realized following the similar method, as shown in Fig. 10. At first, the outline of the mandrel could be built. The central line of this mandrel is the braiding axis. The projected curve could be obtained on the cross section of braid following the same method as that of regular polygonal prism. The braiding surface could be built by “swept surface” tool by taking the projected curve as the sweeping profile and the braiding axis as the path. The main difference is that the path is not a straight line but a curve. Due to this difference, all braiding strands could be obtained one by one

Fig. 10 Non-axisymmetric braided structures **a** aimed surface **b** braiding surface **c** the completed braided structure



instead of by circle pattern method. This means that it is necessary to build all helical surfaces in order to realize the intersection with the braiding surface. The helical surface could be realized by helically sweeping a section, which lie on the cross-sectional plane and the length of which is longer than the radius of the projected curve so that it could intersect with the braiding surface, along the braiding axis. So the helical surface is also a kind of non-axisymmetric structure.

Based on the braiding surface and the helical surface, the strands could be obtained based on the intersection methods one by one. The complete braided structures overbraiding the non-axisymmetric mandrel could be obtained by assembling strands in two directions together, as shown in Fig. 10c.

Discussion

This paper presents a modeling method for braiding structures overbraiding the polygonal prism and their combined structures including axisymmetric and non-axisymmetric structures. This method is given based on the analysis of the braiding motions. The whole braiding process is realized by two parts: the carriers and the take-up roller. The carriers with the strands run along two interlacing tracks on the braiding plane. Based on the trend of carrier motion, the strand movement on the braiding plane could be decomposed into radial motion and circumferential motion. When the carriers interlace with each other, the take-up roller is rolling to take the braided structures away from the braiding zone to ensure the braiding process continually. The rolling of take-up roller makes the strand have an axis motion. The axial motion would combine two different surfaces with motions on the braiding plane including the braiding surface and the helical surface to form two surfaces together which include all motion information, and thus, the braiding strand could lie on these two surfaces at the same time; in other words, the braiding strand could be obtained by the intersection of braiding surface and helical surface.

These two surfaces have different meanings for the formulation of braided structures. The braiding surface is of the similar outline with that of the mandrel and defines profile of the braided structure. From the mandrel surface to the braiding surface, it could be reasonable to treat it as a transformation which adds a series of rising and falling on the mandrel surface. These rising and falling structures could form the crimps of braided strands and provide the space for strands in another direction to pass through without overlapping with each other.

For braided structures overbraiding the regular polygonal prism, the cross section could keep the same; thus, the braiding surface could be obtained by sweeping the projected curve along the braiding axis directly. While, for braided structures overbraiding combined polygonal prism, the cross section would be changed along the axis, therefore, the projected curve would have to be adjusted following the outline of the mandrels. In this case, two guide lines are introduced to control the size of the projected curve along the braiding axis. As to the braided structures overbraiding the non-axisymmetric mandrels, the modeling method is the same

with that of regular structures, and the main difference would lie on the outline of braiding surfaces which would lead that all strands should be built one by one instead of using circle pattern tool. The simulated structures show that this modeling method could reflect the crimp of strands and the interlacing characteristic of whole braiding structures.

Conclusion

For complicated braided structures, it would be difficult to describe the curve of strands by mathematical expressions which make it impossible to simulate based on equations, while the development of CAD techniques would make it possible to obtain the strands based on the relationships of spatial characteristics. This paper presents a modeling method for braided structures overbraiding polygonal prism based on CAD, such as SolidWorks®, CATIA®, etc. Two kinds of surfaces are abstracted from the analysis of the strand motion and the path of the strand in braided structures could be the intersection of these two surfaces. Among these two surfaces, the helical surface defines the outline of the braided structure and the crimp and the helical surface determines the position of strands and the braiding angle; therefore, different braided structures could be realized by modifying these two surfaces. As important application, the braided structures overbraiding polygonal prism and their combined structures including axisymmetric and non-axisymmetric structures were introduced in detail based on the SolidWorks® 2013. The simulated models could reflect the crimp of strand and the interlacing characteristic of braided structures.

References

1. A. Rawal et al., Geometrical modeling of near-net shape braided preforms. *Text. Res. J.* 0040517514559587 (2014)
2. P. Potluri et al., Geometrical modelling and control of a triaxial braiding machine for producing 3D preforms. *Compos. Part A Appl. Sci. Manuf.* **34**(6), 481–492 (2003)
3. D. Brunnschweiler, The structure and tensile properties of braids. *J. Text. Inst. Trans.* **45**(1), T55–T77 (1954)
4. G.W. Du, P. Popper, Analysis of a circular braiding process for complex shapes. *J. Text. Inst.* **85**(3), 316–337 (1994)
5. J.F.A. Kessels, R. Akkerman, Prediction of the yarn trajectories on complex braided preforms. *Compos. Part A Appl. Sci. Manuf.* **33**(8), 1073–1081 (2002)
6. A. Rawal, P. Potluri, C. Steele, Geometrical modeling of the yarn paths in three-dimensional braided structures. *J. Ind. Text.* **35**(2), 115–135 (2005)
7. A. Rawal, P. Potluri, C. Steele, Prediction of yarn paths in braided structures formed on a square pyramid. *J. Ind. Text.* **36**(3), 221–226 (2007)
8. A. Tuba, 3D geometrical modelling of tubular braids. *Text. Res. J.* **82**(5), 443–453 (2012)

9. Y. Kyosev, *Braiding Technology for Textiles* (Woodhead Publishing 2014)
10. Y. Kyosev, Generalized geometric modeling of tubular and flat braided structures with arbitrary floating length and multiple filaments. *Text. Res. J.* (2015)
11. Y. Kyosev, Machine configurator for braided composite profiles with arbitrary cross section, in *16th European conference on composite materials*. Seville, Spain, 2014
12. J. Ravenhorst, R. Akkerman, *A Spool Pattern Tool for Circular Braiding* (2011)

Investigation of the Bending Rigidity of Double Braided Ropes

Lawrence R. Msalilwa, Yordan Kyosev, Amit Rawal
and Uttam Kumar

Abstract This work presents an investigation about the bending rigidity of double braided ropes. The braid structure is subjected to bending condition by fixing one end and leaving the other end to hang freely and bend under its own weight to a set deflection limit and its length is measured. The length and deflection are then used to calculate the bending stiffness and bending moment using the beam deflection equation. The bending behavior of single braided and double braided tubular ropes is also studied and compared. Highest bending rigidity was obtained with double braided tubular ropes compared to single braided tubular ropes. It is observed that, braided structures are very weak under transverse loading, their strength are improved when more structural layers are braided together. High braiding angle of braid structures is observed to improve bending stiffness and bending moment.

Keywords Double braiding · Bending stiffness · Area moment · Boundary condition

Introduction

Braiding is generally used for producing narrow rope-like materials by interlacing diagonally three or more strands of filaments or yarns. The bundles of filaments in a braid are interlaced in a similar way to that of the interlacements of ribbons formed in the Maypole dance. This results in a tubular woven structure in which the constituent

L.R. Msalilwa · Y. Kyosev (✉)

Research Institute for Textile and Clothing (FTB),
Hochschule Niederrhein—University of Applied Sciences, Mönchengladbach, Germany
e-mail: Yordan.kyosev@hs-niederrhein.de

L.R. Msalilwa

Department of Mechanical and Industrial Engineering, University of Dar es Salaam,
Dar es Salaam, Tanzania

A. Rawal · U. Kumar

Department of Textile Technology, IIT Delhi, New Delhi, India

filaments follow helical paths, simultaneously forming the interlacements between them. Circular braiding has been traditionally used for making tubular structures but there is an ever-increasing interest to use these structures for various composite applications [1]. A tubular braid without any core undergoes large lateral contraction when extended by a tensile force along its axis, but when elastic materials are inserted in the hollow braid they can potentially act as reinforcement in energy absorbing composite. These elastic materials do not prevent, only resist the lateral contraction to some extent. Moreover, the use of braided filaments over elastic core can potentially reduce the density and cost of composite [1]. There are several application areas where braided structures are widely used in the composites production of high performance parts and where not so high strength and lightness of the parts, as in the airspace and automotive production. Many recreational equipment such as snow skis, boat hulls, hockey sticks, golf shafts, wake boards, sail masts, bicycle components, baseball bats, canoe paddles also are using braided reinforcements [2, 3]. For several home and industrial applications such overbraided parts can replace small parts from metal or plastic. These braided structures are subjected to different loading conditions specifically bending condition, which they need to overcome during its application.

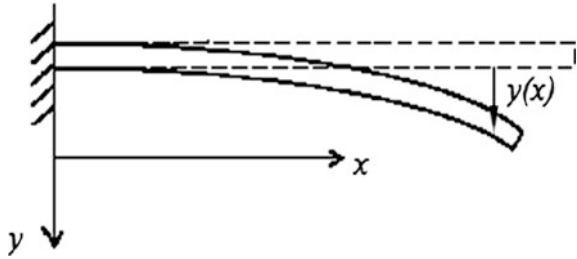
In this study, double braided tubular ropes are modeled as beams to investigate the braid bending properties. The plane stress problem of beams is very classical in elasticity theory and is encountered frequently in practical cases. Timoshenko and Goodier [4] investigated isotropic beams for different cases, such as tension, shearing, pure bending, bending of a cantilever by transverse load at the end and uniform load and other cases of continuously loaded beams. The solutions for constant body force cases were also presented. Jiang and Ding [5] gave the general solution of two-dimensional orthotropic media expressed with two harmonic displacement functions by using the governing equations. Then based on the general solution in the case of distinct eigenvalues, a series of beam problem, including the problem of cantilever beam under uniform loads, cantilever beam with axial load and bending moment at the free end was solved. For beams fixed at both ends subjected to uniform load, Gere and Timoshenko [6] presented the deflection and stress expressions with Euler–Bernoulli beam theory. Ding et al. [7] presented an analytical solution for fixed-end beam subjected to uniform load. A stress function methodology was used to obtain a set of analytical solutions for both ends fixed beams subjected to uniform load.

This work has the aim to investigate the bending rigidity of braid structures consisting of an elastic braid core fixed in one end under uniform distributed load; bending moment, bending stiffness, and deflection of the structure are determined.

General Bending Theory

When a beam is subject to a load, it deforms. The purpose here is to determine the shape of a deformed beam from its geometry and material properties as well as the loads applied to the beam.

Fig. 1 The vertical deflection of the neutral surface from the horizontal at a distance x from the left end is denoted by $y(x)$



As it deforms, a beam develops stresses within it that keep each section of the beam in equilibrium. Both shear and normal stresses are present. In this study, it is assumed that the loads are such that the deformation of the beam is small and that vertical planes through the cross section of the beam remain planes, although they are slightly rotated from their original vertical orientation (see Fig. 1). The normal stresses are such that they exert a bending moment on any section caused by supports and the loads.

The bending moment exerted on the beam by the normal stresses acting there is determined not only by the radius of curvature at that point and the young modulus of the material, but also by the shape of the cross section of the beam through its “area moment” a quantity that not only depends on the area, but also its shape. The equation that examines the relation of bending moment and radius of curvature in a beam is given by,

$$\frac{M}{I} = \frac{E}{R} \quad (1)$$

where M is the bending moment, I is the second moment of area about the centroid, E is the modulus of elasticity, and R is the radius of curvature.

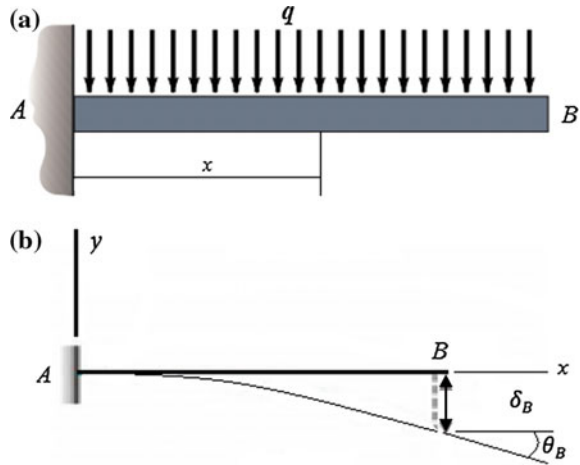
Rearranging Eq. (1) above, we have

$$\frac{1}{R} = \frac{M}{EI} \quad (2)$$

The product EI is called the bending or flexural stiffness of the beam. The curvature is the key to finding the shape, as it is related to the deflection of the beam, $y(x)$, as function of position x along the beam. Figure 1 shows the meaning of the deflection as a function of position along the beam. In the limit of small deflections, when the slope of the deformed beam, dy/dx , is much smaller than 1, the curvature is just the second derivative of the deflection with respect to position.

However, the analysis and design of a beam usually require more precise information on the deflection and the slope of the beam at various points. Of particular importance is the knowledge of the maximum deflection of the beam. We need to obtain a relation between the deflection δ_B ($y(x)$), measured at the given point on the axis of the beam and the distance x of that point from some fixed origin (see Fig. 2a). The relation obtained is the equation of the curve into which the axis of beam is transformed under the given loading as seen in Fig. 2b.

Fig. 2 A uniform cross section cantilever **a** held at one end and loaded uniformly along its length and its exaggerated shape **b** supporting a uniform load



Allen [8] stated that, to be able to solve the deflection of beam δ_B , a reasonable assumptions known as boundary conditions are to be considered. Typically, the assumptions are as listed below;

1. The beam does not deflect where it is supported,
2. If the beam is a cantilever supported at one end by being held in a larger structure, such as a wall, that does not allow the beam to rotate at its point of support,
3. The beam is assumed to be horizontal at the point of support.

Experimental Setup and Deflection Equation

Double braided tubular ropes were produced by producing the tubular braid first and then overbraiding this layer to form a double braided tubular rope. Various double braided tubular ropes were produced having different braiding angle and diameter of the braid structures. After that, a simple test was performed to obtain the braid bending stiffness. Before starting the experiment, we first measured the weight of the sample and also selected the angle, i.e., 41.5° for this case, which was to be used as the deflection limit and help measure the length of the sample that caused the deflection (see Fig. 3). During experiment the sample was fixed on one end and the other end left free to hang allowing it to bend freely under its own weight. Various samples were tested in which case its length and deflection were recorded. Pictures were taken to record the braid length and the braid deflection. The length was read on the ruler scale attached to the experimental setup and deflection was read from the paper with a square unit boxes as shown in Fig. 3b.

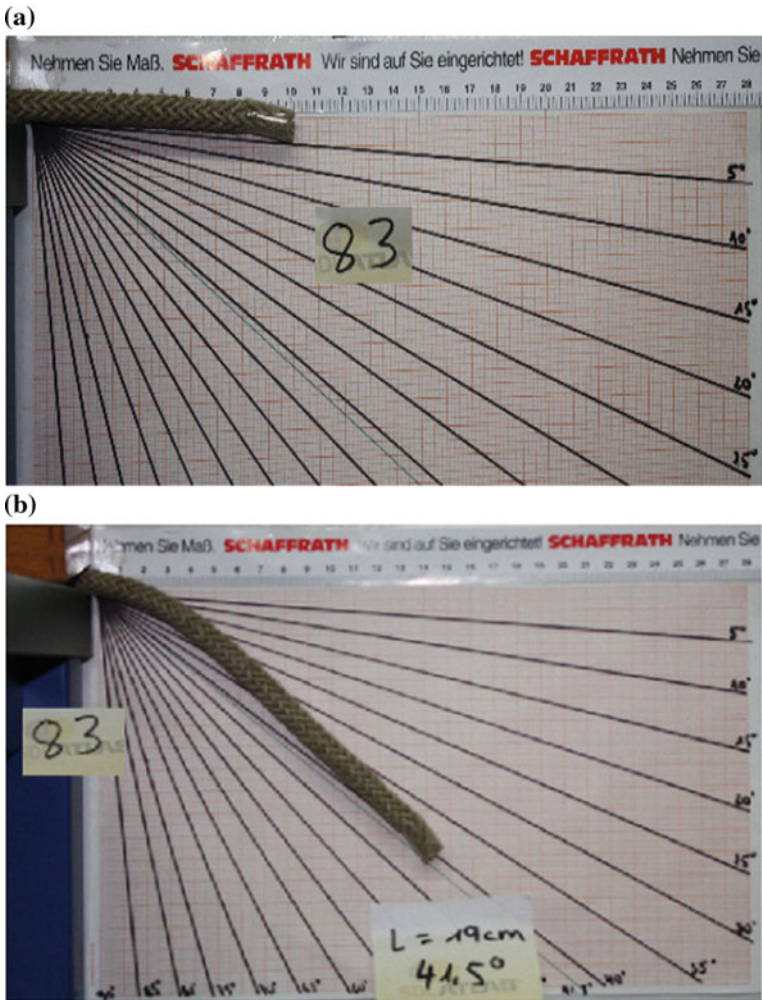


Fig. 3 Braid bending stiffness measurement: **a** before deflection; **b** after deflection

To be able to calculate the bending moment and bending stiffness (flexural stiffness) within the beam, we need to develop equations that will help to determine the deflection curve for cantilever beam AB subjected to uniform load of intensity q also determine the slope θ_B and the deflection δ_B at the free end as shown in Fig. 2a, b above.

Now consider a beam of constant cross section with a uniformly distributed load and supported at one end (Fig. 2), let q be the weight per unit length of the beam. At any distance x from point A , there is a positive shearing force qx where qx is the weight per unit length of the beam up to that section and, since the weight may be taken to act halfway along the length x , there is a bending moment M as shown by Eq. (3) below

$$M = -\frac{qL^2}{2} + qLx - \frac{qx^2}{2} \quad (3)$$

Substituting Eq. (3) into (2) above we have

$$EI \frac{d^2y}{dx^2} = -\frac{qL^2}{2} + qLx - \frac{qx^2}{2} \quad (4)$$

Integrate Eq. (4) with respect to x and we get

$$EI \frac{dy}{dx} = -\frac{qL^2x}{2} + \frac{qLx^2}{2} - \frac{qx^3}{6} + C_1 \quad (5)$$

Integrating again to obtain the deflection curve

$$y(x) = -\frac{qx^2}{24EI} (6L^2 - 4Lx + x^2) + C_2 \quad (6)$$

C_1 and C_2 are constants of integration and must be found from the boundary conditions. These are

$$\begin{aligned} \text{at } x = 0, \quad y &= 0 \text{ (no deflection)} \\ \text{at } x = 0, \quad dy/dx &= 0 \text{ (horizontal)} \end{aligned}$$

Substitute $x = 0$ and $dy/dx = 0$ in Eq. (5) and we get

$$C_1 = 0$$

Thus, Eq. (5) can be written as

$$\frac{dy}{dx} = -\frac{qx}{6EI} (3L^2 - 3Lx + x^2) \quad (7)$$

Substitute this into Eq. (6) with the known solution $y = 0$ and $x = 0$ results in $C_2 = 0$

Putting the results for C_2 into Eq. (6) yields,

$$y(x) = -\frac{qx^2}{24EI} (6L^2 - 4Lx + x^2) \quad (8)$$

For an Euler–Bernoulli beam with large deflection and small strains as shown in Fig. 3, the deflection caused by its weight is as shown on Eq. (8).

The main point of interest is the slope and deflection at the free end where $x = L$. Substituting $x = L$ into (7) and (8) gives the standard equations.

Then,
Slope at free end

$$\theta_{\max} = \theta_B = \frac{dy}{dx} = -\frac{qL^3}{6EI} \quad (9)$$

Deflection at free end

$$\delta_{\max} = -\delta_B = -y(x) = \frac{qL^4}{8EI} \quad (10)$$

Thus, the bending stiffness can be obtained by

$$EI = -\frac{qL^4}{8\delta_B} \quad (11)$$

where δ_B is the tip deflection of the beam.

The measured and calculated deflections, weights per unit length and their corresponding lengths are listed in Table 1 for all different types of braid structure tested. The calculated bending stiffness and bending moment are listed on the same table as well.

Discussion of Results

It is known that braided structures have high resistance to deformation under tensile loading especially for braids with lower braiding angles [9–11]. It is different when subjected to bending effect. Figure 4a, b shows the bending stiffness–braiding angle relationship for each braid structure with different braid cover and having same tubular braid core. A significant difference in bending stiffness is seen at different points of cover-core braiding angle combination. An increase in bending stiffness is observed with an increase in braiding angle of the structures. Few braid structures showed high increase in bending stiffness at the beginning as the braid angle increased, and at higher braiding angles the bending stiffness started to decrease. A peak of bending stiffness was seen at the 43°–19° cover-core braiding angle. Generally it is proved that bending stiffness is improved when a cover-core braid structure has a higher braiding angles despite of the differences that have occurred which might have been caused by the variations in geometric structures. On the other hand, braid structures with high bending stiffness values found to deflect at high length value to reach a slope limit set, i.e., 41.5° (for this case) compared to the low stiffness braid structures.

The bending moment for double braided ropes showed similar behavior as the bending stiffness did, as seen in Fig. 5. In all cases, the bending moment was seen to increase with increase in braiding angle except for one case in Fig. 5c where the

Table 1 Measured and calculated bending parameters for braid structure

Sample no.	Braid outer Dia. (mm)	Core Dia. (mm)	Braid angle cover (deg.)	Braid angle (deg.)	Braid core angle (deg.)	Weight/unit length- q (g/m)	Length for 41.5° (m)	Deflection- δ_B (mm)		Bending Moment ($\times 10^{-3}$ Nm)	Flexural Stiffness- EI ($\times 10^{-3}$ Nm ²)
								Theoretical	Experimental		
1	8.13	-	38	-	-	30.2	0.26	141.2	171	10.01 ± 0.96	1.20 ± 0.19
2	7.37	-	19	-	-	22.5	0.11	57.0	64	1.22 ± 0.28	0.06 ± 0.02
3	7.71	-	21	-	-	23.5	0.12	62.5	73	1.52 ± 0.31	0.08 ± 0.03
5	7.81	-	31	-	-	27.5	0.15	81.5	98	3.03 ± 0.48	0.21 ± 0.05
6.1	10.93	8.13	42	38	-	66.0	0.38	206.4	231	46.75 ± 2.87	8.17 ± 0.91
6.2	11.00	-	35	-	-	64.0	0.29	154.8	179	25.50 ± 2.03	3.34 ± 0.47
6.3	12.90	-	36	-	-	60.0	0.24	129.3	149	16.67 ± 1.58	1.83 ± 0.3
7.1	10.20	7.81	45	31	-	63.0	0.13	69.0	-	4.98 ± 0.86	0.29 ± 0.08
7.2	10.41	-	36	-	-	-	-	-	-	-	-
7.3	11.41	-	33	-	-	55.5	0.17	92.4	106	7.87 ± 1.03	0.62 ± 0.14
8.1	10.47	7.52	42	26	-	64.5	0.32	173.8	184	32.40 ± 2.32	4.77 ± 0.61
8.2	11.02	-	37	-	-	54.0	0.33	179.3	202	28.84 ± 2.06	4.38 ± 0.55
8.3	10.47	-	30	-	-	53.0	0.19	103.2	123	9.38 ± 1.11	0.82 ± 0.17
9.1	9.86	7.71	43	21	-	57.0	0.29	154.8	187	22.71 ± 1.84	2.98 ± 0.42
9.2	9.83	-	34	-	-	52.5	0.35	190.1	214	31.55 ± 2.15	5.08 ± 0.61
9.3	10.64	-	33	-	-	51.0	0.16	86.9	98	6.40 ± 0.90	0.47 ± 0.11
10.1	9.52	7.37	42	19	-	56.5	0.42	229.8	246	49.59 ± 2.83	9.65 ± 1.0
10.2	9.50	-	34	-	-	51.5	0.33	179.3	202	27.51 ± 1.98	4.18 ± 0.53
10.3	10.45	-	28	-	-	51.5	0.18	97.8	114	8.18 ± 1.02	0.68 ± 0.14

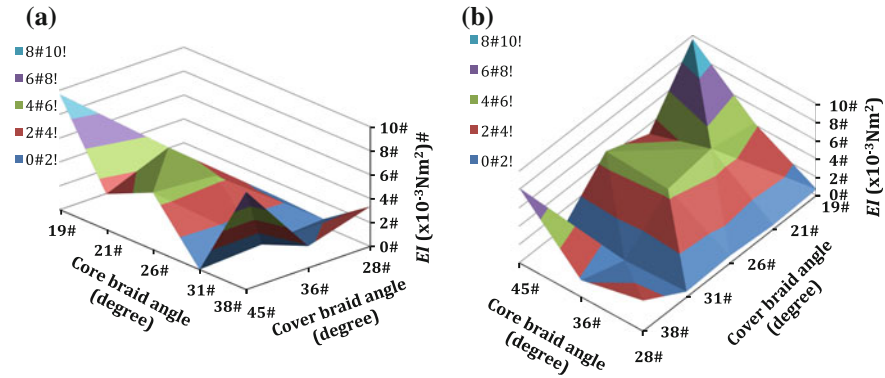


Fig. 4 a, b Different views showing relationship between bending stiffness and braiding angle

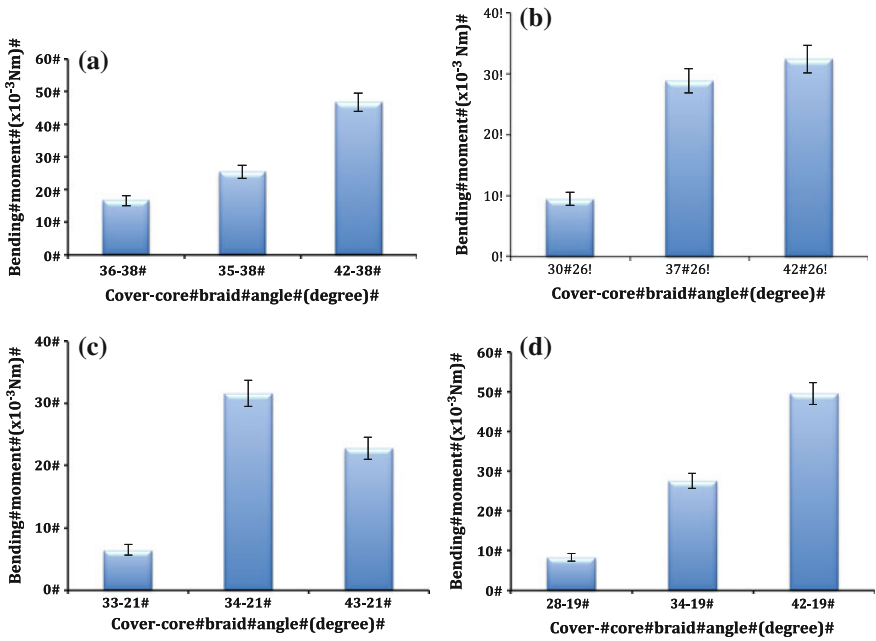


Fig. 5 a–d Relationship between bending moment and braiding angle of double braided tubular ropes having three different braid cover and same core

bending moment seen to decrease at higher braiding angle. The bending moment for single braid tubular ropes in Fig. 6a showed low values compared to double braided tubular ropes, which showed higher values as presented in Fig. 5. This shows that the stiffness of the braided structure can be improved by using more layers as the double braided ropes depending on the application. The braiding angle

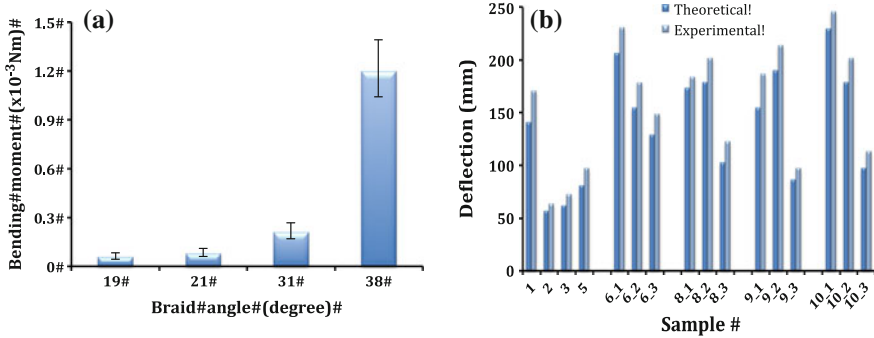


Fig. 6 a Bending moment graphs for single layer braided tubular ropes with different braiding angle. b Comparison of experimental and predicted deflection values of braided structures

combination is very important to consider, as the smaller braiding angle structures were very weak to exhibit their own weight when subjected to bending test. It can be clearly seen that they recorded low bending values due to very low carrying ability of the braid structure in their transverse direction. The 31° braid structure can sustain higher transverse load than 21° braid structure, resulting in higher maximum bending moment. For the braid structure with increased braiding angle, the bending moment induced transverse load become less significant.

Figure 6b shows a comparison between the predicted and experimental deflection of the beams for different tested braid structures. A small difference was observed between the results, experimental results recording higher values of deflection than the predicted values. Nonlinearity of the behavior of braided structures under different loading conditions might have caused these discrepancies since the theoretical model were suitable for linear deformation structures. The deflection percentage increase of the experimental results ranges between 6 % the lowest and 17 % being the highest. However, the predicted and experimental deflections are in good correlation.

Conclusions

Bending test was performed in order to investigate bending properties of double braided tubular ropes. The influence of braiding angle, geometric parameters on the bending properties of braided structure was investigated. Highest bending properties were obtained with double braided tubular ropes compared to single braided tubular ropes. It was observed that, braided structures are very weak under transverse loading, their strength are improved when more structural layers are braided together. It was found that braid structure produced at high braiding angle exhibited the highest bending properties. It was clear that the bending stiffness and bending moment varied with braiding angle for different braid structures. However, the

bending stiffness and bending moment increased with increasing the braiding angle and when the braiding angle varies in a certain range. The differences in the sizes like braid structure diameter did not show any significant effect; however, their structure size difference was minor. The predicted deflection results revealed a good agreement with experimental results, although the experimental results were higher than the predicted deflection results.

References

1. A. Rawal, H. Saraswat, R. Kumar, Tensile response of tubular braids with an elastic core (2012)
2. A. Bicking, W. Oxenham, Variables and methods for aesthetic braid design. *J. Text. Apparel Technol. Manag.* **7**(4), (2012)
3. A. Cagri, Predicting the Elastic Properties of Two Dimensionally Braided Tubular Composite Structures Towards the Design of Braid-Reinforced Polymer Medical Catheters, Ph.D. thesis, University of Alberta, 2010
4. S.P. Timoshenko, J.N. Goodier, *Theory of Elasticity*, 3rd edn. (McGraw Hill, New York, 1970)
5. A.M. Jiang, H.J. Ding, The analytical solutions for orthotropic cantilever beams (I): Subjected to surface forces. *J. Zhejinag Univ. Sci.* **6A**(2), 126–131 (2005)
6. J.M. Gere, S.P. Timoshenko, *Mechanics of Materials* (PWS-KENT Publishing Company, Boston, 1984)
7. H.J. Ding, D.J. Huang, H.M. Wang, Analytical solution for fixed-end beam subjected to uniform load. *J. Zhejinag Univ. Sci.* **6A**(8), 779–783 (2005)
8. T.J. Allen, *Bending of Beams* (Hobart & William Smith Colleges, 2008)
9. A. Rawal, R. Kumar, H. Saraswat, Tensile mechanics of braided sutures. *Text. Res. J.* 2–3 (2012)
10. S.L. Phoenix, Mechanical response of a tubular braided cable with an elastic core. *Text. Res. J.* **48**, 81–91 (1978)
11. R.H. Hopper, J. R, J.W. Grant, P. Popper, Mechanics of a hybrid circular braid with an elastic core. *Text. Res. J.* **65**, 709–722 (1995)

Tensile Properties of Double Braided Flax Fiber Ropes

Lawrence R. Msalilwa, Yordan Kyosev, Amit Rawal
and Uttam Kumar

Abstract In this study, the mechanical behavior of double braided tubular ropes under tensile loads is studied experimentally and analytically. The outer braid is referred as the braid cover and the inner braid is considered as an elastic tubular braid core. A predictive model of the mechanical response of the braids based on the constituent monofilament (yarn) properties and braid geometry based on known research works was used. The model has accounted for the changes in the braid geometry, including braid angle and diameter. Both braid angle and diameter are found to be critical design parameters. Image analysis is employed to experimentally characterize the structural parameters of the braids and their deformation. The structures are tested in tension and their stress–strain response is recorded. The experimental results have been compared to the theoretical stress–strain curves of braid cover-core structures and the results have been observed to agree well between them, though the theoretical model underestimates the Young’s modulus of the braid cover-core structure.

Keywords Double braiding · Modeling · Tensile strength · Braid geometry · Modulus

L.R. Msalilwa · Y. Kyosev (✉)

Research Institute for Textile and Clothing (FTB), Hochschule Niederrhein—University of Applied Sciences, Mönchengladbach, Germany
e-mail: Yordan.kyosev@hs-niederrhein.de

L.R. Msalilwa

Department of Mechanical and Industrial Engineering, University of Dar es Salaam, Dar es Salaam, Tanzania

A. Rawal · U. Kumar

Department of Textile Technology, IIT Delhi, New Delhi, India

© Springer International Publishing Switzerland 2016

Y. Kyosev (ed.), *Recent Developments in Braiding and Narrow Weaving*,

DOI 10.1007/978-3-319-29932-7_6

Introduction

Braiding is a material preform manufacturing technique where a braiding machine deposits continuous, intertwined, fiber tows to create desired reinforcing braid architecture [1]. Due to its ease, versatility, structural integrity, durability and flexibility, the braiding process has proven to be essential in the development of numerous applications; from the more simple processes like apparel and furniture trimmings, shoes laces, fishing line, etc., to the more complex like medical devices, composite materials, parachute cords, climbing ropes. Complex and performance-dependent applications benefit from braids' impact resistance and strength properties; these properties are a result of the braid's bias entwined structure that features a seamless unit from beginning to end. This quality is unique to the braiding process as it is the only textile that is structured in this manner.

Circular braiding has been traditionally used for making tubular structures but there is an ever-increasing interest to use these structures for various composite applications [2]. A tubular braid without any core undergoes large lateral contraction when extended by a tensile force along its axis, but when elastic materials are inserted in the hollow braid they can potentially act as reinforcement in energy absorbing composite. These elastic materials do not prevent, only resist the lateral contraction to some extent. Moreover, the use of braided filaments over elastic core can potentially reduce the density and cost of composite [2].

Several researchers have formed the relationship between the geometrical and tensile properties of tubular braided materials however; the understanding of tensile mechanics of braided structures is relatively scarce, although braiding is an old technique [3, 4]. Few literatures have been discussing the mechanical behavior of the tubular braids with an elastic core of uniform cross section under tensile loading [2, 3]. In this study, mechanical behavior of double braided tubular ropes, the inner core being an elastic tubular braid has been investigated.

The mechanics of circular braids with an elastic core were studied by Phoenix [3] and Hopper et al. [5]. Both works focused on the impact of the core on the transition between the unjammed and jammed states and on the overall behavior of the braid. The level of flexibility of the core on the mechanical response and strain to failure of the braid–core system was investigated. The influences of yarn crimp, helix angle and core nonlinearity, were considered in the analyses and highlighted as important elements in the braid mechanical response. Rawal et al. [2] investigated the tensile response of the tubular braid having elastic core. Rawal et al. developed the model for tensile behavior of tubular braids consisting of an elastic core based on defined braid geometry, core properties, and tensile properties of helically undulated strands of filaments and considered monofilament type as the constituent filaments, but the proposed model has been extended for strands consisting of low twist multifilament yarns with non-hybrid weave. Subsequently, the tensile model of tubular braids consisting of an elastic core has been validated with the experimental work of braids having twill weave (also known as regular braid) [2]. The elastic deformation of braided tubular structures was analyzed by Yükksekaya [6] to give an optimum

radial force for medical applications. The relations among braid angle, helical length, braid diameter, and elastic radial forces were developed. Rawal et al. [4] studied tubular braids and presented 3D coordinates of the braiding yarn paths over different mandrels with different cross sections, but they have ignored the yarn crimp (the sinusoidal path in the radial direction). Jung et al. [7] developed a geometric model so that precise material properties of the 3D circular braided composite can be estimated. They described the yarn paths as curved lines using third-order spline, which are close to real geometric formation of the 3D braided composite. In [9] is developed mechanical model of hybrid braids. The comparison between the experimental and predicted values shows good accuracy of the model, with the remark, that the strength of the fabrics with high braiding angle is underestimated.

This work aim at investigating the tensile properties of braided structures having an elastic circular braided core subjected to tensile load using the proposed simple model generated after studying the available geometrical models for tubular braids with an elastic core, and present the experimental and numerical study results. For the model used, the constituent filaments considered are monofilament types but the proposed tensile model of braid cover-core system has also been extended for low twist multifilament yarns with non-hybrid weave [2]. Monofilament braid structures consist of a single strand of filament, whereas multifilament braid structures are made up of several filaments or strands that are generally twisted or braided together. Multifilament braided structure offer higher tensile strength, pliability and flexibility in comparison to monofilament structures.

Experiment

Production of Braided Preforms

Double braided tubular ropes were produced by producing the tubular braid first and then over braiding this layer to form a double braided tubular rope. The production was done on a tubular braiding machine with 16 carriers. The braiding machine consisting of two sets of yarn carriers rotating on a circular track in which half of the carriers rotate in clockwise direction and the remaining half of the set rotates in counterclockwise direction. Various double braided tubular ropes, were produced, by varying the braiding machine fabric delivery speed (rate of take-up) and, therefore, changing the braiding angle of the structure as shown on Table 1.

Table 1 Braiding angle variations with take-up speed rate

Sample no.	Braiding angle (deg.)	Take-up speed (m/min.)
1	38	1.62
2	19	4.85
3	21	4.71
4	26	3.48
5	31	2.62

The outer braid was braided with 16 filaments/braid and the inner tubular braid having 8 filaments/braid, and the inner tubular braid being a core of the braided structure. Twisted flax yarns with fineness of 1372 tex, maximum tensile load 230 N and strain at breaking point of 4.8 % [8] was used to produce the structure, and a regular braid of two by two (2/2 repeat) were produced. Five single layer tubular ropes were produced and then overbraided to form double braided tubular ropes. Each single layer tubular rope was overbraided in three different braid structures (covers), i.e., 6-1, 6-2, 6-3, etc., having different cover parameters such as the diameter and the braiding angle to easily determine their behavior when subjected to tensile testing conditions. Before testing, ropes were measured the original parameters such as the diameters, length, weight, etc., to help during further analysis of the structures.

Tensile Test Performance

A tensile test experiment was carried out on a Zwick tensile test machine. The experiment was performed in displacement control mode at a stroke rate (i.e., cross-head displacement rate) of 500 mm/min for the tensile test. Since the structures were not prestretched before the test, a preload of 5N was actually applied to the tested braid structure. The amount of this displacement was defined as an interval from the beginning of the test until the point at which load increase is observed. Load–displacement curve was recorded during the test. During loading, all the output data (strain, displacement of cross-head, and load) were collected by an acquisition system and transferred to the PC. The data were then used to calculate the tensile properties parameters.

Model Validation

The experimental results have been validated with the previously published work of tubular braids having elastic core [2–5]. A typical stress–strain relationship is given below.

$$\sigma = \frac{4}{N\pi d^2(1+C) + \pi D^2 \cos \alpha} \left\{ N(\cos^2 \alpha - \nu \sin^2 \alpha)f(\varepsilon_f) + \frac{\pi D^2 E_c \varepsilon \cos \alpha}{4} \right\} \quad (1)$$

where α is the braid angle, ε_f is the filament strain, d is the filament diameter, σ is the true tensile stress, N is the number of constituent filaments, ν is the Poisson's ratio, F_f is the load experienced by the filament, D is the braid diameter, E_c is the core modulus and C is the braid crimp.

It must be noted that filament strain (ε_f) and braid angle (α) has been updated based on the changes in axial strain (ε) using following equations.

$$\varepsilon_f = \left[(1 + \varepsilon)^2 \cos^2 \alpha_i + \frac{\sin^2 \alpha_i}{(1 + \varepsilon)} \right]^{1/2} - 1 \quad \text{and} \quad \cos \alpha = \frac{\cos \alpha_i (1 + \varepsilon)}{(1 + \varepsilon_f)} \quad (2)$$

Similarly, the core diameter has been updated at defined level of axial strain using following equation.

$$D^2 = \frac{D_0^2}{(1 + \varepsilon)} \quad (3)$$

Hence, the *true* tensile stress (σ) has been updated accordingly at defined level of axial strain. The reader is referred to reference [2] for detailed derivations and geometrical considerations.

Results and Discussion

This part is about the study of double braided tubular ropes subjected to axial tensile loading, where theoretical results are determined and compared with experimental results. In the theoretical part, the model to estimate the true tensile stress of tubular braid having an elastic tubular braid core was generated as shown in Eq. (1). The braid cover-core system was assumed to consist of an elastic core in order to simplify the formulation of the model of tensile response of tubular braids; but during calculations the core was considered to be tubular braid for the effective results.

From the results presented in Figs. 1a–d shows that, the braiding angle has a considerable role in controlling the tensile properties of double braided tubular rope. Observing the theoretical model, the increase in braiding angle responded to the decrease of the tensile strength based on the Eq. (1). For the same values of tensile strength, the extensibility of the braid cover-core system appeared to increase with increasing the braid angle. The braid cover-core system with low braid angles found to have high strain values in most of the braid structures analyzed at maximum tensile load. However, the result recorded from the braid structures with low braid angle was high with slight different between them. Generally, braiding angle has seen to have more influence on the mechanical behavior of double braided tubular ropes, although other structure parameters such as diameter also have contribution to alter the tensile properties of the braided structures. The tensile properties of the tested double braided tubular ropes are given in Tables 2.

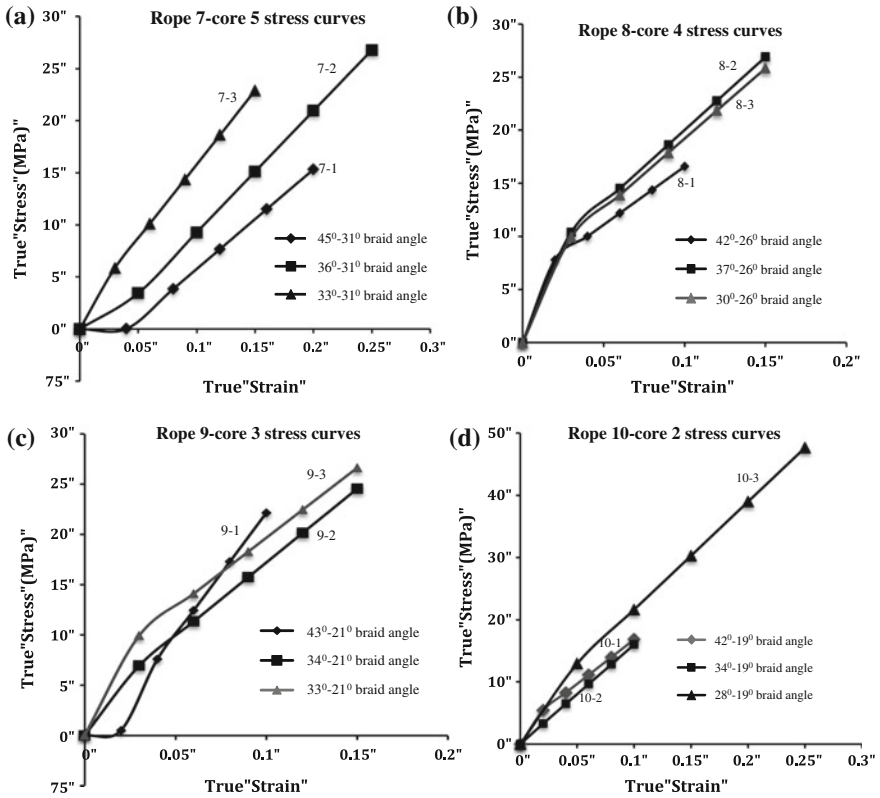


Fig. 1 a–d Tensile stress comparisons for different tubular braid consisting same tubular braid core

The experimental and theoretical result curves for true stress–strain comparison are shown in Figs. 2a–d. Observed that the theoretical and experimental stress–strain curves are in good agreement. However, an experimental stress–strain curve obtained for a braid cover-core system deviates significantly from theoretical stress–strain curves specifically at low strain values and seems to come closer and crosses at high values of strains. If we compare the theoretical curves which looks linear at all points, the experimental curves observed to be nonlinear where the values appears to vary at different strain values. Nonlinearity of the experimental tensile properties causes deviation from predicted tensile properties; these deviations may be due to high elongation behaved by experimental stress–strain curve of the braid cover-core system at the beginning. This difference is also believed to be due to geometric effect, clarity of the theoretical model developed to predict the values and, random variation can be expected in the loads of the individual strands.

Table 2 The structural parameters, experimental and predicted tensile strength and elastic modulus results for double braided tubular ropes

Sample no.	Braid outer dia. (mm)	Core dia. (mm)	Braid angle cover (deg.)	Braid angle core (deg.)	Stress- σ (MPa)		Elastic modulus- E (MPa)		Theoretical		Experimental	
					Theoretical	Experimental	Theoretical	Experimental	Theoretical	Experimental		
6-1	10.93	8.13	42	38	26.7	28.2	58.6	129.8				
6-2	11.00		35		23.4	12.2	79.1	114.0				
6-3	12.90		36		23.5	26.9	84.7	260.0				
7-1	10.20	7.81	45	31	15.3	40.4	95.6	228.1				
7-2	10.41		36		26.8	36.9	116.8	479.8				
7-3	11.41		33		22.9	19.4	141.9	72.0				
8-1	10.47	7.52	42	26	16.6	34.9	109.7	247.5				
8-2	11.02		37		26.9	35.9	137.7	318.9				
8-3	10.47		30		25.8	45.4	132.7	454.0				
9-1	9.86	7.71	43	21	22.2	37.6	243.1	428.2				
9-2	9.83		34		24.5	45.9	146.7	305.7				
9-3	10.64		33		26.6	41.6	139.0	243.7				
10-1	9.52	7.37	42	19	16.8	19.5	142.4	146.3				
10-2	9.50		34		16.0	47.5	159.0	332.9				
10-3	10.45		28		47.7	50.0	173.6	450.7				

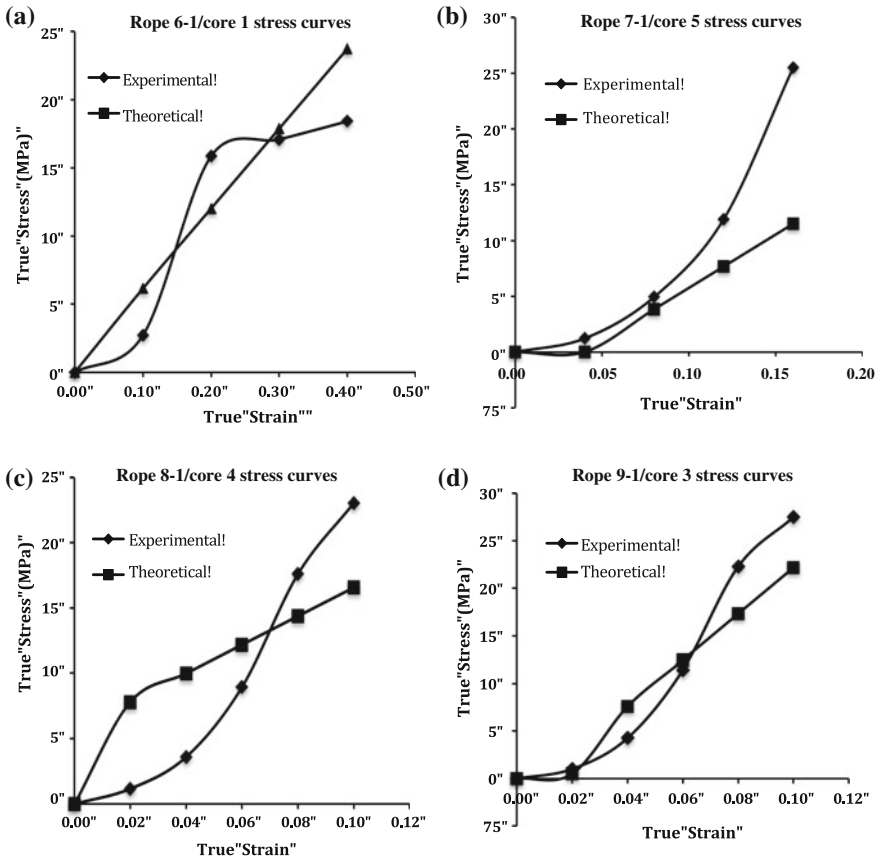


Fig. 2 a–d Comparison between experimental and theoretical true lateral contraction—true axial strain

Conclusions

The geometric properties for double braided tubular ropes have been plotted as a function of braiding angle and true strain, from the experimental and theoretical results of this study on the tensile loading of braids. Both experimental and theoretical results observed that increasing the braid angle enhances the extensibility of braid cover-core system and changes the tensile strength. The analytical models gave consistent and accurate predictions for the tensile strength and Young’s moduli of several of the braid structures. However, the agreement of predicted and experiment elastic modulus values, was, not as good except for some braid structures the results were in good agreement. The reasons for this discrepancy are not fully investigated; there is a need for improved methods of analysis and wider range of test data with regard to braid angles, and other geometric parameters.

References

1. A. Cagri, Predicting the elastic properties of two dimensionally braided tubular composite structures towards the design of braid-reinforced polymer medical catheters, PhD thesis, University of Alberta, 2010
2. A. Rawal, H. Saraswat, R. Kumar, Tensile response of tubular braids with an elastic core. *Compos. Part A: Appl. Sci. Manuf.* **47**, 150–155 (2013)
3. S.L. Phoenix, Mechanical response of a tubular braided cable with an elastic core. *Text. Res. J.* **48**, 81–91 (1978)
4. A. Rawal, R. Kumar, H. Saraswat, Tensile mechanics of braided sutures. *Text. Res. J.* 2–3 (2012)
5. R.H. Hopper, J.W. Grant, P. Popper, Mechanics of a hybrid circular braid with an elastic core. *Text. Res J.* **65**, 709–722 (1995)
6. M.E. Yükksekaya, Analysis of elastic deformation of braided tubular structures for medical applications. *J. Eng. Sci.* **7**(2), 277–285 (2001)
7. K. Jung, S. J. Kim, T.J. Kang, K. Chung, J.R. Youn, Optimum modeling of 3D circular braided composites, ICCM-14, San Diego, California 14–18 July 2003
8. M. Lawrence, K. Yordan, Prediction of the mechanical properties of braided flax/epoxy 3D shape composites. Research Institute for Textile and Clothing, 2012
9. K. Hristov, E.A. Carroll, M. Dunn, C. Pastore, Y. Gawayed, Mechanical behavior of circular hybrid braids under tensile loads. *Text. Res. J.* **74**, 20–26 (2004)

The Numerical Prediction of the Tensile Behaviour of Multilayer Woven Tapes Made by Multifilament Yarns

Yordan Kyosev, Stepan Lomov and Katalin Küster

Introduction

Woven belts and tapes are used in wide area of technical applications and as reinforcement for composites. Contrary to the art design of the woven fabrics, where the colour and pattern appearance is more important than the mechanical parameters, in the technical products the strength, stiffness, compressibility and other mechanical properties have the importance.

At the current time the authors found more than 20 CAD programs for the design of woven fabrics [6], from which only few are able to visualize the woven fabrics in 3D object as photorealistic, but in simplified way. The industrial weavers in the most cases use the CAD to design the fabrics for the fashion way, this is marked larger and this explains why there are more solutions.

In the contrary, for technical calculations the only software which calculates the 3D special positions of the yarns in the woven fabric, based on their mechanical parameters and fast analytical algorithms seems to be WiseTex [7, 9]. More elaborate methods involve calculations of the yarns mechanical interactions using finite element (FE) representation of a textile [1, 3, 13], and are mostly applied to calculation of the fabric deformations during draping rather than the initial yarns configuration. Recently, these FE methods are applied also to calculate initial yarn configuration as well [2, 11].

Y. Kyosev (✉) · K. Küster

Faculty of Textile and Clothing Technology, Hochschule Niederrhein—University of Applied Sciences, Mönchengladbach, Germany
e-mail: Yordan.kyosev@hs-niederrhein.de

S. Lomov

Department of Materials Engineering, Katholieke Universiteit Leuven, Louvain, Belgium

S. Lomov

Centre of Design, Manufacturing and Materials (CDMM) of Skoltech, Moscow, Russia

© Springer International Publishing Switzerland 2016

Y. Kyosev (ed.), *Recent Developments in Braiding and Narrow Weaving*,

DOI 10.1007/978-3-319-29932-7_7

This work presents an example of the use of WiseTex for numerical investigation of dense woven narrow tapes. For simulation of composites, the researcher normally takes one product, analyses it using micro-CT and tries to reconstruct its geometry in WiseTex with the goal to export the geometry to some FEM software and work with it. The approach of this work is different, because the aim of it is more applied. Here it was started with the yarn data, woven pattern and density with the aim to receive information about the properties and the behaviour of the tape without its production.

Modelling Steps

Woven Fabric Topology (Weave)

The correct definition of the weave type is one of the basic information required for the modelling of the woven tapes. For single layer structures the marking where the warp yarns are over the weft yarns is sufficient. For double layer structures it is common to use the diagonal line for marking the warp position in the middle layers, but this method has limitation—if extended for structures with more than two weft layers, it will be connected with the use of different symbols (Fig. 1).

Using the numbers or clicking the corresponding positions in the graphical editor of WiseTex (Fig. 2) allows definition of the position of each warp yarn at each

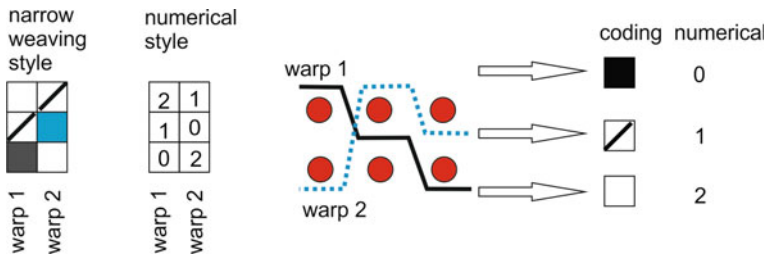


Fig. 1 Coding styles—using the numbering of the warp yarn position and its equivalent, commonly used in the narrow weaving in the case of two-layer structures for machines with low-middle-high positions of the frames (in German: T-M-H “Tief-Mitte-Hoch” machines)

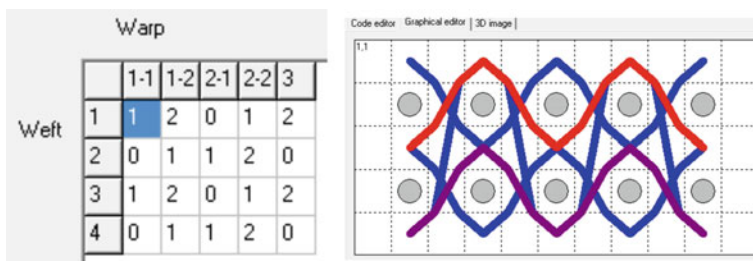


Fig. 2 Coding of two-layer sample used in this example and its graphical presentation

crossing point with the weft yarns. It has to be stressed that for the modelling purpose the topology of the structure has to be defined, independent of the way of weaving this structure—if it is produced with one single shuttle or weft insertion needle or if it is produced with two shuttles/weaving needles simultaneously.

Fabric Parameters

The safety belts and other technical tapes are usually woven as dense woven structures. For these structures the yarn cross section is not constant. As visible on Fig. 3, multifament yarns spread their filaments in the areas, where no side contact with other yarns is disturbing and narrow these in a dense bundle in the positions, where no place is available.

Some programs, like TexGen allows definition of yarns with different cross section at different points. TexGen is in its public available version pure geometrical modeller do not consider at this point the mechanical properties of the yarns. Additionally, definition of yarns with different areas of their cross sections in different places, causes problems in the theory and algorithms for computations, connected with the packing density of the fibres in these places.

WiseTex tries to calculate the change of the cross sections under forces of the warp and weft interaction. However, this calculation asks for detailed compressibility data of the yarns, especially of the yarn flattening under compression. In the

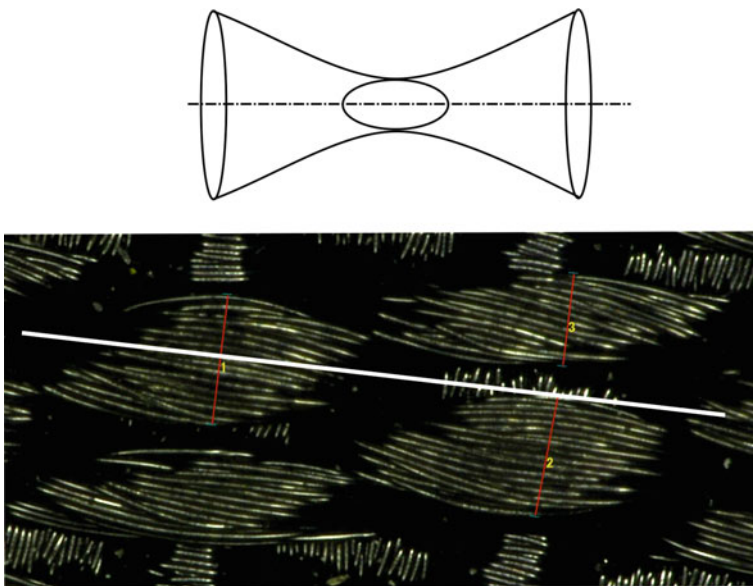


Fig. 3 The yarn cross section in dense woven fabrics (tapes, belts) of multifilament yarns is not constant and changes depending on the position of the yarns and its neighbours

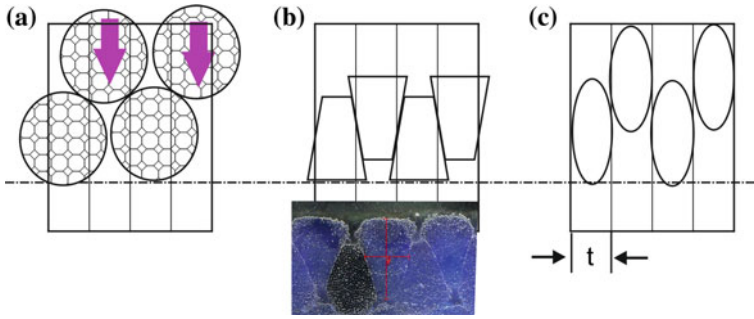


Fig. 4 Yarn spacing as basic for the cross-section definition **a** original state at the moment of weaving, **b** idealized (*up*) and real (*down*) final state **c** option for modelling with narrow yarns

absence of these flattening data, in the model with some *equivalent* cross section will be worked, which preserves as more properties as possible of the original one and allows to perform the calculations with the current model.

Figure 4 describes the basic idea of the selection of the yarn spacing in warp direction. Case a) is the idealized representation of the yarns just before the weaving process (interlacement and beat up force) for the current step was performed. The yarns here are presented with larger cross section, they have lower packing density. Observing the images of the cross sections is visible, that after weaving, the yarns in this case take trapeze-like form (Fig. 4b). In order to preserve the number of the yarns per unit length and allow the crimp between the yarns, the cross section for the modelling has to be selected based on the yarn density

$$d \leq t = \frac{10}{N}$$

so that the diameter *d* is not larger than the space *t* for the *N* yarns in 10 mm.

The generated in this way geometry for one two-layer tape is presented in Fig. 5. In relaxed state the fabric has minimal potential energy. During the computation of

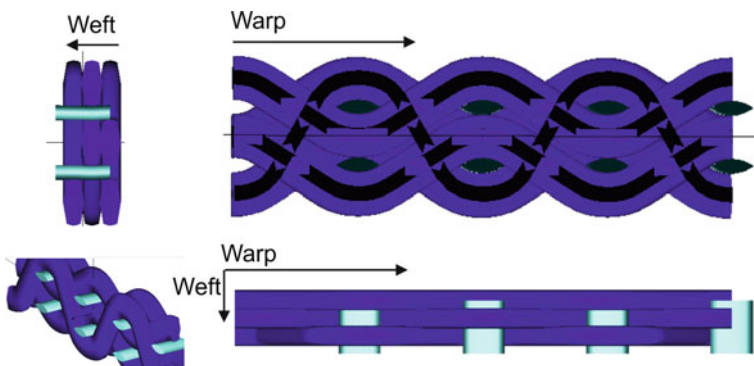


Fig. 5 Geometry calculated by WiseTex

this state, the potential energy in each yarn is computed, which covers the energy of tension, bending and compression:

$$W_{\text{yarn}} = W_{\text{tension}} + W_{\text{bending}} + W_{\text{compression}}$$

WiseTex calculates all these energies and solve minimizations task giving the relaxed geometry, if such one is found. If this task is solved for set of given elongations of the warp yarns, the complete force-elongation curve can be simulated. This simulation shows good accuracy, if the input data in the model is prepared correct and enough [4, 8, 10].

Actually, getting the correct yarn properties is still connected with uncommon measurements for the industrial users. The following examples demonstrate the influence of some single parameters over the simulation.

Yarn Parameters and Force—Elongation Curve

As mentioned above, the geometrical parameters of the equivalent yarn should be specified based on the density of the yarns. The tension parameters can be directly entered from a force-elongation curve of standard tensile test as presented in Fig. 6.

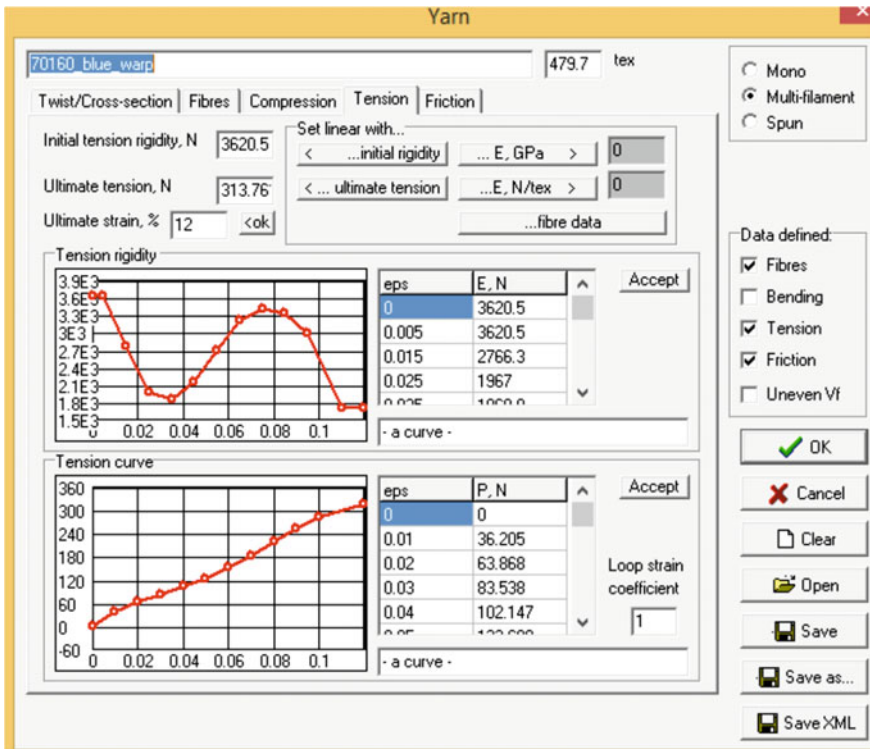


Fig. 6 Yarn data—ultimate strain 12 %, ultimate tension 313 N

The ultimate values of the force and elongation can be taken from the curve or entered manually, if instead of force-elongation curve the elasticity modulus is provided.

Yarn Lateral Compression

The lateral compression behaviour of the yarns influences the properties of the fabric, but it is not common property for testing in the textile testing laboratories. Assume the yarn has initial cross section with thickness d_{10} and width d_{20} (Fig. 7). After applying some force Q , measured here in Newton per millimeter yarn length, the cross section deforms to such lower thickness d_1 and in some cases slightly larger width d_2 . This test can be performed on a standard equipment for testing fabric thickness as described in EN ISO 5084:1996 for fabrics, but by placing the yarns in the middle of the testing circle, for instance using guiding openings plastic sheets, mounted on both sides of the testing circle. More elaborate methods for the yarn compression test are described in [5, 12].

Let us consider that the standard circle with diameter $D = 50.5 \pm 0.2$ mm is used with corresponding surface of $2000 \text{ mm}^2 = 20 \text{ cm}^2 = 0.0020 \text{ m}^2$. The fabrics thickness and compression test according to EN ISO 5074:1996 is preformed with pressures 0.1 kPa and after that 1 kPa. The forces acting over the pressing plate B (Fig. 8) for these pressures will be $100 \text{ Pa} \times 0.0020 \text{ m}^2 = 0.2$ and 2 N, respectively. So over one yarn piece, which is placed as a diagonal under the pressing circle (Fig. 8) with length $L = D = 50$ mm, the forces for these two standard loads will be

Fig. 7 Change of the yarn cross-section dimensions during lateral compression

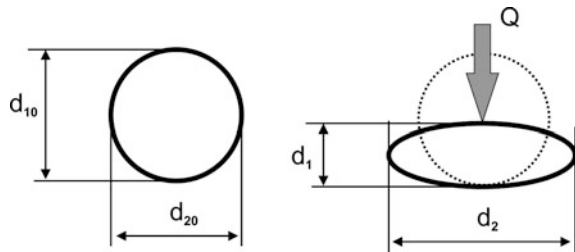
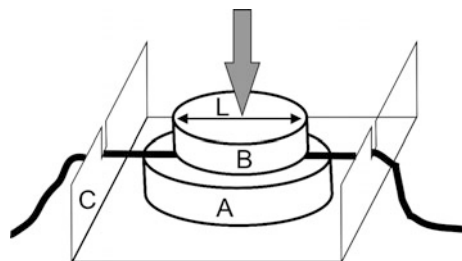


Fig. 8 Modified equipment for lateral compression test



0.2 N/50 mm = 0.004 N/mm and
 2 N/50 mm = 0.04 N/mm, respectively.

Using some different weights from the standard used allows performing measurements of the cross-section change at several points and in this way getting more accurate curve about the compression behaviour. The change of the width of the yarn during this deformation can be taken using optical evaluation, but it requires special equipment.

Figure 9 presents the values of the relations between the current diameter and the initial one for the used warp yarn in this example.

Yarn Bending Rigidity

The simplest method for measuring the yarn bending rigidity is the so-called cantilever method (Fig. 10). In this case the left end of the yarn is fixed (pressed horizontally) and moving the pressing body the free hanging length is increased

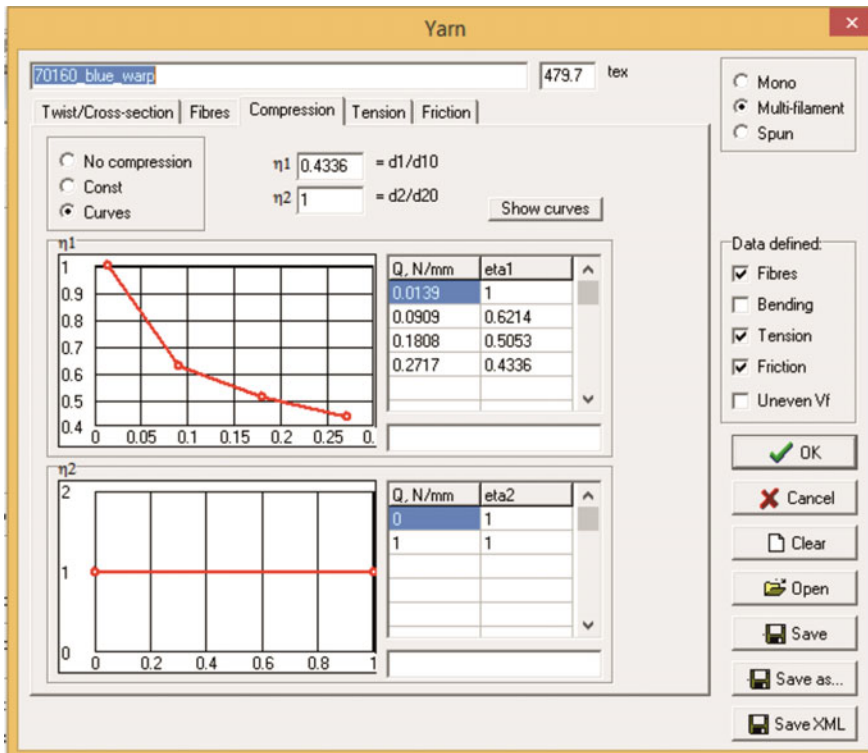
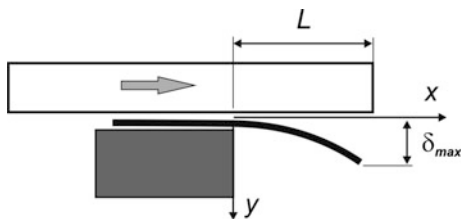


Fig. 9 Compression curves for the yarn

Fig. 10 Cantilever beam method for measuring the bending rigidity of the yarns



until some deflection δ_{\max} is reached. If this deflection is small in comparison to the free length, it can be calculated based on the linear beam theory

$$\delta_{\max} = \frac{w \cdot L^4}{8 \cdot EI}$$

From here

$$EI = \frac{w \cdot L^4}{8 \cdot \delta_{\max}}$$

Assuming here L and δ_{\max} are in mm, w is the linear density in N/mm, then the bending rigidity EI will be in Nmm^2 . The linear density is actually usually given in $\text{tex} = \text{g/km}$, so conversion from tex to N/mm here will be required as follows:

$$w \left[\frac{\text{N}}{\text{mm}} \right] \approx \left[\frac{100 \text{ g}}{\text{mm}} \right] = \left[\frac{0.1 \text{ g}}{\text{m}} \right] = \left[\frac{0.0001 \text{ g}}{\text{km}} \right] = \text{tex} \cdot 0.0001$$

So, the equation will then be

$$EI = \frac{\text{tex} \cdot L^4}{8 \cdot \delta_{\max}} \cdot 0.0001$$

Of course the measurement using this method is connected with several sources for errors—if the yarn is twisted, it tries to untwist at the end, moves itself to one or the other side and this twist changes the rigidity as well. For multifilament yarns without twist, the orientation of the single filaments in the fixation point changes the geometrical moment of inertia of the “beam” and changes the rigidity as well. Still, using some approximated values for the rigidity of the yarns is significantly better ignoring the bending rigidity of the yarns.

Numerical Investigation

For the two-layer woven belt from multifilament PES yarn, presented as well on Figs. 2 and 5, the in-plane deformation was simulated. Setting free edges in the weft (F_y) direction means that there is no force on the selvages, so the program looks for

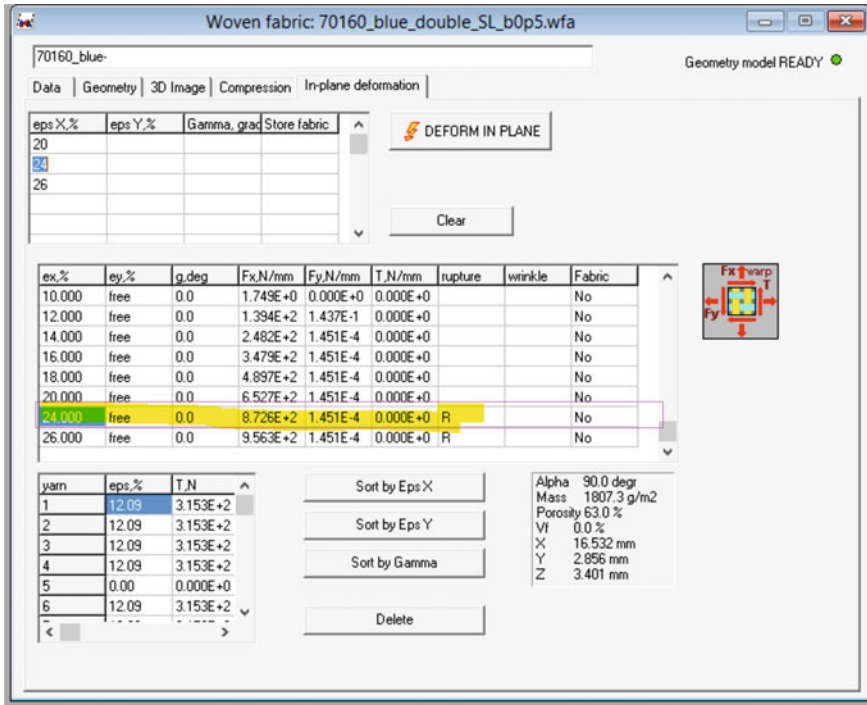


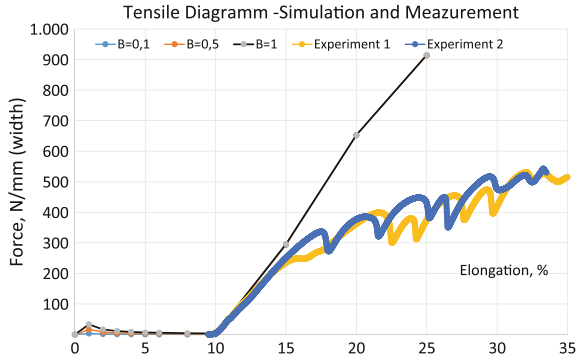
Fig. 11 Yarn load at rupture

fabric geometry at all given elongations from 1 to 26 % and checks the loading of the single yarns during this simulation.

As visible in Fig. 11, at 24 % fabric elongation some of the yarns reach their ultimate elongation, so rupture is expected. As the software does not “kill” the broken yarn during the simulation, the force is shown to increase after reaching this value, for simplicity of the calculation algorithm.

Figure 12 summarizes the simulated force-elongation diagrams of this structure for different bending stiffnesses of the yarns starting from 0.01 Nmm² up to 1 Nmm². Two effects can be recognized in the figure—first one is that increasing the bending stiffness leads to slight increase of the force at the same elongation. The second effect is in the range between 0 and 3 % elongation—in this area the yarns with lower bending stiffness cause the first increase of the force and then it goes back down. One of the hypotheses for this behaviour is that for these bending values the reaction of the deformation for the yarns is more significant than the tensile force. After reaching some level of the force the yarns adjust their positions, so that no more motion is expected and the material starts loading. Another hypothesis for the initial difference is that in this region the calculation is numerically not stable, because of the flexibility of the structure—there are different states of the fabrics possible, which have nearly same value of the potential energy.

Fig. 12 Simulated and measured force-elongation curves. The deviation between both starts when the yarns in the real fabrics become broken. The initial elongation point of the measurement curves is shifted to elongation of 9.5 % where the deformation of the material starts

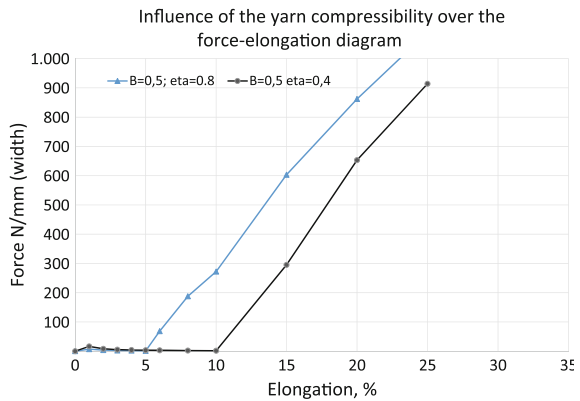


In any case this initial region of deformation is connected with changes of the position of the yarn axis which cannot be modelled in the same way as in the real tape, because of the differences between the yarn cross section form in the real and the modelled yarn and thus the differences in their positions.

The simulated tapes show rupture at 24 % elongation, where the demonstrated two experimental curves show first ruptures earlier—at about 15 and 20 %, but the deviation of the elongation at the first broken yarn in the remaining measurements (not shown in the figure for clarity) is large and can be caused by different factors like yarn irregularity, not exact placement in the testing clamp, etc., which are not included in the simulation.

Figure 13 demonstrates the influence of the yarn compression—where the fabric is simulated once with the same data as in Fig. 12 (yarn reaches 40 % of its initial thickness after load) and once for more incompressible yarns (yarn reaches 80 % of the initial thickness). The difference in the compressibility of the yarns causes 5 % additional initial elongation in the current case.

Fig. 13 Force-elongation diagram—influence of the yarn compressibility over the starting point of material loading



Conclusions

This work presents investigation about the numerical simulation of double-layer woven tape made of multifilament polyester yarns in dense weave, common for technical tapes. The numerical experiments demonstrate that the compression of the yarns has significant influence on the elongation values of the fabrics during loading and it causes shifting of the equilibrium points. This is probably the reason why the simulated forces values are overestimated compared to the measured force-elongation curve. Bending rigidity of the yarns has influence as well, but is mainly expressed by slightly increasing the force at the given elongation.

In any of the variants, the simulated behaviour is near the real one which proves that WiseTex is able to provide approximation of the properties of the fabrics even with roughly estimated yarn data.

For the applications and users, where exact prediction of the tensile behaviour is required, it is actually required the exact geometry of the fabric to be entered, the exact mechanical properties of the yarns to be measured and probably some extension of the software in order to deal with the different cross-section areas of the yarns. One way for current extension today is the use of the FEM export functionality of WiseTex, and simulation of the behaviour with external software. This way provides significantly more flexibility in the settings and parameters of the simulation but also requires significantly higher qualification of the person, who has to do it, which is in most of today's narrow weaving companies not a feasible solution.

Acknowledgements Stepan Lomov is a Toray Professor of a Toray Chair for Composite Materials in KU Leuven. His work reported here was partially funded by Centre of Design, Manufacturing and Materials (CDMM) of Skoltech (Russia) under agreement MRA-335 with KU Leuven.

References

1. P. Boisse, A. Gasser, B. Hagege, J. Billoet, Analysis of the mechanical behavior of woven fibrous material using virtual tests at the unit cell level. *J. Mater. Sci.* **40**(22), 5955–5962 (2005). doi:[10.1007/s10853-005-5069-7](https://doi.org/10.1007/s10853-005-5069-7)
2. G. Grail, M. Hirsekorn, A. Wendling, G. Hivet, R. Hambli, Consistent finite element mesh generation for meso-scale modeling of textile composites with preformed and compacted reinforcements. *Compos. A Appl. Sci. Manuf.* **55**, 143–151 (2013). doi:[10.1016/j.compositesa.2013.09.001](https://doi.org/10.1016/j.compositesa.2013.09.001)
3. N. Hamila, P. Boisse, Simulations of textile composite reinforcement draping using a new semi-discrete three node finite element. *Compos. B Eng.* **39**(6), 999–1010 (2008). doi:[10.1016/j.compositesb.2007.11.008](https://doi.org/10.1016/j.compositesb.2007.11.008)
4. F. Heuwinkel, *Analyse Mechanischer Eigenschaften von Bandgeweben* (Hochschule Niederrhein, 2011)

5. D.S. Ivanov, S.V. Lomov, Compaction behaviour of dense sheared woven preforms: Experimental observations and analytical predictions. *Compos. A Appl. Sci. Manuf.* **64**, 167–176 (2014). doi:[10.1016/j.compositesa.2014.05.002](https://doi.org/10.1016/j.compositesa.2014.05.002)
6. Y.K. Kyosev, in *Simulation of Wound Packages, Woven, Braided and Knitted Structures*. ed. by D. Veit (Simulation in Textile Technology, Elsevier, 2012), pp. 266–314
7. S. Lomov, A. Gusakov, G. Huysmans, A. Prodromou, I. Verpoest, Textile geometry preprocessor for meso-mechanical models of woven composites. *Compos. Sci. Technol.* **60**(11), 2083–2095 (2000)
8. S.V. Lomov, I. Verpoest, Model of shear of woven fabric and parametric description of shear resistance of glass woven reinforcements. *Compos. Sci. Technol.* **66**(66), 919–933 (2006)
9. S.V. Lomov, I. Verpoest, J. Cichosz, C. Hahn, D.S. Ivanov, B. Verleye, Meso-level textile composites simulations: Open data exchange and scripting. *J. Compos. Mater.* **48**(5), 621–637 (2014). doi:[10.1177/0021998313476327](https://doi.org/10.1177/0021998313476327)
10. S.V. Lomov, A. Willems, D. Vandepitte, I. Verpoest, in *Simulations of Shear and Tension of Glass/PP Woven Fabrics*. eds. by N. Juster, A. Rosochowski. The 9th International Conference on Material Forming ESAFORM, pp. 783–786
11. N. Naouar, E. Vidal-Sallé, J. Schneider, E. Maire, P. Boisse, Meso-scale FE analyses of textile composite reinforcement deformation based on X-ray computed tomography. *Compos. Struct.* **116**, 165–176 (2014). doi:[10.1016/j.compstruct.2014.04.026](https://doi.org/10.1016/j.compstruct.2014.04.026)
12. G. Stamoulis, C. Wagner-Kocher, M. Renner, An experimental technique to study the transverse mechanical behaviour of polymer monofilaments. *Exp. Techn.* 26–31 (2005)
13. E. Vidal-Salle, P. Boisse, Modelling the structures and properties of woven fabrics, in *Modelling and predicting textile behaviour*, ed. by X. Chen (Woodhead Publishing; In association with the Textile Institute; CRC Press, Cambridge, Boca Raton, Fla, 2010), pp. 144–179

Part III
Technical Applications

End Fasteners of High Performance Fibre Ropes

Markus Michael, David Holschemacher and Peter Streubel

Keywords High performance · Fibre rope · End fastening · End termination · End connection · Dynamic tensile test · Bionical

Mechanical components made from high-strength synthetic fibres become more important because of their potential for lightweight construction. Subjects of present investigations are ropes and rope-like structures. A problem to be solved is the realization of end fasteners. Every rope can, irrespective of design, material and diameter, only be loaded with the force that can be borne by the end fastener. This is a weak point in rope structure which leads to high oversizing of the rope. Connecting mechanisms known from steel wire ropes cannot be transferred to the fibre ropes because of fibre's higher sensibility to bending and compressive forces, and due to their creep behaviour. Common rope fastener mechanisms (e.g. splices, socketed fasteners) can bear about 95 % of the Mean Break Load of the rope [1]. High-strength fibre ropes are, due to their high specific strength, predestined for being used in dynamically loaded applications in conveying engineering. Admittedly, the state of knowledge regarding needed rope fasteners and for adequate force transmission is insufficient. The requirements imposed on the design of fasteners are high. Among other things, rope fasteners must endure static and dynamic loads, exhibit the same temperature stability as the rope and have the same degrees of freedom. In contrast to this, application-specific restrictions, like easy assembly and disassembly, lightweight and compact design and a low price, can be found. In practice, it is proven to separate connection variants into detachable and non-detachable connections ([1, 2] cf. Fig. 1).

Detachable fasteners are based on mechanical linkage concepts, where the application of force is realized by reversible clamping or friction contacts. The coupling mechanisms, usually applied in wire rope applications, are only suitable

M. Michael · D. Holschemacher (✉) · P. Streubel
Endowed Professorship of Technical Textiles and Textile Mechanical Components,
Chemnitz University of Technology, Chemnitz, Germany
e-mail: david.holschemacher@mb.tu-chemnitz.de

M. Michael
e-mail: markus.michael@mb.tu-chemnitz.de

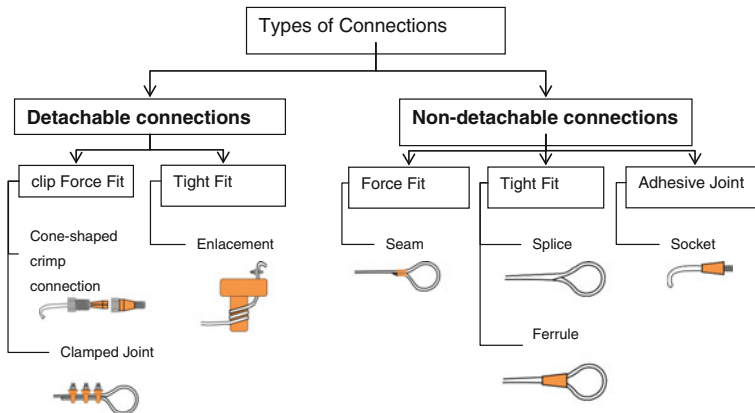


Fig. 1 Available connections, established for fibre ropes

for fibre ropes to a limited extent, because of the fibre-specific behaviour of ‘working in’ and creep of fibre ropes. Non-detachable fasteners, e.g. splices, can bear about 100 % of the Mean Break Load of the ropes, but those require well-trained personnel, and a subsequent correction is not possible. The fields of application for new high performance textiles are versatile and steadily increasing, what leads to a need of an innovative connection concept. The linkage concepts actually used are very expensive or not suitable for fulfilling the high requirements concerning reproducibility, adjustability and dimensional accuracy. New approaches with a performance superior to existing technical solutions can be found within interdisciplinary research in the field of human’s physiology. In connection with this, the chondral entheses is taken as a model from biology. Comparing the entheses zone and technical solutions, it can be shown that an optimum in tensile strength is gained by superimposing different mechanisms of action. The high potential of this concept originates in the interaction of structural alignment of mechanical attenuators and a firmly bonded composition of materials.

Investigation of Commonly Used End Fasteners

The majority of investigations in the past, concerning high performance fibre ropes, dealt with the strength and lifespan of the rope itself. Concerning end fasteners, however, very limited data of comparable research is available. The same applies to test standards. While static tensile tests are described in DIN EN ISO 2307, there is no standard or established test specification for tests with dynamic payloads, taking into account the special factors such as the medium tension, amplitude as well as the influence of the rope’s materials and construction. In practice, dynamic payloads on ropes, and thus also on the end fasteners, occur mostly randomly and in

different size and frequency. Representing those stresses as realistically as possible has been one of the major objectives of this investigation. In order to achieve optimal comparability of the results, an idealized dynamic payload with a sinusoidal load–time sequence was chosen to be applied for the tension–tension tests. Concerning the end fasteners, especially load-free states followed by jerkily increasing loads are representing critical stresses. For each end fastener the bearing number of load cycles N has been determined. Since high performance fibre ropes are mechanical structures with a limited lifetime, the limit of oscillation cycles was set to $N = 3 \times 10^6$. For those test specimens that reached the set limit, static tension tests to investigate the remaining break load have been performed. To ensure no significant influence of temperature, the frequency of oscillation was set to 5 Hz. All tests were performed under laboratory conditions with relatively short free rope lengths and free from environmental influences. Major object of this investigation was to enable the comparison between known end fasteners for high performance fibre ropes for static and dynamic applications. All tests have been performed with the same rope design and fibre material shown in Table 1. For this rope a mean break load of $F_B = 31.5$ kN was determined in static tension tests.

During tests, various end fasteners have been investigated, such as conventional ones for fibre ropes like splices and knots, as well as those mainly used for steel wire ropes like ferrules, swaged sockets and wedge sockets. Additionally, a sewed splice as a hybrid solution and a bonded joint has been tested. Figure 2 shows an overview of the investigated end fasteners.

Initially, static tensile tests according to DIN EN ISO 2307 have been performed with the materials testing machine Z150 from manufacturer Zwick/Roell. For each

Table 1 Manufacturing parameters of the tested rope construction

Material	Aramid fibre technora® T221
Diameter	6 mm
Rope construction	Hollow braid, 12 strands
Braid length	43 mm
Mean Break Load	$F_B = 31,5$ kN

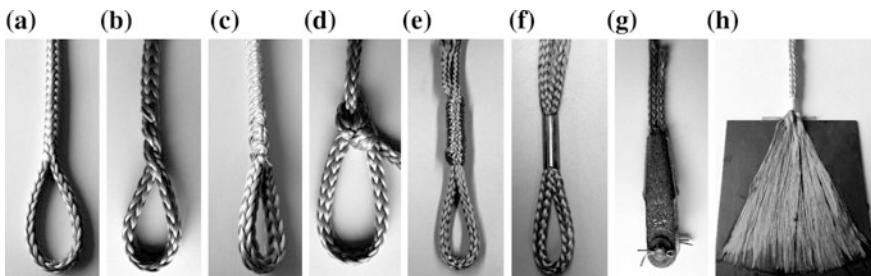


Fig. 2 Overview of the investigated end fasteners: **a** eye splice, **b** Locked Brummel splice, **c** sewed splice, **d** bowline knot, **e** hangman’s knot, **f** swaged socket, **g** wedge socket, **h** bonded joint

Table 2 Mean break loads determined in the static tension tests

End fastener	Break load F_B in N	F_B in % of rope mean break load	Standard deviation s in N	Coefficient of variation in %
Eye splice	30.900	98	635.4	2.2
Locked Brummel splice	30.912	98	591.9	1.9
Sewed splice	31.020	100	973.1	3.0
Bowline knot	9.300	30	967.2	7.6
Hangman's knot	12.420	39	732.8	5.9
Swaged socket	8.737	28	243.3	2.8
Wedge socket	12.570	40	806.6	6.4
Boned joint	19.286	61	2378.0	12.3

end fastener the tests have been executed 10 times. The determined break loads are shown in Table 2.

Best results of the investigated end fasteners in the static tensile tests were obtained by splice variations. Reaching break loads of almost 100 % of the rope's mean break load, the splice variations provided the maximum potential in bearing peak loads, significantly outperforming the other test fasteners. With a break load of 61 %, good potential regarding bearing peak loads could be obtained by the boned joint, although the tests revealed the unfavourable geometrical design. Connecting a cylindrical component with a plain one results in pull of forces that lead to gradual delamination and thus to a reduction of the glued surface. The remaining fasteners showed results below 50 % of the rope's mean break load, and therefore should be used with caution when used in applications where high peak loads can occur.

Further, dynamic tensile tests have been performed as described previously. For this purpose, the servo-hydraulic pulsator 8501 by the manufacturer Instron with a capacity of 100 kN was utilized. During dynamic tensile tests, the sinusoidal load/time sequence has been applied to the unloaded specimen in a force-controlled mode. The test was performed until either the preset force could not be applied anymore due to failure or the limit number of load cycles $N = 3 \times 10^6$ has been passed without failure. For each type of end fastener, the tests have been performed three times. Table 3 shows the determined number of the endured number of load cycles for the investigated fasteners.

The Locked Brummel splice and the sewed splice again performed best by reaching the limited number of loading cycles under all tested circumstances. No damage to the rope or fastener could be determined by visual inspection, so that those fasteners can be assessed fatigue endurable by means of the used test specification. Regarding the test results, both fasteners can be used in applications with

Table 3 Endured number of load cycles

End fastening	0–15 % F_B	0–20 % F_B	15–30 % F_B
Eye splice	–	–	3×10^6
Locked Brummell splice	3×10^6	3×10^6	3×10^6
Sewed splice	3×10^6	3×10^6	3×10^6
Hangman’s knot	No results yet	117.617	–
Wedge socket	3×10^6	–	–
Bonded joint	No results yet	587.921	–

high tensile forces, large peak loads, as well as those application with minimum loads around zero. Ferrules to be used as end fasteners for high performance fibre ropes work very well under dynamic payloads up to 15 % of the rope’s mean break load. Appropriate applications can make good use of the fastenings advantages such as easy and fast on-site assembly and disassembly. Higher load levels lead to slipping effects and thus cause failure. The bonded joint once again obtained good results in the tests with an oscillating force between 0 and 20 % of the rope’s mean break load. The endured numbers of load cycles show a good resistance to fatigue and by that the high potential of that type of fastener. The results indicate the fastener to work best at lower forces. Unfortunately, those tests have not been performed yet. Nevertheless, the bonded joint shows good potential for further improvement.

For those test specimens that reached the set limit of load cycles, static tension tests have been performed to investigate the remaining break load. The results are shown in Table 4. All investigated specimens reached remaining break loads of more than 80 % of their initial break loads, which confirms that those fasteners can be seen as long-term fatigue resistant.

The presented results enable the comparison of various known end fasteners for high performance fibre ropes for different types of applications. A special test specification for dynamic tensile tests for end fasteners of high performance fibre ropes that deliver comparable results has been developed. The results open up a broad field of application for the splice variations Locked Brummel splice and sewed splice. Good results, as well as a high improvement potential, have been shown for the bonded joint. Thus, a bolt with special shape to be bonded to a rope is

Table 4 Remaining break load of fatigue endurable fasteners

End fastener	Remaining break load in N	Remaining break load as % of the fasteners initial break load
Eye splice	26.526	85.8
Locked Brummel splice	25.016	80.7
Sewed splice	25.884	82.2
Wedge socket	7.284	83.4

currently under investigation. Further experiments and tests are required to determine further influence factors, such as material, rope design, medium tension and amplitude. Final objective will be the deriving of a calculation model.

Bionical Approach to End Fasteners

Additionally to the known end fasteners, new approaches have been investigated as well. The connection between tendon and bone as a biological solution represents such an interesting approach. Focus is the adaption of the link between a low-modulus (tendon) and a high (bone)-modulus material and extrapolation of this biological concept to technology and special fields of mechanical engineering. The passage between tendon and bone is separated into five sectors (cf. Fig. 3). Initially, the fibres are aligned along the direction of the work load, what results in a uniform distribution of load on the number of collagen fibrils, involved in transferring tensile forces. The passage between muscle and tendon is discounted, in this case. Within the second sector, non-mineralised cartilage cells are working as attenuator. This special arrangement of components provides a compensation of the differences in moduli between the tense collagen tissue of the tendons and the osseous tissue. Within the following sectors, the content of minerals of the chondral tissue is varying and steadily increased towards the bone. The gradients in material properties, generated by this setup, are smoothing the passage between low-modulus connective tissue and high-modulus osseous tissue.

For depletion of load peaks, in the 4th sector the collagen fibres are reinforced by highly elastic collagen bands (retinacula). Each retinaculum is providing a direct

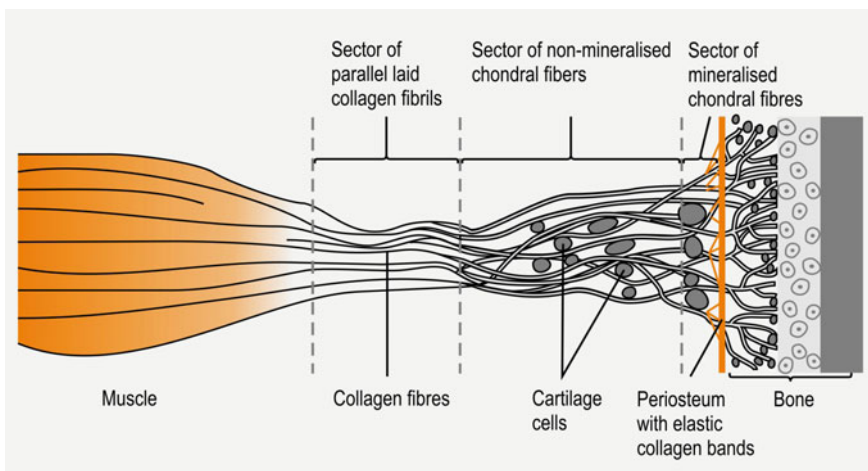


Fig. 3 Enthesis in accordance with Schnüke [3]

contact between tendon's collagen fibres and periosteum. The tendon is fixed and protected from load peaks. In the 5th sector, the collagen fibres are permeating the cortical substance of the osseous tissue and are firmly bonded. A fluent passage from collagen to osseous tissue is the result, what helps to avoid discontinuities within the material composite. A superposition of mechanical attenuation and firmly bonded intergrowth ensures that pulling the enthesis out of the bone can only happen at diseased modifications of the osseous tissue.

For setting up such a connection, a bolt is inserted in the fibre rope, which acts as a coupling element between force transmission point and rope (cf. Fig. 4). This principle of operation is based on the mechanisms acting inside the connection between the periosteum and the bones. When loaded with a tensile force, the tubular tension member (e.g. tendon, rope ...) is constricted and a friction with a direction opposite to the tensile load is generated between bone (bolt) and periosteum (rope).

The termination shown above has been investigated regarding its break load at a tensile test machine (ZWICK/ROELL Z 150). For first orientating investigations of the pull-out force of the termination, a braided fibre rope with a diameter of 12 mm has been made from polyester fibres. The break load of the rope, measured in accordance with DIN EN ISO 2307, has been determined with 35.5 kN. The pull-out force at a termination containing the longest bolt with an insertion length of 320 mm was about 26 kN, so about 73.2 % of the rope's break load. During tension tests, stick-slip effects between bolt and rope occur. These stick-slip effects are caused by the rope structure which cannot be totally relieved, even when in close to break load. The influence of the bolt's design and geometry on the ascent of the graph, the break load and stick-slip effects have to be investigated. The influence of the length of the bolt has already been investigated in two tests. Therefore, the initial bolt with a length of 320 mm has been shortened by 80 mm. All the other geometry factors have been kept. The result of shortening the length of the bolt was an increase of termination's break force from about 26 kN up to 29.5 kN, which is about 83 % of rope's break load. The optimal length of the bolt is estimated to be between 200 and 320 mm for a braided fibre rope with a diameter of 12 mm. Following parameters have shown to have a significant influence, during the first tensile tests: length of bolt, design of bolt, roughness of surface of bolt. Further tests are needed to investigate the quantity of the influence of these three parameters. Additionally, the behaviour in transverse deformation in dependence on the rope

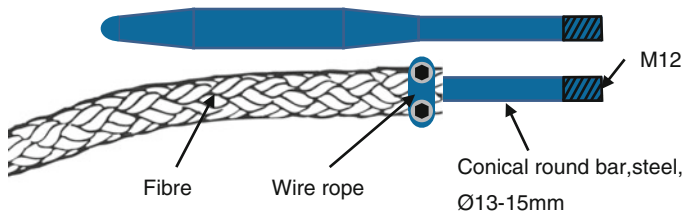


Fig. 4 Setup of innovative terminations

kinematics is to be described mathematically. These steps are necessary to develop special designs for bolts that are not depending on specific rope constructions and that do show optimized load bearing characteristics.

References

1. R. Verreet, *Seilendverbindungen* (PR Werbeagentur & Verlag GmbH, Aachen, 2003)
2. S. Gelbrich, *Beitrag zur Entwicklung von Kräfteinleitungselementen für hochbeanspruchte Faserverbund-Zugstreben im Bauwesen* (Technische Universität Chemnitz, 2008)
3. M. Schünke, *Topographie und Funktion des Bewegungssystems* (Georg Thieme Verlag, Stuttgart, 2000)

Influence of Braid Carrier Tension on Carbon Fibre Braided Preforms

Sree Shankhachur Roy, Wentao Zou and Prasad Potluri

Introduction

The process parameters of two-dimensional braiding can influence the braided preform specification. A few major process parameters in braiding are the speed of the carrier, haul off and core diameter. In addition to these parameters, the fibre tension determined by the bobbin carrier tension plays a role in the preform thickness. Braid carrier tension has a combined operation of providing a set tension to the fibre tow as well as compensation of the tow. As the fibre tow from the bobbin is guided around the roller guide, usually the compensation operation removes the slack and keeps the tow under tension. The tension force required for compensation can be as little as 70 g. Despite the requirement of a very low tension for compensation, braiding machines are delivered with springs capable of providing tension as high as ~ 700 g. A larger tension can be used with the aim of producing a compact braided preform. This study attempts to investigate the effect of selecting a higher tension on the preform and the effect on the subsequent composite structure.

The compensator unit in a braid carrier is usually connected to a torsion spring (circumferential braider) or compression spring (radial braider). In this study, two tension values (1.5 and 3 N) were selected using the torsion spring for braiding purpose. Although these tension values were not as high as those used for filament winding for composite braiding was carried out to study the effect on preforming and subsequent preform consolidation for composite. Tension variation at different points of fibre passage was also recorded. Since carbon fibre has been widely used as a reinforcing material for composite structures it was used for this study.

The original version of this chapter was revised: The surname of the second author's name was corrected. The erratum to this chapter is available at DOI [10.1007/978-3-319-29932-7_17](https://doi.org/10.1007/978-3-319-29932-7_17)

S.S. Roy (✉) · W. Zou · P. Potluri
Textile Composites Group, The University of Manchester, Manchester, UK
e-mail: shankhachur.roy@manchester.ac.uk

If a tubular-braided structure is pulled the helical fibre orientation changes that influence the diameter and length of the structure. If the braided structure is placed on a rigid core, change in diameter will apply pressure on the core when the braid is pulled. In this study the principle of pressure applied due to the pull is aimed to be used for carbon fibre preforming. However, the preforms for composites are usually over-braided onto a mandrel and hence pulling the braid to apply radial pressure is not convenient. In order to facilitate the ‘pulling’ effect on the braid, tension on individual strands were changed at pre-braiding stage. The carrier tension on individual fibre tow will eventually apply the consolidation pressure as discussed in the following sections.

The ‘Chinese Finger Trap’ Principle

The tubular-braided structure has a phenomenon of fibre shearing under tension. During the process, the braid length increases changing the fibre orientation and subsequently the diameter decreases. The method replicates the principle of ‘Chinese handcuff’ [1] otherwise mentioned as ‘Chinese finger trick’ [2]. The Chinese finger trap principle is widely used in children’s toy (Fig. 1) which is a cylindrical braided structure. In the trick when someone tries to pull the fingers out of the braided toy, it tightens the grip by reducing diameter and applying pressure. The principle is used in various scientific applications from straightening fracture [3] in medical science to picking samples from the Moon during space exploration [4]. In all such applications, a braid structure is used to apply uniform pressure that acts as a grip as the structure is pulled.

As the trick presents the change in diameter with the change in length, fibres oriented in opposite direction in braid shears producing a ‘scissoring effect’ [5]. The fibre shearing changes the braid angle (Fig. 2) and the braid diameter. In this study, the mandrel diameter was constant and six layers were over braided in a stacked preform. Additional layers change the braid diameter and thus a change in braid angle is possible. Hence, take up speed was calculated using the following equation [6] for the change in diameter in order to keep the braid angle constant.

$$v = \frac{N_h \tan \alpha}{2 \omega_h R} \quad (1)$$

Fig. 1 Braided ‘Chinese finger trap’ that uses the principle of strand shearing under tension



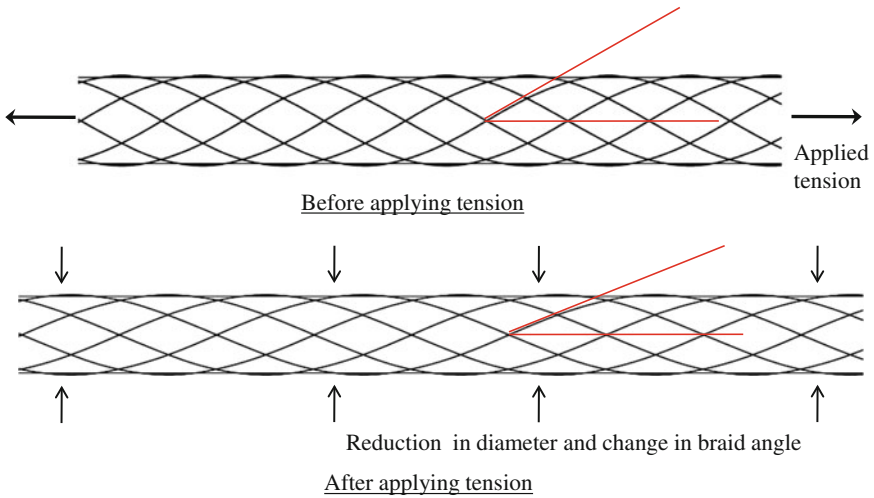


Fig. 2 Schematic of the principle of longitudinal tensioning of biaxial braided preform showing states of braid before applying tension (*top*) and after applying tension (*bottom*)

Tow Tension at Carrier and Braid Fell Point

A circumferential braider was used for over-braiding a mandrel of ~ 50.5 mm diameter with two different tension settings. A low size content (0.3 %) carbon fibre (T700 SC) was chosen so that the effect of change in tension on tow dimension can be observed. As shown in the Fig. 3 the tension applied by the compensator roller guide that is connected to the torsion spring is F . The measured tension through the eyelet is F_2 ($\approx F/2$) while the fibre tow does not have any contact with the eyelet. The tension measurement was carried out using an ISO (961-161) calibrated push-pull type digital force gauge (Sauter FK 250). The resolution of the handheld equipment was 0.1 N with a minimum precision of 1.25 N. During the measurement a loop with

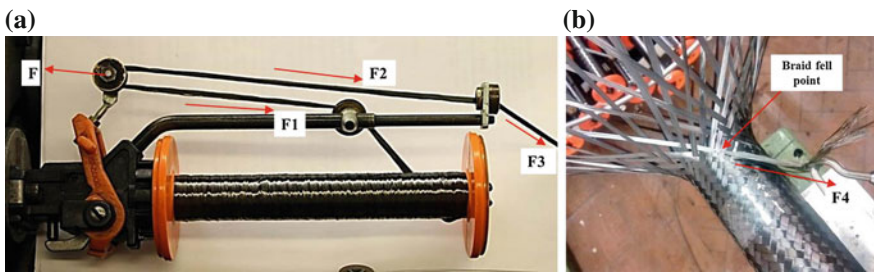


Fig. 3 Fibre passage on a circumferential braider at the University of Manchester **a** A carrier with the bobbin with different tension at different points along the fibre passage **b** tension measured at the braid fell point

Table 1 Fibre tow tension variation between the carrier eyelet and braid ($\pm 45^\circ$) fell point (330 mm convergence)

Desired tension setting through carrier eyelet (N)	Measured tension through carrier eyelet, F2 (N) \pm 95 % CI	Measured tension at fell point, F4 (N) \pm SD	$F4/F2$
1.5	1.4 \pm 0.44	2.28 \pm 0.05	1.63
3	3.1 \pm 0.54	4.2 \pm 0.05	1.35

a knot was created at the end of the tow and the loop was connected with the hook of the tensioner for measurement. The tension data was recorded for all 48 carriers.

Further to the point of contact with braid ring the fibre tows converge to the fell point of braid onto the mandrel. In the convergence zone the counter-rotating tows come in contact with each other as the tows approach the fell point. However, the contact points vary at different angles between the tows that will lead to a varying friction resistance [7]. Thus, the tow tension is likely to be different at the fell point compared to the tension measured at carrier. The tension measured through the eyelet of a carrier was different to the tension at braid fell point as presented in Table 1. For lower tension this difference is higher than that with higher tension. The applied pressure from the helical fibre passage of the braid is thus the tension at the fell point instead of that at the carrier.

The tow tension was measured by cutting a tow from the braid at fell point and pulling through the interlacement. In this method, after over braiding a mandrel the braider and the take up was stopped and then the tension was measured from different tows. The tension measured in this way included the all frictional resistance and fibre slippage on the passage of a tow from the carrier to the braid. Although due to the regular interlacement pattern (2/2) it was not feasible to take the tow out of the braid from the first tow at the fell point. Instead the tow was taken out at a tangent to the mandrel circumference at the crossover point. This was kept consistent between the measurements. Total number of these measurements was 12 for each tension setting. The results of the difference in tension through eyelet of the carrier and at fell point are presented in Table 1.

Braiding Carrier Tension and Applied Pressure

Previous studies [6, 8] on braided preform and composite fabrication discussed the consolidation using nesting factor along with to what extent the thickness reduction occurs for braided preform. However, no specific process parameters that can cause thickness reduction and preform consolidation were discussed. Filament winding is widely used for developing cylindrical composite structures. The process uses a very high tension for preform consolidation. Several previous studies [9–11] investigated the consolidation of filament wound preform as an effect of winding tow tension. Although the principles of braid and filament wound structure formation are different, braiding fibre tows follows helical path and wraps the core

around similar to that in filament winding. The angle of wrapping and the tension applies force underneath.

Thus, interlacing tow tension for braid will have similar effect on the thickness of the preform. Cai et al. [10] presented an equation for each filament wound layer where the authors considered that the fibre tension (T) and consequently the applied radial pressure (p) are in equilibrium condition as shown in Eq. 2 [10].

$$T \cos^2 \alpha = pr \tag{2}$$

In the above equation, r is the radial position of the filament wound layer and α is the angle between fibre and the horizontal axis. In another study carried out by Banerjee et al. [9] the fibre tow width was considered in order to calculate the applied pressure by a fibre tow band on the underlying fibre layer during filament winding of a cylindrical mandrel. The equation presented by the authors [9] is as follows.

$$p_0 = \frac{F^{k+1} \sin^2 \alpha}{r_f^{k+1} w^{k+1}} \tag{3}$$

In the above equation p_0 is the applied pressure, by k+1 layer. Other notations F, α , r_f and w represents initial fibre tension, angle between the fibre and cylinder longitudinal axis, radius of the mandrel with the added layer and band width of the tow, respectively.

During braiding although tow tension was unaltered throughout the process, the consolidation of the preform was recorded in terms of change in thickness. It is apparent from the Eqs. 1 and 2 that if the fibre angle, tow width and tension remains constant with increasing radius the pressure will decrease and hence, the thickness reduction due to the added multiple layers will be less.

Prediction for Applied Pressure Generated by an Interlacing Point of a Biaxial Braid

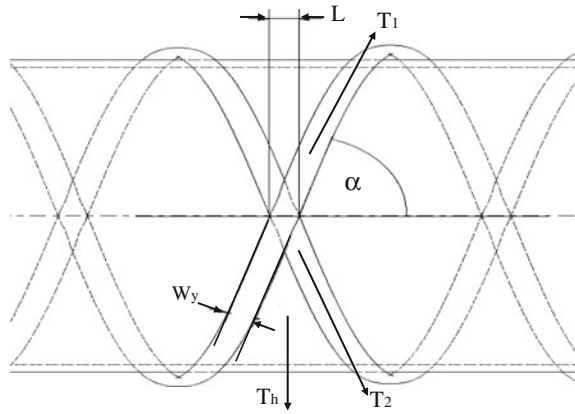
The schematic presented in Fig. 4 shows the crossover point of two tows that replicates a simplest interlacement case for a biaxial braid over braided on a circular cylindrical mandrel. The parameters of the braid those influence in applying pressure are braid angle (α), fibre tow width (W_y), tow tension (T) and mandrel radius (R).

Both tow tensions will apply the total force on the mandrel at crossover point. Considering the tension of both tows equal ($T_1 = T_2 = T$) the radial (hoop) component of the individual tow tension will be,

$$T_{1h} = T_{2h}$$

Length of the crossover unit in axial direction: L

Fig. 4 Schematic of the effect of tow tension and width when helically wrapped around a mandrel



From the schematic presented in Fig. 4, force applied in the circumferential direction,

$$T_h = T_{1h} + T_{2h} = T_1 \sin \alpha + T_2 \sin \alpha \tag{4}$$

$$\text{As } T_1 = T_2 = T \text{ therefore } T_h = 2T \sin \alpha \tag{5}$$

Pressure (P_h) applied on the mandrel by two yarns at crossover point over a length of L ,

$$P_h = \frac{T_h}{L \times R}$$

$$P_h = \frac{2T \sin \alpha}{L \times R} \tag{6}$$

The length of the mandrel covered by the tow crossover, L can be expressed using the tow width as follows:

$$L = \frac{W_y}{\sin \alpha}$$

Replacing the L with the above expression on the Eq. 6,

$$P_h = \frac{2T \sin^2 \alpha}{W_y \times R} \tag{7}$$

Equation 7 is applicable for biaxial braid structures. In case of triaxial braid there is an axial tow that is embedded in between the two crossing over biaxial tows.

Measurement of Braid Parameters

In this study, six layers of braiding were carried out in a single stack of preform. The braiding was repeated for minimum 5 times for two different tension settings and braid angles. As the carrier tension was unchanged, with the change in angle the change in braid thickness for both tension settings was recorded. The cover factor of the first and sixth layer of the biaxial braid for both tension settings were calculated using equation [12] and compared (Table 2 and Fig. 5).

$$\text{Cover factor} = 1 - \left(1 - \frac{W_y N_c}{4\pi R \cos \alpha} \right)^2 \tag{8}$$

The cover factor of $\pm 45^\circ$ and $\pm 60^\circ$ braid was 0.81 and 1.0, respectively. As the diameter was changed from 1st to 6th layer the surface coverage of $\pm 45^\circ$ braid changed from ~ 98 to ~ 95.5 %. Thus, the increase in tow spacing (~ 0.3 mm) at sixth layer left uncovered surface (~ 0.1 mm) between the adjacent tows. For such uncovered preform, braid diameter measurement can have errors if a digital or vernier calliper is used as the jaws of a calliper can be placed on the uncovered area. In

Table 2 Tow width, tow spacing and cover factor variation between different layers within a stack of $\pm 45^\circ$

	Tow width (mm) \pm SD	Tow spacing, (mm) \pm SD	Braid angle ($^\circ$) \pm SD	Cover factor
1.5 N 1st layer	4.11 \pm 0.26	4.69 \pm 0.43	45.1 \pm 0.8	0.983
1.5 N 6th layer	4.02 \pm 0.25	4.99 \pm 0.71	45.6 \pm 0.6	0.956
3 N 1st layer	3.65 \pm 0.36	5.01 \pm 0.27	43.8 \pm 0.6	0.941
3 N 6th layer	3.87 \pm 0.45	5.27 \pm 0.41	44.9 \pm 1.2	0.939

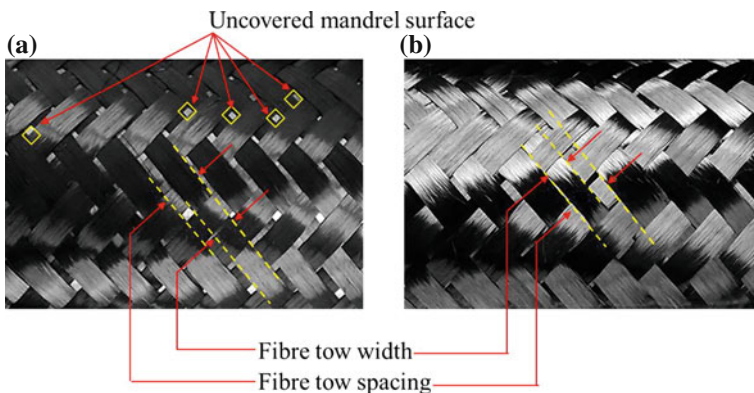


Fig. 5 $\pm 45^\circ$ braid tow width, tow spacing and uncovered area **a** first layer **b** sixth layer

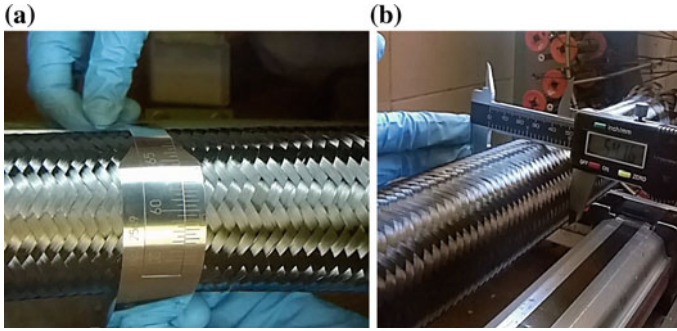


Fig. 6 Outer diameter of the braid measurement using **a** vernier diameter measurement tape **b** digital callipers

addition, as the mandrel diameter around the circumference had deviation the measurement at different radial points varied. To avoid such variation, a stainless steel vernier diameter measuring tape (Fig. 6a) was used. This approach reduced the possibility of incorrect measurement by eliminating the chance of braid diameter measurement from an uncovered section. Also it cancel outs error induced by variable mandrel diameter around the circumference. For individual layers of each preforms, thickness were measured at ten different points along the braid. The mean values with standard deviation of each layer thickness have been reported in this article.

Effect of Tow Tension Change on Braided Preform

In a multilayer braided preform the layers will have nesting effect. However, the effect of tension and subsequent applied pressure is a contributing factor of braid layer thickness reduction in a stack. The extent to which the braid stack thickness is reduced with respect to the first braided layer thickness can be determined by using Eq. 9 [13].

$$\text{Nesting Factor (NF)} = \frac{t_s}{\sum_{i=1}^n t_i} \quad (9)$$

In the above equation, t_s = stack thickness and t_i = individual ply thickness.

As the braided layers were added to the preform, the stack thickness was calculated by using Eq. 10 where D_m and D_b are the diameter of the mandrel and the last braided layer respectively.

$$t_s = \frac{D_b - D_m}{2} \quad (10)$$

The tow tension at the fell point (Table 1) was used in Eq. 7 for both braid angles and respective tow widths to predict the applied pressure.

The calculated applied pressure by the braided tows was higher for 3 N tension setting, as a result braid stack thickness appeared to be more consolidated (Fig. 7a) for both $\pm 45^\circ$ and $\pm 60^\circ$ braid. Although the difference in thickness between 1.5 and 3 N tension settings is not very high, the reduction in thickness is higher for $\pm 60^\circ$ compared to that of $\pm 45^\circ$ braid. For $\pm 45^\circ$ braid no distinguishable difference in stack thickness between the tension settings are visible in the first three layers. One of the reasons that can be influencing this is the lack of surface coverage by the braid. The cover factor of the braid hence will also influence the nesting factor that is discussed in the following section. The predicted pressure applied by $\pm 60^\circ$ braid is ~ 1.5 times higher than that of $\pm 45^\circ$ braid. According to Eq. 7, tow tension and applied pressure are directly proportional if the other parameters remain constant. However for both braid angles, as the tow tension (F4) was increased from 2.28 N to 4.2 N (~ 1.8 times), the pressure increased was twice. This is a result of individual layer thickness variation that eventually changes the effective radius and also decrease in tow width in the braid for higher tow tension.

Nesting factor (NF) indicates the reduction in stack thickness with respect to the first layer thickness. Higher the nesting factor, the thickness reduction of a stack of layers is lower and vice versa. As Fig. 8 shows, the NF in a stack is less for a $\pm 60^\circ$ braid compared to that of $\pm 45^\circ$ braid. For this study, $\pm 45^\circ$ braid had cover factor less than 1 and also the cover factor decreased with increasing braid diameter (Table 2). This is a key reason that will allow the layers to nest more reducing the stack thickness. For $\pm 45^\circ$ braid NF was high for higher tension (3N) indicating less

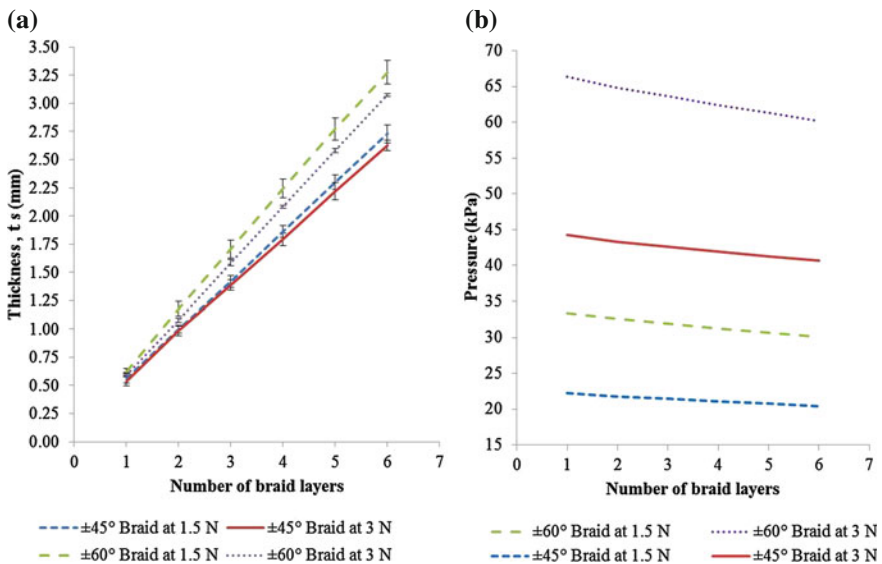


Fig. 7 a Braided stack thickness (t_s) as the layers added the preforms braided for both tension (F4) settings b Calculated pressure applied by tow tension at braid fell point

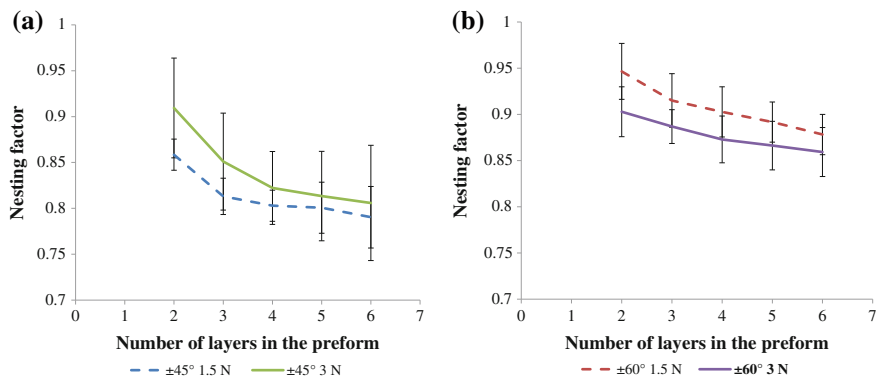


Fig. 8 Change in nesting factor for both tow tension settings as layers were added in the stack of **a** $\pm 45^\circ$ braid **b** $\pm 60^\circ$ braid

nesting as the cover factor change from first to sixth layer was not as high as that of 1.5 N. In contrast for $\pm 60^\circ$ the NF was less for higher tow tension thus the layer thickness reduction was high. For $\pm 60^\circ$ braid the higher nesting of layers for higher tension was mainly an effect of applied pressure from the tow tension as the surface was fully covered. This indicates that the layer nesting for $\pm 45^\circ$ braid was a result of both lack of surface coverage as well as the applied pressure. Hence, the effect of tow tension and subsequent pressure on preform consolidation as well as nesting for $\pm 45^\circ$ braid cannot be explained with clarity. Nonetheless for $\pm 60^\circ$ braid as the surface was fully covered the nesting was predominantly influenced by the applied pressure from tow tension. For higher tension, the thickness reduction was higher resulting a smaller NF as it is presented in Fig. 8b. For both the angles, layer nesting tends to reduce with increasing number of layers as well as decreasing pressure from tow tension.

Influence of Tension on Braided Composite Tubes

During the preform consolidation study, minimum five samples were produced. However, only one sample from each tension settings for both angles was used for manufacturing composite tubes (Fig. 9). Vacuum assisted resin infusion method was used with flexible tooling for the manufacturing purpose. Further compaction of preform occurred during the composite manufacturing as vacuum was drawn inside the envelope.

Composite tubes were manufactured and all the tubes had wrinkles. Wrinkles (Fig. 9) are generally considered as imperfection for structural composite tubes. The tube wall thickness was measured using a micrometre both with the wrinkles and without the wrinkles. The preform thickness was reduced (Table 3) over 25 % for $\pm 45^\circ$ braid in composites whereas this reduction was ~ 15 % for $\pm 60^\circ$ braid. This

Fig. 9 Two $\pm 45^\circ$ braided composite tubes manufactured using vacuum assisted resin infusion method at Northwest Composites centre, The University of Manchester

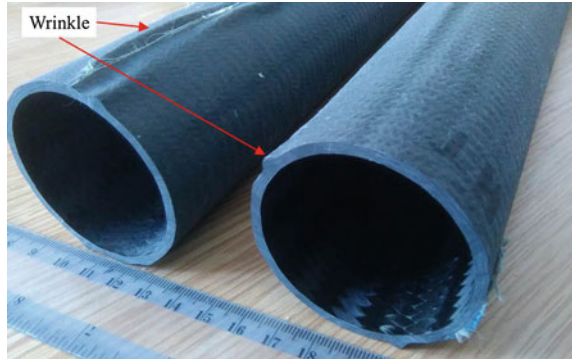


Table 3 Composite tube wall thickness with and without wrinkle and thickness reduction

Braid type with tow tension setting	Preform thickness (mm) \pm SD	Composite tube wall thickness without wrinkle (mm) \pm SD	Wall thickness reduction (%)	Composite tube wall thickness with wrinkle (mm) \pm SD
$\pm 45^\circ$ at 1.5 N	2.75 \pm 0.08	1.89 \pm 0.08	31	7.83 \pm 0.04
$\pm 45^\circ$ at 3 N	2.63 \pm 0.05	1.95 \pm 0.09	26	5.57 \pm 1.02
$\pm 60^\circ$ at 1.5 N	3.28 \pm 0.01	2.75 \pm 0.06	16	5.26 \pm 0.45
$\pm 60^\circ$ at 3 N	3.07 \pm 0.01	2.64 \pm 0.08	14	5.25 \pm 0.87

observation suggests that $\pm 60^\circ$ braid structure was more consolidated at preform stage than that of $\pm 45^\circ$ braid. Between the two tension settings, for higher tow tension, the reduction in thickness was less compared to that of the lower tow tension. Yet for $\pm 45^\circ$ the thickness reduction was about 10 % higher than that of $\pm 60^\circ$ braid indicates that lack of surface coverage provided scope for further thickness reduction with the addition of atmospheric pressure on the envelope.

Conclusion

The effect of braid carrier tension on preforming was aimed in this study. It was observed that the tension at the braid fell point was different and higher than that is usually measured at the carrier. Also, although nesting was a widely used parameter for indicating thickness reduction in a stacked preform, effect of tow tension for stacked preform thickness reduction was observed during this study. As a result of the tow tension at the crossover point of two tows the applied hoop pressure was predicted. Future investigations can validate this prediction by practical measurement of the pressure. Although the prediction indicated the effect of applied pressure from crossover points, it was only recognizable from the data collected from the $\pm 60^\circ$ braided preforms. The data for $\pm 45^\circ$ braid did not clearly show any

major effect of pressure as the nesting of the layers in the preform was influenced by the lack of surface coverage. Increasing tension had an effect on tow width for low size content T700SC 60E carbon fibre that eventually decreased the cover factor. The $\pm 60^\circ$ braid preform was more consolidated than $\pm 45^\circ$ braided preform. Higher tow tension braided preform had better consolidated preform and the thickness reduction percentage from preform to composite wall reflects this observation. Future work with different tension and different braid angle is likely to provide additional important observation to draw additional conclusion for this investigation.

References

1. F.K. Ko, C.M. Pastore, A.A. Head, *Atkins & Pearce Handbook of Industrial Braiding* (Atkins & Pearce, 1989)
2. Q. Zhang, D. Beale, S. Adanur, R. Broughton, R. Walker, Structural analysis of a two-dimensional braided fabric. *J. Text. Inst.* **88**, 41–52 (1997)
3. K. Akhtar, D. Akhtar, J. Simmons, A readily available alternative to Chinese finger traps for fracture reduction. *Ann. R. Coll. Surg. Engl.* **95**, 159–159 (2013)
4. Child's Toy May Catch Samples of Moon, In *Science Fields, Science News by Society for Science & the Public*, vol. 90, pp. 72–73 (1966). <http://www.jstor.org/stable/3951079>
5. A.-M. Harte, N.A. Fleck, On the mechanics of braided composites in tension. *Eur. J. Mech. A. Solids* **19**, 259–275 (2000)
6. P. Potluri, A. Manan, M. Francke, R.J. Day, Flexural and torsional behaviour of biaxial and triaxial braided composite structures. *Compos. Struct.* **75**, 377–386 (2006)
7. N.D. Chakladar, P. Mandal, P. Potluri, Effects of inter-tow angle and tow size on carbon fibre friction. *Compos. A Appl. Sci. Manuf.* **65**, 115–124 (2014)
8. A. Endruweit, A.C. Long, A model for the in-plane permeability of triaxially braided reinforcements. *Compos. A Appl. Sci. Manuf.* **42**, 165–172 (2011)
9. A. Banerjee, L. Sun, S.C. Mantell, D. Cohen, Model and experimental study of fiber motion in wet filament winding. *Compos. A Appl. Sci. Manuf.* **29**, 251–263 (1998)
10. Z. Cai, T. Gutowski, S. Allen, Winding and consolidation analysis for cylindrical composite structures. *J. Compos. Mater.* **26**, 1374–1399 (1992)
11. H.T. Hahn, E.A. Kempner, S.S. Lee, The stress development during filament winding of thick cylinders. *Compos. Manuf.* **4**, 147–156 (1993)
12. P. Potluri, A. Rawal, M. Rivaldi, I. Porat, Geometrical modelling and control of a triaxial braiding machine for producing 3D preforms. *Compos. Part A Appl. Sci. Manuf.* **34**(6), 481–492 (2003)
13. P. Potluri, T.V. Sagar, Compaction modelling of textile preforms for composite structures. *Compos. Struct.* **86**, 177–185 (2008)

Sensor Integration in Carbon Fiber Reinforced Plastics (CFRP) to Detect Tension Differences

Jens Schäfer, Cristin Konkart and Thomas Gries

Abstract Fibre-reinforced polymers (FRP) are well known for their high performance characteristics as low weight, strength, and stiffness. Nowadays they play an essential part in the automotive, mechanical, or plant engineering. Because of the two component-material (fibers and matrix), damage calculation and lifetime prediction are difficult to forecast. To diagnose the future potential of fiber composites, more detailed data have to be examined. A new monitoring system integrated inside the FRP construction can measure material wear and fatigue, as well as material load. Such recording and evaluation systems are necessary to locate precisely the critical structural changes inside the composite to reduce production and maintenance costs.

Keywords Fibre-reinforced polymers (FRP) · Braiding · Integrated sensor systems · Structural health monitoring system (SHM)

State of Art

Standard FRP systems commonly used in automotive, mechanical, or plant engineering are not yet equipped with such monitoring systems. Especially large components need an online monitoring system, also for areas which are difficult to reach [1]. There are three categories given, to integrate sensors in general. Table 1 presents the possible sensor position combined with the advantages and disadvantages.

Structural health monitoring (SHM) systems are normally placed on the surface, because it is the easiest way to apply SHM. There are already some systems on the market which are available like strain gauges, optical strain gauges [3], ultrasonic

C. Konkart
Hochschule Niederrhein, Mönchengladbach, Germany

J. Schäfer (✉)
Institut für Textiltechnik of RWTH Aachen University,
Otto-Blumenthal-Str. 1, 52074 Aachen, Germany
e-mail: Jens.Schaefer@ita.rwth-aachen.de

Table 1 Sensor position possibilities named by their advantages and disadvantages [2]

Sensor position	Advantages	Disadvantages
On the surface	<ul style="list-style-type: none"> • Reusable • Structurally not affected • Process integrated 	<ul style="list-style-type: none"> • High tooling costs • High robustness
Integration inside the component construction	<ul style="list-style-type: none"> • Precise damage information/location (material-wear, fatigue, and load) • Multifunctionality 	<ul style="list-style-type: none"> • Influence of compound structure • Costs for sensor material
Contactless	<ul style="list-style-type: none"> • No influence of compound structure • Lower robustness for sensor material possible 	<ul style="list-style-type: none"> • Lower sensitivity • Many process information gets lost

sensors, and eddy current sensors [4]. These systems are not fully developed and make it impossible to give any statement about FRPs' inside conditions. So researches are interested to develop new sensor integration systems, which can be combined during the production process to overcome most of the disadvantages.

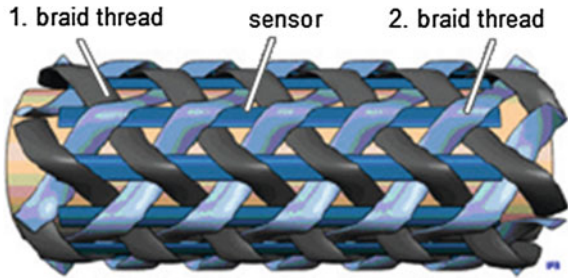
In 2015, for instance, the Otto-von-Guericke award went to a research group analyzing the mechanical stresses in glass, fiber, wind, and turbine blades. [1] Thereby a conductive yarn was integrated during the stitch bonding process. At present most of the wind turbine blades are oversized because of the missing evaluation about structural modification. The entire turbine must be shut down for an inspection. In terms of cost and time calculation, this is unavoidable and such an inspection is suspended as long as possible. The combination of unnecessary material consumption and the large amount of inspection costs makes an integrated sensor system indispensable for the market. Often the test parts are destroyed during the testing process which again leads to higher costs. A nondestructive test method would be a great step forward to understand more about material-wear, fatigue, and load. In this research project, a new measurement system is integrated directly inside the fabric during a braiding process.

The braiding process will be done with carbon fibers combined with a sensor wire [5]. With the evaluation of the sensor data it will be possible to draw conclusions about precise structural changes. This not only leads to a reduction in production time and resources, but also to continuous long-term monitoring of highly stressed FRPs.

Processing

To distinguish the lifetime cycle of three-dimensional CFRP constructions, a simple round tube is used in this particular study. A rotation braiding (Horn gear method) system is used to braid the carbon fibers around a metal tube [2]. The construction consists of three layers, where a constantan standard wire (CuNi44) is integrated

Fig. 1 Braid construction with filler yarn



during the braiding process. CuNi44 is commonly used in strain gages. The sensor material should be flexible enough to be used in the braiding process and must have a similar coefficient of thermal expansion in temperature as the matrix. The CuNi44 wire comes in contact with the carbon braid. Thus the wire needs to be isolated. A painted wire is used. The sensor takes the filler yarn position, which includes only little tension on the braid. During the braiding process, a lot of pressure can be forced on the braiding yarns. This is technically not convertible for the sensor. The filler yarns are used as sensors only in the second layer (Fig. 1).

The CuNi44 stranded wires are connected with a soldering terminal to create a stable connection point. The braided tubes have an outer diameter of 76 mm. The distance between two soldering terminals is approximately 120 mm. The carbon fiber reinforced plastic (CFRP) is generated by a vacuum infusion process using a standard epoxy resin. After a 24 h curing process at room temperature, the CFRP tubes are tempered at 80 °C in the oven. For the final tensile tests of the CFRP tubes, glass fiber fabrics (GFF) are fixed as cap strips at the edges of the tubes. The dimension of the tube is shown in Fig. 2. For the tensile test, this particular form is necessary to fit into the available test machine.

After the glass fiber fabrics are fixed with epoxy resin and cured for 24 h at room temperature, the outer layers are abraded till an outer diameter of 87 ± 0.2 mm is reached. The application process of the cap stripes is presented in Table 2.

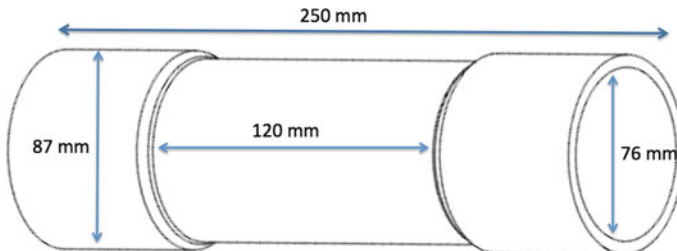





Fig. 2 Technical drawing of the test tube

Table 2 Production steps of CFRP tubes

(1) Cured CFRP tube	(2) CFRP tube with GFF as cap stripes	(3) CFRP tube with milled of cap stripes
		

The tensile test is performed referring to DIN 53835 part 1. The tubes are tested in five cycles. The adjusted forces vary between 15 and 60 kN at the maximum load. At each turning point, a break of 5 s is included. The tensile speed is set at 1 mm/min. The sensors are connected so that the electrical force can be measured with 5 mA.

Results

Primarily, the regression lines will be presented in the results. The regression line stands for all data measured within the five cycles (average value).

As presented in Fig. 3, three sensor braids are measured under the same force of 30 kN. All three linear regression lines show a similar helix angle and a positive correlation coefficient greater than 0.7. Only the correlation coefficient of measurement 8, with a value of 0.75 shows lower results than the other two measurements (0.99 and 0.94). The low correlation coefficient can be explained according to the wide dispersion between each measurement cycle.

In the following table, data's from an intact sensor (left column of table) and from a broken sensor (right column of table) are visualized. The difference between both graphs is clearly recognizable and can be seen as an optical detector. One out of seven tested sensors (M 5) shows this particular wide dispersion and a strong voltage drop after the first cycle. Within each cycle the graph lowers down and does not show the normal diagonal rise presented under measurement 4. It is clearly recognizable that sensor 5 is broken and inoperable.

The reason for the damage cannot be clearly defined. However, the first cycle has a linear increase. Immediately after the second cycle has started, the graph loses voltage in a wavy form. Possible reasons for this increase could be the following:

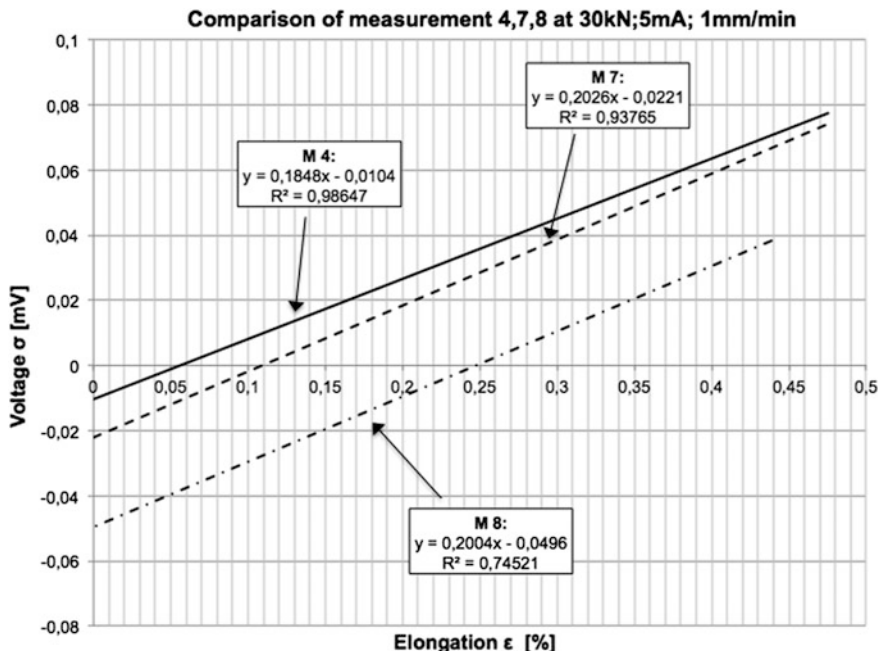


Fig. 3 Comparison of measurement 4, 7, 8 with correlation coefficient at 30 kN

damage during braiding process, vacuum infusion, contacting, or during the stretch process itself. Within the next step both graphs are compared on their regression lines. The low result of 0.27 R² for measurement 5 explains the wide range of measurement points of the broken sensor (presented in Table 3). The high correlation coefficient of measurement 4 indicates that all measurement points during the five cycles have a small variance. They show only small differences between each cycle (Fig. 4).

In the final comparison, one sensor is used for two measurements to analyze the decrease of forces over more than five cycles. Measurement 2 is taken at 15 kN force. Measurement 3 and 4 are taken with the same sensor; first at 15 kN (M 3) and then at 30 kN (M 4). All three regression lines have a diagonal increasing course. The helix angles are similar to each other (Fig. 5).

The graph of measurement 2 presents a straight increase till 0.04 mV at the load point of 15 kN. During the whole test of measurement 2, the graph shows low dispersion, which is also recognizable at the high value of 0.96 for the correlation coefficient. Measurement 3 shows a slightly lower correlation coefficient of 0.73. The dispersion between each cycle of measurement 3 is much wider compared to

Table 3 Optical comparison of a intact working sensor (M 4) an a broken sensor (M 5) under the same conditions

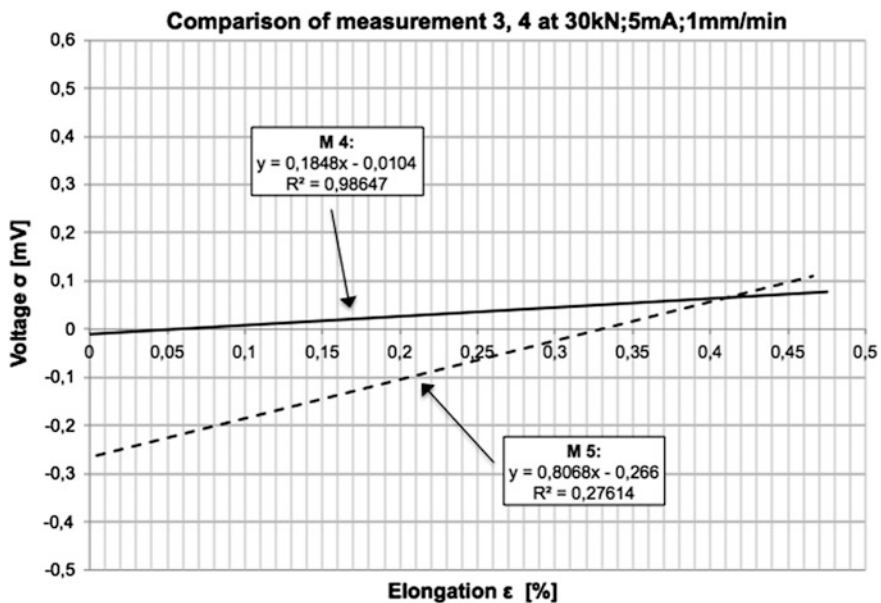
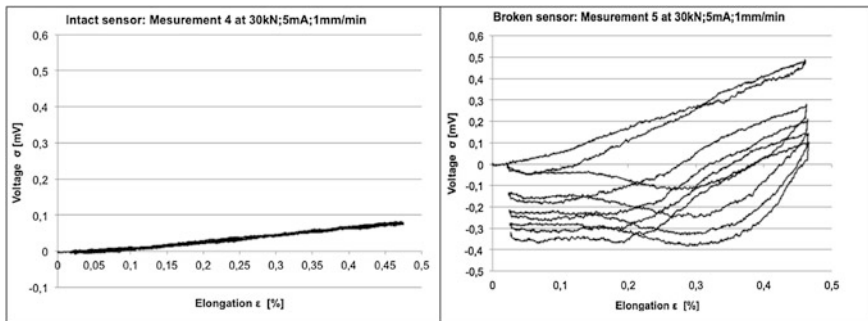


Fig. 4 Comparison of measurement 4 and 5 with correlation coefficient at 30 kN

measurement 2. Interestingly, measurement 4, which is done with the same sensor as measurement 3, now shows even better results within the correlation coefficient. Similar positive results are also recorded at force increase till 60 kN.

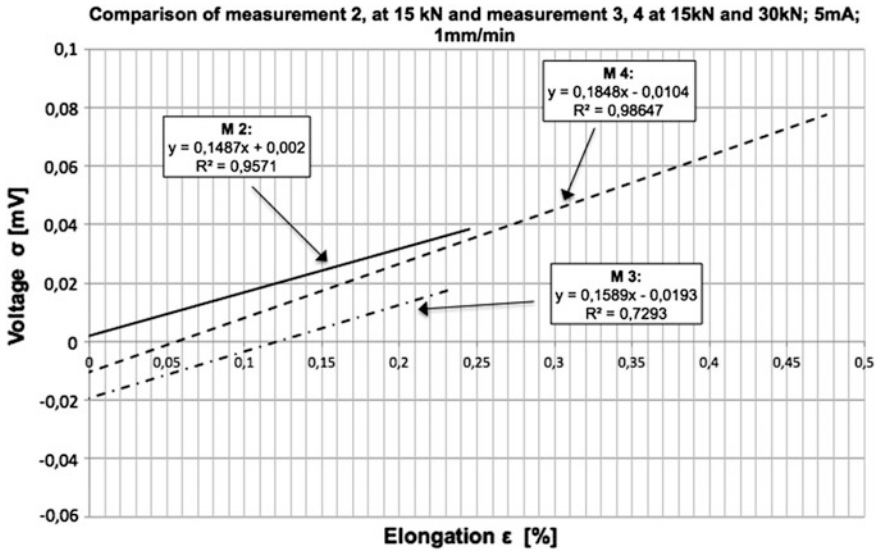


Fig. 5 Comparison of measurement 2, 3, 4 while increasing force at 15 and 30 kN

Conclusion

It can be summarized that such a constantan stranded wire integration seems to be a possible option for measuring the elongation of braided carbon fiber tubes. The sensor enables researcher a quite simple integration and quick response about the inner characteristics of the composite. The tests were performed over five cycles at 15, 30, and 60 kN already. The graphs always show a linear incline in connection of force and elongation. The graphs of measurements 4, 7, and 8 (Fig. 3) show a similar helix angle between 20° and 30°. After increasing the force from 15 to 30 kN at the same sensor, the sensor wire worked without complications. This means that 10 cycles are measurable while force gets increased. These results show a promising dynamic application flexibility, but they have to be verified profoundly. It is also easy recognizable when a sensor is broken and not longer operational. In the next step this fast detection method should be analyzed in detail. To make any statement about the type and intensity of the damage the sensor results have to be investigated in future research.

Within this particular research, sensor integration in CFRP has been tested for the first time. The results show great application possibilities, but longer test cycles and the integration systems themselves have to be improved before a needed realization and positioning in the FRP market can be reached.

References

1. AIF Forschungsnetzwerk, Mittelstand; Otto von Guericke-Preis 2015: Textilbasierte Sensoren sparen Ressourcen und sorgen, für Sicherheit; online source: <http://www.aif.de/home/detailansicht/news/otto-von-guericke-preis-2015-textilbasierte-sensoren-sparen-ressourcen-und-sorgen-fuer-sicherheit-1.html>, 13.11.15
2. Handbuch Verbundwerkstoffe: Werkstoffe, Verarbeitung, Anwendung; 2., Auflage; M. Neitzel, P. Mitschang, U. Breuer, Hanser Verlag 2014, München
3. Sensorbasierte Kohlfasertextillamierungen für Monitoring und Verstärkung, 2011; S. Käseberg; M. B. Schaller; M. Kuhne. <https://gghmbh-public.sharepoint.com/Documents/005%20Sensorbasierte%20KFT%202011.pdf>; 12.10.15
4. Ein Methodenvergleich- ZiP an Kohlefaserverbundwerkstoffen mittels Wirbelstrom- und ultraschallbasierender Prüfverfahren, M. Schulze; S. Goldbach; H. Heurer; N. Meyendorf; Dresden 2011
5. Textile Fertigungsverfahren: Eine Einführung; 2., Auflage T. Gries, D. Veit, B. Wulfhorst; Hanser Verlag 2015, München

Investigation of the Relations Between the Parameters in the Radial Braiding Process

Viktor Reimer, Su Alptekin and Thomas Gries

Introduction

Fiber-reinforced plastics have demonstrated their potential as a lightweight material for the future. However, in order for widespread use in mass production to be possible, automated processes are required. One approach for the automated manufacture of complex structures is the over braiding technology, which is characterized by its high productivity and high automation potential [1].

During the production process, the reinforcement tows (or rovings) interlace around an external core in a predefined orientation and the braided product is taken-off with a defined speed (Fig. 1). This external core is called a “mandrel,” although sometimes cylindrical mandrels are simply referred to as cores [4].

In this over braiding process tows are first wound on spools and placed on carriers, that carry them along the sinusoidal carrier path placed within the machine. The carriers are divided into two groups; clockwise and counterclockwise carriers (see Fig. 1). Radial over braiding machines usually have two braiding rings to guide the tows as they converge.

The ring must be large enough for the mandrel to pass freely through it. The presence of a second ring in the braiding zone allows braiding in the reverse direction. In this way, the braided product can be taken-off in either direction.

An industrial robot performs the take-off of the braided product. The mandrel can be automatically handled by the robot enabling integration into an automated

V. Reimer (✉) · T. Gries
Institut für Textiltechnik (ITA) of RWTH, Aachen University,
Otto-Blumenthal-Str. 1, 52074 Aachen, Germany
e-mail: viktor.reimer@ita.rwth-aachen.de

S. Alptekin
Faculty of Textile and Clothing Technology,
Niederrhein University of Applied Sciences, Krefeld, Germany

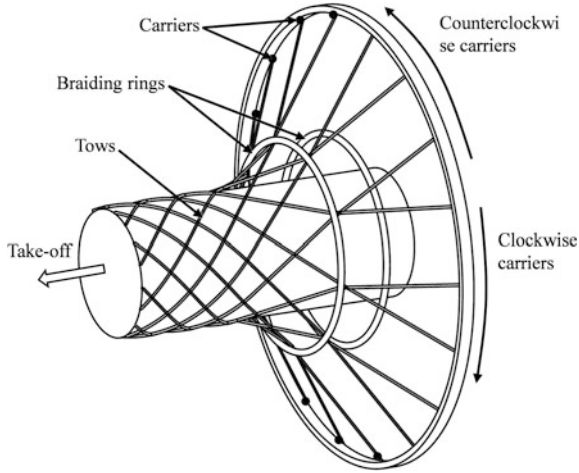


Fig. 1 Illustration of the over braiding process

manufacturing cell [1]. For many composite components it is important to provide a full coverage of the composite material and well-spread fibers, before it is taken-off by an industrial robot.

The cover factor reflects the proportional coverage of the mandrel. Along with the braiding angle, cover factor C and braid thickness are important parameters in determining and characterizing the appearance and performance of the braided structure. The cover factor is defined as the ratio of covered mandrel surface to total mandrel surface [6].

In order to determine the correct cover factor for cylindrical mandrels, a distorted bias braid structure has to be considered. The braid structure is divided into single, representative unit cells to estimate the total coverage. In this case, the braid structure is divided into single unit cells to assess the structural distortion on the mandrel (Fig. 2).

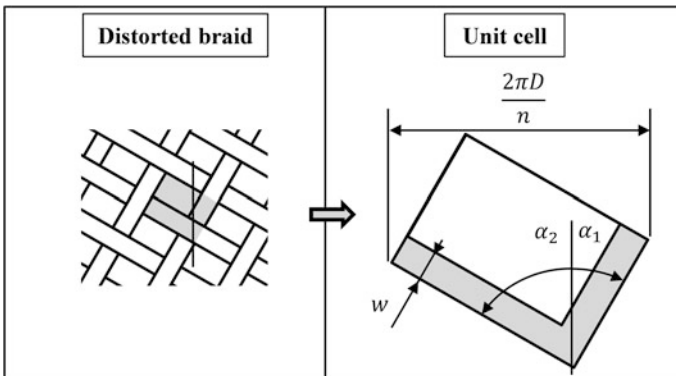


Fig. 2 An example of a distorted bias braid structure on a cylindrical mandrel

According to Rosenbaum [6], the following geometrical conditions must be satisfied in order to ensure full coverage of the mandrel with a distorted bias structure:

$$\frac{w}{\cos \alpha} = \frac{2 \times \pi \times D}{n} \quad \text{or} \quad \frac{w}{\cos \alpha} = \frac{2 \times \pi \times D}{n} \rightarrow C = 1 \quad (1)$$

As can be seen in the above relationship, tow width is an important factor in coverage. Greater tow width means better coverage of the mandrel.

A recent study “*Online tow spreading in the braiding process and its effects* [5]” examines the differences in tow width when different core diameters are used. For this experiment, machine and material parameters were held constant. According to this study, the size of a produced braid depends on three parameters: braiding angle α , tow width w and number of tows n . These three parameters determine the maximum core diameter D , which can be fully covered according to the following equation: measurement process is

$$D = \frac{w \times n}{2 \times \cos \alpha} \quad (2)$$

To take full advantage of the given mathematical Eqs. 1 and 2, the material properties have to be taken into consideration. Glass and carbon fibers have different tow widths and spreading properties and it is also important to consider the structural differences between these materials when determining the maximum core diameter of mandrel, D that can be completely covered ($C = 1$).

Full coverage of the mandrel is important as it improves the structural and mechanical quality. It is, however, not always properly attained due to lack of control over the process.

Motivation

Over braiding is a complex process with numerous controllable and uncontrollable parameters influencing the end product. The assistance of proper documentation is needed to provide better process control and in turn higher quality products. Knowing the features and limits of each machine in question is also critically required to performing process analysis.

This study analyzes the interactions between the braiding parameters in the radial braiding process and their influences on the braid geometry. The main purpose is to provide comprehensive documentation for the over braiding process, in order to help build up a process environment for a good and constant product quality.

The resulting information is intended to be used to prepare a database of optimal parameters. This database may then be used in the development of a self-optimization system for the manufacturing cell [2].

Approach

With the help of practical experiments on ITA's 2D radial braiding machine "RF 1/144-100" [3], critical influences and interactions between braiding parameters were investigated through several designed experiments and by monitoring the main influential variable: the braiding angle.

The braiding angle is of great importance as it significantly influences the final quality of the braided structures and the braid geometry. The braiding angle was monitored using a machine vision system with a camera sensor supplied by Apodius GmbH, Aachen. The measurement process is shown in Fig. 3.

Following design of experiments (DoE) principles, a central composite design (CCD) was used for the practical experiments. During these experiments the vibration frequency was found to be another critical influencing factor on mandrel coverage.

Vibration frequency controls the deposition of tows on the mandrel by influencing their distribution around the mandrel. An illustration of this effect can be seen in Fig. 4. As the tows are collected at the braiding ring, the braiding ring transmits its own vibrating motion to them. The tows are reformed and spread out as the vibration passes through them. In this way, the friction and tension caused by collision of the tows can be controlled and reduced. This function allows better and more even deposition of fibers.

The influence of this vibration frequency and the findings of recent studies were practically tested and verified with one factor at a time (OFAT) method for a more comprehensive analysis. Parameter values for control variables are shown in Table 1. The resulting braiding angle is presented as a constant parameter because all the parameters that have a direct influence on it were controlled. A braiding ring of diameter 130 mm was chosen for the 50 mm mandrel.

During the experiments, levels of the vibrating ring frequency and their influence on the braid geometry were tested. Vibration frequency ranges from 0 to 10 on an arbitrary scale, as labeled on the vibration motor control box. Only levels 5–7 were



Fig. 3 Apodius monitoring device with camera

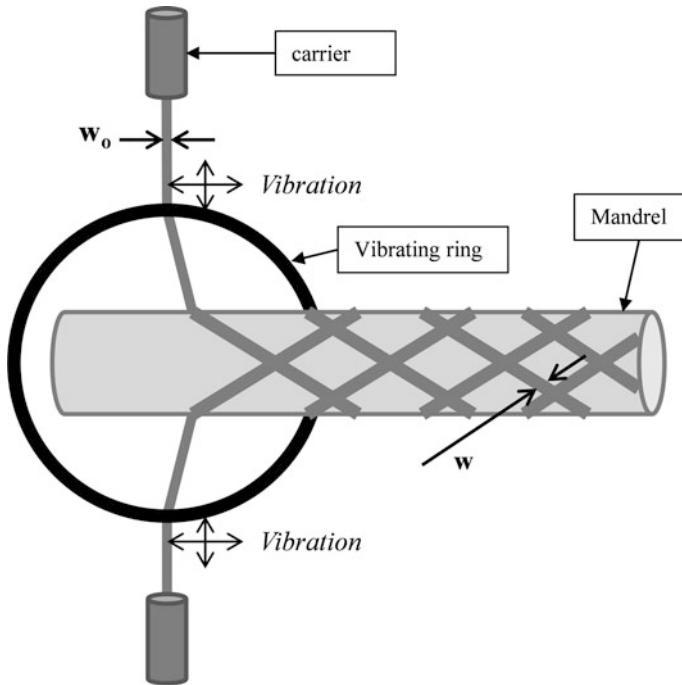


Fig. 4 Illustration of the vibration frequency of the braiding ring in the braiding process

Table 1 Parameter settings that were constant

Material	Carbon or glass
D	\varnothing 50 mm
α	45°
V_T	0.0036 m/s
$\omega_{HornGear}$	50 RPM

used in the experiments, as unsafe and destructive behavior has been observed in the machinery when operating above level 7 and no significant effect was produced when operating below level 5. Between these levels the vibration can be adjusted to create different levels of influence. Carbon and glass materials were both tested in repeated trials. In order to create situations with both closed and open structures for the experiment, the number of tows was also changed. Changing the number of tows means changing the amount of carriers and their arrangement within the machine.

Tow width measurements were performed with a Vernier caliper at 12 to 13 different points, distributed over the mandrel surface, as represented in Fig. 5. The standard deviation of the tow width was calculated from these measurements. The summary data presented in the following section takes the average of these measurements unless otherwise stated.

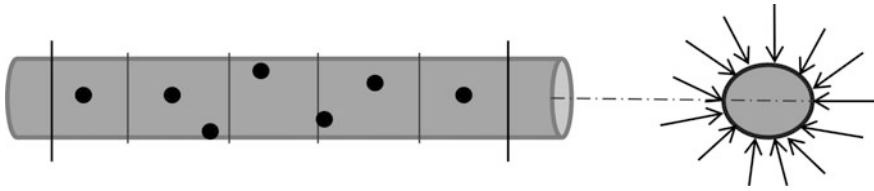


Fig. 5 Measuring tow width on the mandrel

Table 2 Experiment results with carbon and glass fibers

Vibration frequency levels (N_f)	Tow width after its deposition (w)			
	Carbon roving ($w_o = 5$ mm)		Glass roving ($w_o = 2.5$ mm)	
	With 48 carriers	With 36 carriers	With 72 carriers	With 48 carriers
5	5.01	5.13	2.44	2.73
5.5	5.25	5.23	2.46	2.98
6	5.25	5.53	2.47	3.11
6.5	5.25 ^a	5.62	2.49	3.17
7	5.25 ^a	5.84	2.59	3.32

^aFull coverage achieved with vibration frequency level 6

For each material, experiments were carried out with two different numbers of tows. Initial widths of the carbon and glass roving materials were measured directly after the bobbin winding. By comparison with this initial state, it is possible to estimate the change in tow width due to the vibration of the braiding ring. These measurements were also used to estimate the amount of tows required to create open and closed structures. A plan of the experiments was developed, the results of which are displayed in Table 2.

Results and Discussion

Vibration of the ring directly increases the tow width by spreading out the fibers, as well as distributing the tows evenly through the structure. Furthermore, if full coverage of the mandrel “ $C = 1$ ” is achieved, the tows start squeezing together and stop expanding with the influence of increasing vibration. A closed structure is then formed. When the full coverage does not take place “ $C < 1$ ”, an open structure is formed. Here, the tow width can continue expanding with the increase in vibration until its expansion stops naturally.

Under similar process conditions with both fiber materials, using fewer tows resulted in a more open structure and this allowed the tows to expand more than their original width ($w_o = 5$ mm for carbon and $w_o = 2.5$ mm for glass). The average tow

width values are shown in Figs. 6 and 7 and in Table 2. The variation according to vibration frequency is apparent when compared to the original fiber width.

The increase in carbon tow width stops for the test with 48 tows after the first vibration levels due to full coverage of the mandrel. This prevents the tows from further expanding.

To better understand tow width increase behavior, standard deviations in tow width measurements are calculated for each test. Relationship between tow width increase and standard deviation between vibration frequency levels are presented with the assistance of graphs and tables below in Figs. 6 and 7 and Tables 3 and 4.

Decrease in standard deviation was higher with vibration frequency level 7 in tests with 72 glass fiber tows and 36 carbon fiber tows (Tables 3 and 4). These results, however, are not sufficient to claim that standard deviation decreases in general with the increasing vibration frequency of the ring.

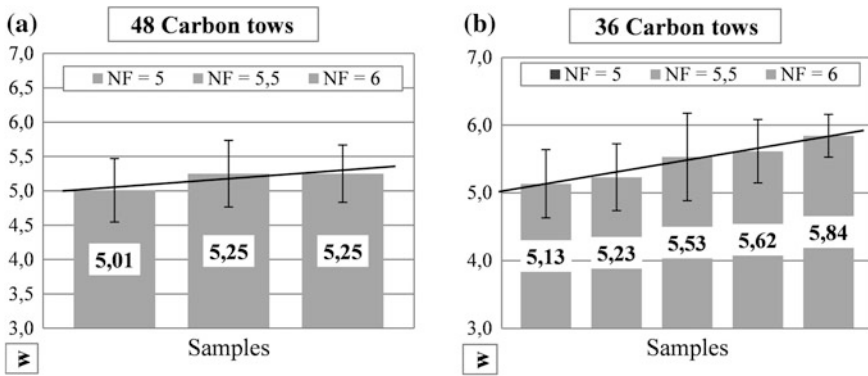


Fig. 6 Influence of vibration frequency on braiding with a 48 and b 36 carbon tows

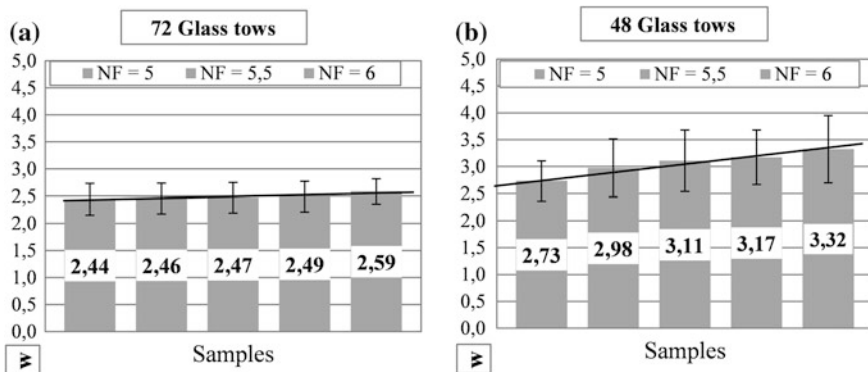


Fig. 7 Influence of vibration frequency on braiding with a 72 and b 48 glass tows

Table 3 Experiment results with 48 and 36 carbon tows

Vibrations frequency levels (N_F)	Average w 48 carbon tows	Standard deviation
5	5.02	0.46
5.5	5.25	0.48
6	5.25	0.42
Vibrations frequency levels (N_F)	Average w 36 carbon tows	Standard deviation
5	5.13	0.5
5.5	5.23	0.49
6	5.53	0.65
6.5	5.62	0.47
7	5.84	0.32

Table 4 Experiment results with 72 and 48 glass tows

Vibrations frequency levels (N_F)	Average w 72 glass tows	Standard deviation
5	2.44	0.29
5.5	2.46	0.28
6	2.47	0.28
6.5	2.49	0.28
7	2.59	0.23
Vibrations frequency levels (N_F)	Average w 48 glass tows	Standard deviation
5	2.73	0.32
5.5	2.98	0.54
6	3.11	0.57
6.5	3.17	0.51
7	3.32	0.62

An example of the over braiding results with 36 carbon fiber tows is shown in Fig. 8. The effect of the vibrating ring is visible on the figures.

Another example to stress the effect vibration frequency level has on the braid structure is shown in Fig. 9. In this example, two extreme cases are presented for over braiding with 72 glass fiber tows: braiding with vibration frequency level of 7 and braiding without any vibration. The effect of the vibrating ring can be plainly seen in these images.

In conclusion, vibration frequency has a significant influence on braid coverage. Higher frequency levels are recommended, when applicable, as they provide a more uniform structure with less of the structural deformations that are caused by uncontrollable parameters. For this choice, the individual influences of each vibration level, motion dynamics of the vibrating ring, changing properties of the fiber material need to be considered.

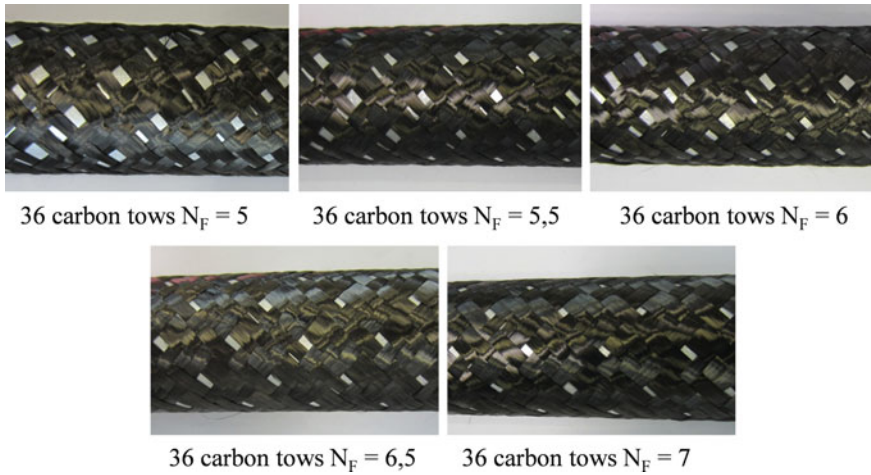


Fig. 8 Cover factor for braiding with 36 carbon tows

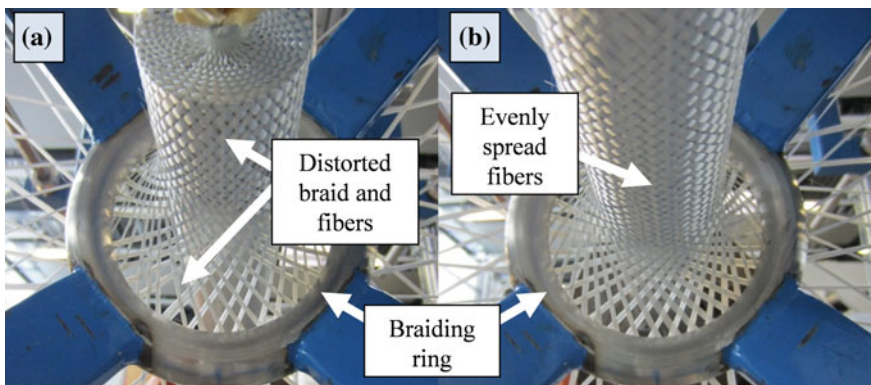


Fig. 9 Influence of the vibration frequency on the process: **a** without vibration, **b** with vibration of level 7

Acknowledgement This research was carried out as part of the cluster of excellence “Integrative Production Technology for High-Wage Countries,” funded by the German Research Foundation (DFG).

References

1. B. Fabich, M. Linke, T. Gries, Overbraiding technology for economic mass production of textile preforms, in *ITMC international conference* (Aachen, 2011)
2. T. Gries, V. Reimer, B. Kuckhoff, M. Lengersdorf, J. Schaefer, Self-optimization of the radial braiding process. (2015), <https://www.produktionstechnik.rwth-aachen.de/go/id/hpfz/lidx/1>. Accessed 5 Apr 2015

3. Herzog. (n.d). Herzog braiding machines, http://www.herzog-online.com/_rubric/index.php?rubric=Products+Composites+EN. Accessed 5 Mar 2015
4. Y. Kyosev, *Braiding Technology for Textiles* (Woodhead Publishing, UK, 2015)
5. M. Mitwalsky, Online tow spreading in the braiding process and its effects, in *SAMPE Europe 35th international conference and forum* (München, 2014)
6. J.U. Rosenbaum, *Flechten: Rationelle Fertigung faserstaerkter Kunststoffbauteile* (TÜV Rheinland GmbH, Köln, 1991)

Narrow Woven Fabrics Applied for Conveyor Facilities

I. Berbig, D. Holschemacher, C. Kern and M. Michael

Keywords Weaving · Warp · Weft · Non-textile elements · Chain · Narrow fabric

Introduction

Technical textiles have a wide range of applications. So you are able to use the good mechanical conditions and also the individual shaping. For more features there is a step further in functional integration of the textile. Regarding to applications in conveying industry textile mechanical components are referred different requirements.

Therefore textile will not be only textile. For function extensions the manufacturing process has to be changed. Additional mechanisms have to be installed. In the following part there are information, what has to be done to integrate non-textile elements into a weaving. It is divided into the warp and weft direction.

Functions which are suitable for warp direction are transmission of energy, signals, forces, etc. It is possible to create a very thin textile for applications where it is necessary to have a very low bending ratio. Possible functions for weft direction are the usage as a chain, the integration of sensory element. So it is possible to know something about the current position in a mechanism [3].

I. Berbig · D. Holschemacher (✉) · C. Kern · M. Michael
Endowed Professorship of Technical Textiles and Textile Mechanical Components,
Chemnitz University of Technology, Chemnitz, Germany
e-mail: david.holschemacher@mb.tu-chemnitz.de

I. Berbig
e-mail: ingo.berbig@mb.tu-chemnitz.de

C. Kern
e-mail: colin.kern@mb.tu-chemnitz.de

M. Michael
e-mail: markus.michael@mb.tu-chemnitz.de

To produce textiles which have been mentioned you have to fit the weaving machine. This has to be done at the supply of the warp, at the heald frames, at the batten, at the weft insertion, at the take down and at the healds.

Objectives

- Adaption of a textile machine
- Integration of functions into moving textile tension and suspension elements
- Function extension of technical textiles
 - Transport of energy
 - Accurate pitch for transmission
 - Integration of sensory elements
 - Bundling of reinforcement elements
 - Construction of narrow textiles which are used for bending technologies

Motivation

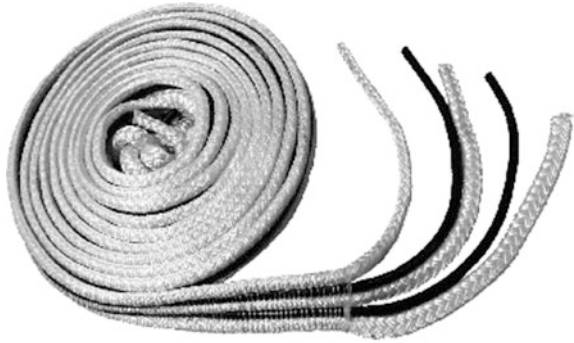
Technical textiles get more and more popular in the bright field of mechanical engineering. There is a design variety, which allows having a lot of functions and fields of application. It is precisely this design variety that can be improved by the integration of additional non-textile elements.

Warp Direction Development of a Multiple-Functional Narrow Fabric

The development of a multi-functional narrow fabric (cf. Fig. 1) to be used as a tension member in a winch has been performed. This narrow fabric enables to join several functional elements, e.g. electric conductors, in one mechanical component. Development of the design of the woven structure and development of the purpose-built manufacturing technology have been the main focusses, in case of the narrow fabric [2].

The special challenge is to apply particularly light and equally powerful tension and suspension elements. These narrow fabrics not only need to withstand the enormous loads of winding, but also maintain their function. This function divides in the mechanics of winding and the function of energy and signal transmission. Further, the textile tension and suspension elements need to be sufficiently equipped so that they are resistant to external influences such as humidity, insolation, precipitations, aggressive media (mining), etc. It is only the implementation of these requirements that enables the application in a winch.

Fig. 1 A multi-functional narrow fabric assembling tension and suspension members, signal transmitters and energy lines in one single element [2]



Dimensioning of the Functional Elements

The selection of the functional conducting paths is based on the ratings of the current and voltage to be transmitted. The special case works with 24 V. To reduce voltage drops as well as the heating of the conductor to a minimum, the conductor cross section was specified to 10 mm^2 , which constitutes the limit of what is currently technically feasible in the manufacture. Principally, solely flexible elements qualify as conductors. In this field, particularly cables for energy chains are easily available for purchase. Further requirements are the resistance to climatic influences, such as UV radiation, humidity or wetness, a wide operating range at varying temperatures and ideally also a certain resistance to tensile loads and torsion. For the tensile elements, conventional materials such as polyester were used. At this point, it was important to find suitable materials for the arrangement in the fabric composite. Similarly significant is the investigation of further influences such as the preload for the weaving process and the geometrical situation. Since the fabric composite is also composed of polyester in warp and weft direction, the variation of the parameters is solely limited to the geometry and the used conducting paths. The rope diameter of 12 mm was chosen to be larger than that of the conducting paths. In this way, the loads, which are induced to the entire composite in transverse direction, can be absorbed by the tensile element. Here, 12-strand single-braids with two strands per carrier are used. An additional sheath construction is not yet foreseen. Moreover, the fabric composite leads to an increase of the transverse rigidity.

Construction of the Narrow Fabric

The narrow fabric (cf. Fig. 2) corresponds to the following structure: Tension members in the form of braided ropes alternate with electrical cables. Due to the larger cross-sectional area of the rope, load relief of the electrical cables during potential bending or winding is ensured. The fabric is built in such a way that any



Fig. 2 Schematic cross section illustration (*left*), fabric composite for preliminary tests (*right*) [1, 2]

additional elements are equally joined in warp direction. The plain weave is used as the prevailing weave. In so doing, stratification can be avoided. If warp raising or lowering is exchanged for the adjacent elements (rope and cable), the danger of layer formation arises. The adjacent ropes are pulled together to such an extent due to the weft yarn tension so that the ropes might arrange on top of each other. For later use, this case must be eliminated. The weft density was chosen to be 4/cm.

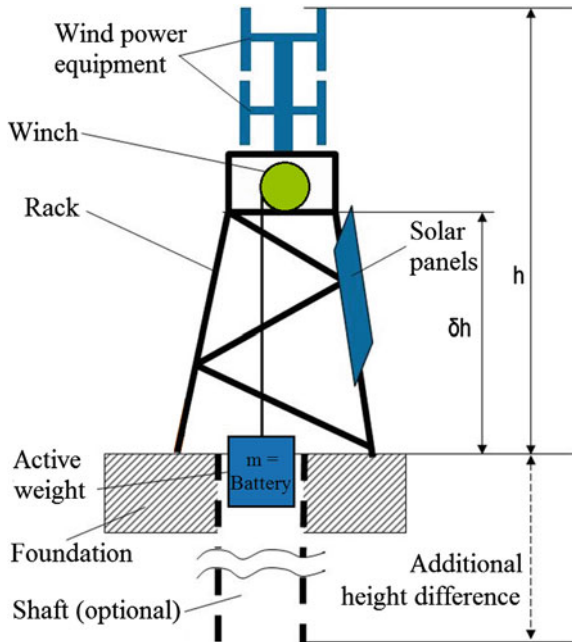
Manufacture of a Multi-Functional Narrow Fabric

The production of a multifunctional narrow fabric requires special technology. In the course of the production, high demands occur particularly on the weaving machine regarding the flexibility of mechanics and control. In the context of the manufacture of a multifunctional narrow fabric, the integration of the functional elements to the weaving process also proves to be particularly critical. While the ropes being a load-bearing element need to be pretensioned before their integration, the cables being a non-load-bearing element can be processed without any pretension. At the same time, it is necessary to realize a preferably symmetrical shedding. This problem was solved by the targeted selection of different guide tracks through a stretching unit. In comparison to warp and weft yarns, the functional elements have considerably larger diameters and bending strengths, which also require certain adjustments: Special heddles need to be developed, the process of the deduction is to be adapted to the limited mechanical resilience of the cables integrated in the fabric composite and the provision of the functional elements requires a respective specialized creel.

Example of Application

A mechanic short-term storage is achieved by a rope winch with a hoisting height of 24 metres. This winch is attached to the pedestal of a hoisting pole and operated with a load of 240 kg in winch operation as well as in alternator operation. The specific challenge is to combine the load with an additional function. In this special case there is an active weight combined with the winch (cf. Fig. 3).

Fig. 3 Model of a pilot power plant with operating winch [2]



Weft Direction Development of a Narrow Fabric as a Part of a Mechanism

The second example is the development of a narrow fabric which can be used as a part of a mechanism. This narrow fabric enables the good performance of a weaving in warp direction with the additional function in weft direction. This function enables the positive connection between power unit and output of a mechanism. The challenge is to apply very good performance, low lengthening and high power-transmission in warp direction and the possibility to initiate power in a defined sector of the narrow fabric in weft direction in form of non-textile elements. These narrow fabrics not only need to withstand the enormous loads of bending, but also maintain their function in form of accurate pitch. Further, the textile elements need to be sufficiently equipped so that they are resistant to influences such as aggressive media occur in mechanisms. Additional to this, these textiles need the ability to create a very strong contact between textile and non-textile elements [4].

Construction of the Narrow Fabric

At first you have to find a weaving form that fits into your strain scheme. So the binding along the warp direction has to be constructed based on the application. This example includes a six layer weaving. All the layers alternate from up to down

and in the opposite direction. This construction has a very good bending behaviour and also a good basis for integration of additional elements in weft direction. To integrate the non-textile elements it is necessary to adapt the shed. The time for the integration has to be special fixed. The element has to be hold until the shed is changed into a new one. Then, it will be fixed by a new weft insertion. The take-up motion is adapted to the new product. So it is possible to pull the textile positive fitted. The frequency of the insertion of the non-textile elements and the form of the take-up motion has to be adjusted exactly. The following figure shows the symbolic structure of the new textile (Fig. 4).

Example of Application

One sector of materials handling is the transportation of goods. Pieces have to be transported from one place to another. One of these possibilities is a chain conveyor. This technology is constructed for its special task. For some goods, it is possible to divide the tasks of the conveyor into two functions. The first one is the carrying of the goods. This could be realized by boards made out of synthetic material with low coefficient of sliding friction. The second one is the force transmission. This task is in unity to the positive fitting impulse. Altogether both tasks have to be combined [4] (Fig. 5).



Fig. 4 Weaving with non-textile elements [4, 5]

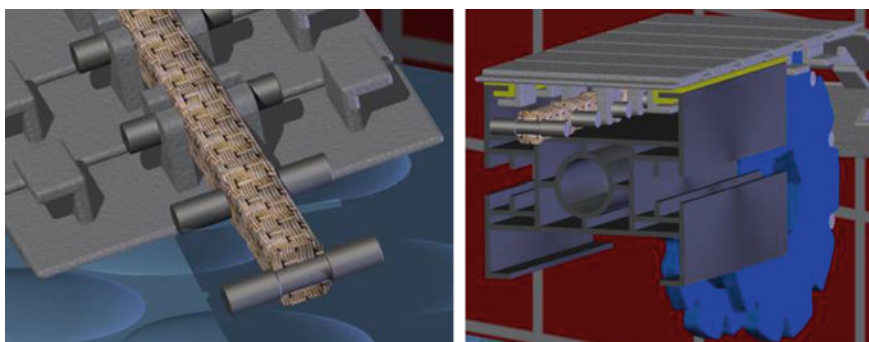


Fig. 5 Model of the chain conveyor [4, 5]

Conclusions

It is possible to enlarge functions of narrow fabrics. It is to be distinguished between warp and weft direction. Suitable for warp direction are the inclusion of wires for energy, signals, forces, etc. The creation of a very thin textile for applications where it is necessary to have a very low bending ratio is a second possibility. To enlarge the functions in weft direction are the usage as a chain and the integration of sensory element. So it is possible to know something about the current position in a mechanism. To get all this technologies you have to adapt the weaving technology in the described way. There are a lot of parts, which have been modified along the warp direction. Also the parts for the weft direction have to be changed.

References

1. I. Berbig, T. Schneiderheinze, M. Michael, D. Holschemacher, Development of multi-functional narrow fabric as tension member for winch operations. in Airborne wind energy conference proceedings 2015, S. 74, ISBN 978-94-6186-486-4 15–16 June 2015
2. D. Holschemacher, I. Berbig, T. Schneiderheinze, M. Michael, Peak shaving for renewable energy systems. in International conference on renewable energy sources and sustainability (RESUS 2015), Conference proceedings (CD) S. 219–224, 3–5 Mar 2015
3. T. Heinze, M. Michael, Entwicklung und Herstellung leistungsfähiger Zug- und Tragmittel in Leichtbauausführung, Euroseil, Fachzeitschrift Ausgabe 2/2008, S. 22, ISSN 0323–3243, September 2008
4. I. Berbig, M. Michael, K. Nendel, Hochleistungstextilien mit Funktionselementen für den Maschinenbau, 12. Chemnitzer Textiltechnik-Tagung, Tagungsband, ISBN 978-3-9812554-3-0, 30.09. und 1. Mar 1. Oct 2009
5. I. Berbig, S. Subbert, E. Putzke, Prof. Klaus Nendel, Innovative Zug- und Tragmittel für die Fördertechnik, 5. Fachkolloquium der Wissenschaftlichen Gesellschaft für Technische Logistik (WGTL), Tagungsband, ISBN: 978-3-939473-56-5, 01. und 2. Oct 2009

Multilayer Textile-Based Woven Batteries

Marina Normann, Yordan Kyosev, Andrea Ehrmann
and Anne Schwarz-Pfeiffer

Abstract In recent years, conventional garments and electronic components have been combined to produce wearable diagnostic systems for monitoring vital signs in medical applications, or novel fashion effects, visual displays, or audio and computing systems. Another area of interest is the integration of sensors and actuators into fibers as the development of high efficiency conducting polymer actuator fibers and conducting polymer fibers with chemical sensing is about to be realized. Sophisticated smart textiles and wearable systems will, however, require wearable energy-storage capabilities. There is a great need to develop fiber-based batteries that contribute to a deeper integration of active smart components in textiles and hence to realize a stand-alone smart textile system. We followed this approach and present in this paper our first results on textile-based batteries. We used combination of different metal coated textile structures serving as electrodes. On both electrodes thin gel-like layers of gelatine-based electrolyte filled with a metal salt were applied. Finally, I-V curves of different structures were measured.

Keywords Gelatine · Natural electrolyte · Flexible battery · Conductive fabric · Smart textiles

Introduction

The overall goal is to develop flexible and drapable 3D batteries, made of textile materials and evolving the vision of self-sustaining smart textile systems to become reality. The need arose from several technological, economical and societal trends

M. Normann · Y. Kyosev · A. Schwarz-Pfeiffer (✉)
Faculty of Textile and Clothing Technology, Niederrhein University
of Applied Sciences, Mönchengladbach, Germany
e-mail: Anne.Schwarz-Pfeiffer@hsnr.de

A. Ehrmann
Faculty of Engineering Sciences and Mathematics, Bielefeld University
of Applied Sciences, Bielefeld, Germany

that can be observed already today and which are predicted to increase tremendously within the next 30 years [1].

Our day-to-day lives in the future will be significantly regulated by smart devices and many of these devices will be integrated in textiles and clothing. Research and development in smart wearable systems and applications for personalized services, especially for health purposes, have significantly increased worldwide over the last years [2]. In order to drive the electronics in a smart wearable textile system, energy storing technology is needed. There are three main electrochemical energy storing technologies used in wearable systems: electrical double layer capacitors, pseudo capacitors, and batteries [3].

A battery can convert stored chemical energy to electrical energy. Just like conventional batteries a textile battery has a cathode as the positive electrode and an anode as the negative electrode. It has an electrolyte which makes the cations and anions move towards the cathode and the anode, respectively. It also has a separator which separates the anode and the cathode [4]. Several researchers worldwide currently explore the potential of textile-based batteries. The electrode materials being used for this purpose range from copper and aluminium wires [5, 6], and nickel-coated yarns [7], to carbon-based textiles [8, 9] to polypyrrole coated textiles [10].

To be of practical use in textile applications, the envisaged electrolyte needs to be gel-like or solid. Especially gel electrolytes have satisfying ion conductivity and combine good interfacial properties from the liquid phase with good mechanical properties from the solid components [11]. Additionally, in most cases a separating membrane can be avoided as the gels take over the separating function.

However, the majority of existing textile battery solutions uses a blend of polymer electrolytes in combination with organic solvents. These organic solvents are poisonous and caustic; therefore they do not fit well with wearability [12]. Based on this fact, we decided to exploit electrolytic layers for textile batteries which are based on biological compounds and are water soluble.

In this paper, we present the development of textile batteries, comprising copper and nickel coated textiles as electrodes. Both textiles were coated with thin layers of gelatine containing either copper sulfate or nickel sulfate, respectively. After coating, the electrode-electrolyte hybrid structures were sandwiched together. In order to investigate their battery performance, I-V curves were plotted. The results are presented and discussed in this paper.

Experimental

Materials

Electrode Materials

Copper and nickel coated fabrics were used as electrode materials. Both materials were purchased from Less EMF. The copper coated textile has a polyester taffeta

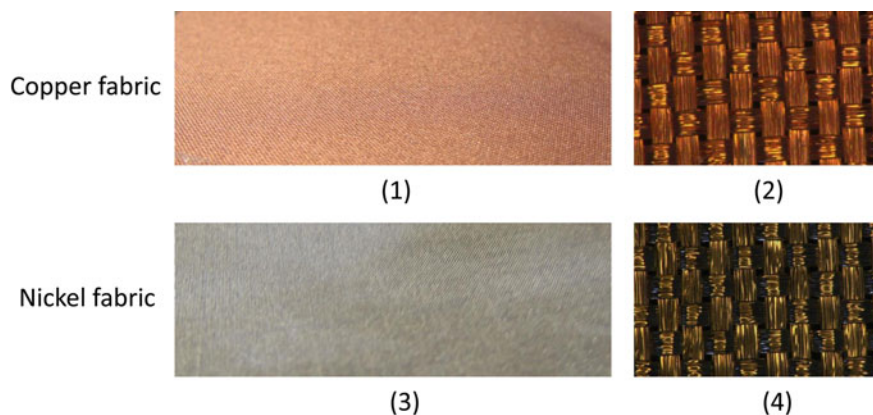


Fig. 1 Copper and nickel coated fabric used as electrode materials, purchased from Less EMF (magnification of pictures on the right 100x)

fabric as base. It has a thickness of 0.08 mm with a weight of 80 g/m² (about 35 % copper). The electrical resistivity R_{square} amounts to 0.05 Ω .

The nickel coated textile is a woven ripstop fabric, having polyester as a base. The thickness is 0.08 mm with a weight of 90 g/m². The electrical resistivity is R_{square} 0.03 Ω .

Both materials are shiny, smooth, light, flexible and highly conductive (Fig. 1). They were cut into rectangles with a length of 5 cm and a width of 4 cm, with an extended tap on the upper side of 1 × 1 cm to allow a proper fixing of clamps to measure the current and voltage output (Fig. 1).

Gel-like Electrolytes

The electrolytic layer is based on commercially available gelatine, powdered and white in colour from Dr. Oetker GmbH. 9 g of gelatine powder were dissolved in 25 ml of demineralized water. After a swelling time of 10 min, 100 ml of demineralized water were added. The mixture was heating up to 90 °C. Subsequently, the gelatine mixture was removed from the heat source and 9.97 g of copper sulfate (purchased from Sigma Aldrich, analytical grade) were added and constantly stirred by magnetic stirrer until the copper sulfate was dissolved to result in a 0.5 M solution. Subsequently, the copper sulfate/gelatine mixture was poured into a Teflon[®]-coated form with a dimension of 20 × 20 cm and hardened. The resulting gel film with a thickness of 3 mm was dismantled and cut into rectangles with a dimension of 4 × 5 cm. The same procedure was followed to prepare the gelatine/nickel sulfate electrolyte gel. 9.67 g of nickel-sulfate (purchased from Sigma Aldrich, analytical grade) were added to 125 ml of water to result in a 0.5 M solution.

Methods

Assembly of Cells

Cells were assembled in a conventional symmetrical two electrode setup. The two half cells were produced separately. The copper sulfate electrolytic gel layer and the nickel sulfate electrolytic gel layer were manually placed and pressed onto the copper and nickel coated fabrics, respectively. Having a copper electrode/copper sulfate electrolyte half-cell on the one hand and, on the other hand, a nickel electrode/nickel sulfate electrolyte cell, it was possible to sandwich both structures together (Fig. 2). The adhesive properties of the gelatine allowed the sandwiched structure to firmly adhere.

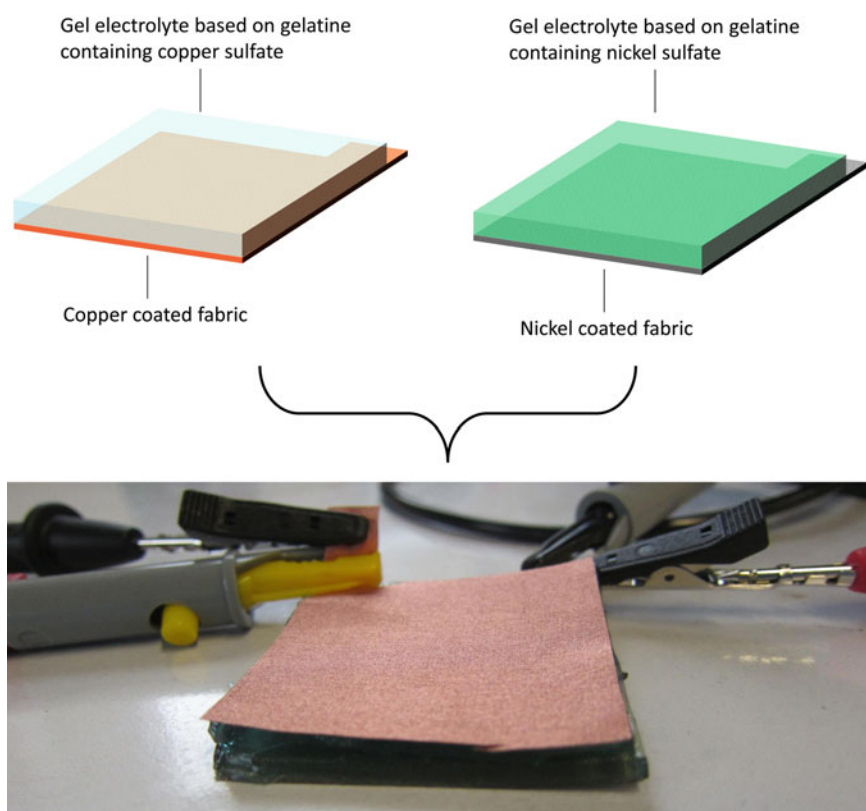
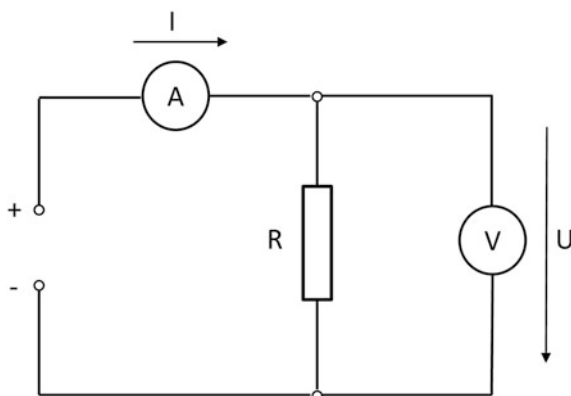


Fig. 2 Preparation and set-up of the textile cell; both electrodes were coated with layers of gelatine containing a corresponding metal salt and were subsequently sandwiched together

Fig. 3 Schematic of electrical circuit to investigate the current—voltage characteristics using variable loads



Measurements of Current and Voltage

In order to evaluate the battery performance, the current-voltage characteristics using a variable resistor were analysed. The set-up consisted of two digital multimeter, type Voltcraft VC820-1 and type Mastech MS 8233EL, to record the voltage and current of the cell when being connected to variable resistor, resistance decade type VOLTCRAFT[®] R-BOX01. The device provides a variable amount of resistance ranging between 1 Ω to 50 k Ω in the circuit, thereby acting as a load. A schematic of the measurement configuration is shown in Fig. 3.

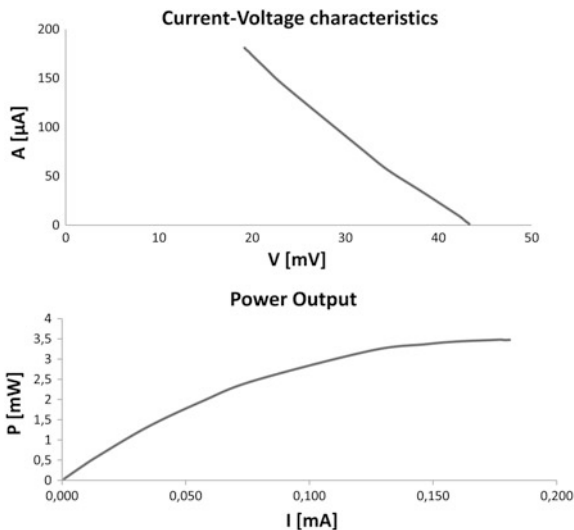
Results and Discussion

Current-Voltage curves as well as the power output curves are important characteristics for energy generating systems. The first gives the terminal voltage provided by the electrochemical cell as a function of the discharge current. The power curve shows power as a function of voltage.

Figure 4 (upper panel) illustrates a typical current-voltage curve of one of the assembled cells. The expected behaviour, that the voltage will drop if current is withdrawn from the system, can be clearly seen. The open-circuit voltage is measured to be 44 mV. The graph further shows that the cell provides a constantly decreasing voltage under different loads. When a load of 1 Ω is applied the cell voltage amounts to 19.2 mV.

The product of current and the accompanying terminal voltage is the electric power delivered by the battery system at any time. The delivered power as a function of current, and hence with decreasing load, is given in the bottom of Fig. 4. It seems like a saturation level and hence, a maximum power point is reached at around 3.4 μ W.

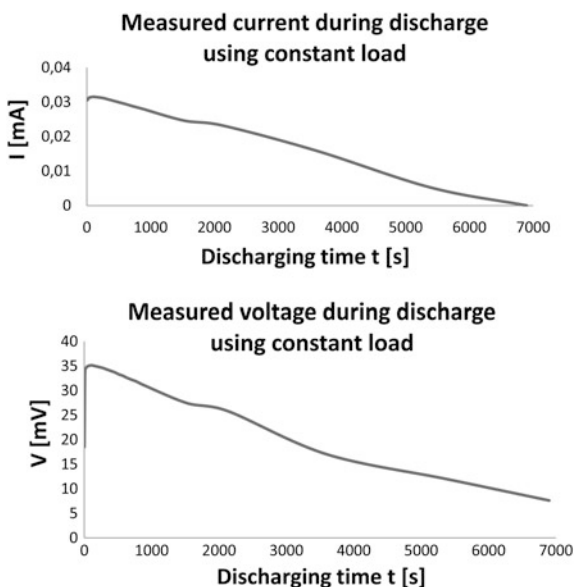
Fig. 4 Current voltage and power output curve of a representative textile nickel—copper battery with a dimension of 5 cm × 4 cm 0,6 cm (length × width × heights)



In order to investigate the capacity of the battery, the cell was discharged using a constant load of 1 $k\Omega$. The corresponding voltage and current curves are displayed in Fig. 5. These experiments result in approximately 16 μAh or 0,48 μWh , respectively.

Under equilibrium conditions the potential difference ε_0 corresponds to the terminal voltage of the cell. Taking a look to the standard electrode potentials E_0 of copper and nickel, which are 0.52 V and -0.25 V respectively, theoretical terminal

Fig. 5 Measured current and voltage value during discharging using a constant load of 1 $k\Omega$



voltage of 0.77 V can be achieved. The measured open-circuit voltage of our system amounts to 7.6 mV. The considerable discrepancy of this result to the theoretical terminal voltage value was also stated by other research groups [3]. Reasons for this outcome might be that the electrode structure may cause problems. Compared to a metal plate, a metal coated textile surface is rough in appearance with open pores between the interlacing warp and weft threads. Hence, the constructed fabric may possess a too low density and the adhesion between the electrode and the electrolyte therefore suffers.

Conclusion and Outlook

In this paper we present our initial results on textile-based batteries. We were able to demonstrate a working textile battery based on copper and nickel. The assembled cells have an open-circuit voltage of 44 mV and a maximum power output of 3.4 μ W.

Future work will now concentrate on improving the battery performance. For this purpose, the electrolyte will directly be printed onto the textile electrode to improve the adhesion. Above that, the electrolytic layer thickness will be progressively decreased using appropriate knives of a hand coating machine. On the longer run, we will substitute nickel by other metals, such as zinc. However, for this purpose a proper coating procedure has to be established.

Last but not least, first weaving trials were performed to result in a narrow fabric 3D jacquard multilayer woven structure in which the nickel and copper yarn electrode layers are separated by a conventional textile layer. The next steps will lead towards solutions on how to integrate the electrolyte.

Acknowledgement This work was carried out in the scope of an internally funded project at Niederrhein University of Applied Sciences. The authors would like to thank Niederrhein University of Applied Sciences for their financial support.

References

1. A. Schwarz, L. Van Langenhove, P. Guermonprez, D. Deguillement, A roadmap on smart textiles. *Text. Prog* **42** (2011)
2. Y.K. Kim, A.F. Lewis, Concepts for energy-interactive textiles. *MRS Bull.* **28**, 592–596 (2003)
3. K. Jost, G. Dion, Y. Gogotsi, Textile energy storage in perspective. *J. Mater. Chem. A.* **2**(28) 10777.(2014). doi:[10.1039/c4ta00203b](https://doi.org/10.1039/c4ta00203b)
4. SA. Odhiambo, de Mey G, C. Hertleer, A. Schwarz, L. van Langenhove, Discharge characteristics of poly(3,4-ethylene dioxothiophene). Poly(styrenesulfonate) (PEDOT:PSS) textile batteries; comparison of silver coated yarn electrode devices and pure stainless steel filament yarn electrode devices. *Text. Res. J* **84**(4), 348. doi:[10.1177/0040517513481871](https://doi.org/10.1177/0040517513481871)

5. Q. Hang, B. Jean-Pierre, R. Julien, V. Alexandru, G. Jean-Francois, S. Makssim (2015) Flexible fiber batteries for applications in smart textiles. <http://arxiv.org/ftp/arxiv/papers/1301/1301.1266.pdf>. Assessed 1 Nov 2015
6. H. Qu, O. Semenikhin, M. Skorobogatiy, Flexible fiber batteries for applications in smart textiles. *Smart Mater. Struct.* **24**(2), 1 (2015). doi:[10.1088/0964-1726/24/2/025012](https://doi.org/10.1088/0964-1726/24/2/025012)
7. Y. H. Lee, J. S. Kim, J. Noh, I. Lee, H. J. Kim, S. Choi, J. W. Choi, Wearable textile battery rechargeable by solar energy. *Nano Lett.*, **13**(11), 5753–5761 (2013)
8. S. Lakshmi, Scientists create weavable Li-ion fiber battery yarn. *J. Nanolett.* May 30, 2014 <http://www.gizmag.com/weavable-li-ion-fiber-battery-yarn/32332/>. Accessed 1 Nov 2015
9. K. Jost, C.R. Perez, J.K. McDonough, V. Presser, M. Heon, G. Dion, Y. Gogotsi, Carbon coated textiles for flexible energy storage. *Energy Environ. Sci.* **4**(12), 5060 (2011). doi:[10.1039/c1ee02421c](https://doi.org/10.1039/c1ee02421c)
10. R. Xu, J. Wei, F. Guo, X. Cui, T. Zhang, H. Zhu et al. (2015) Highly conductive, twistable and bendable polypyrrole–carbon nanotube fiber for efficient supercapacitor electrodes. *RSC Adv* **5**(28), 22015–22021. doi:[10.1039/c5ra01917f](https://doi.org/10.1039/c5ra01917f)
11. Y. Wang, W.H. Zhong Development of electrolytes towards achieving safe and high-performance energy-storage devices. A review. *ChemElectroChem* **2**(1), 22–36 (2015). doi:[10.1002/celec.201402277](https://doi.org/10.1002/celec.201402277)
12. Y. Liu, S. Gorgutsa, C. Santato, M. Skorobogatiy, Flexible, solid electrolyte-based lithium battery composed of LiFePO₄ cathode and Li₄Ti₅O₁₂ anode for applications in smart textiles. *J. Electrochem. Soc.* **159**(4), A349. doi:[10.1149/2.020204jes](https://doi.org/10.1149/2.020204jes) (2012)

Part IV
Materials and Modifications

Chinese HMPE Fibers in Textile Semi-finished Parts—A Competitive Price–Performance Analysis

Jens Mammitzsch, David Häser and Andreas Kretschmer

Abstract High-modulus polyethylene fibers are well-known in manufacturing of composites, e.g., for armoring shells, lightweight structures, and textile-reinforced composites, and textile-based mechanical components for technical applications. Due to the appearance of several HMPE fiber types from Korea and China at the market of HMPEs, new materials are available for manufacturing textile-based composites. A challenge is that there is no independent data on the mechanical properties or on the performance of such fibers in technical applications. The University of Chemnitz in Germany has carried out investigations on the strength and the behavior of textile semifinished parts (fiber ropes) in technical applications, because especially the Chinese fibers are less expensive than well-known non-Chinese fiber brands. A final comparison of the costs of textile manufacturing of braided ropes led to a comparison of the price–performance-relation.

Introduction

HMPE fibers are becoming more and more important for technical applications, e.g., composite manufacturing, protective textiles, and mechanical components for conveyor applications and engineering applications. Approaching engineering applications from an economical point of view, it is clearly visible that not only the performance properties are important for successfully applying HMPE fibers in such applications. The costs of the fiber materials are also influencing decision making, especially under the focus of estimated costs for overheads, maintenance, and replacement of the textile-based component or composite part. For introducing

J. Mammitzsch (✉) · D. Häser
Endowed Professorship of Technical Textiles and Textile Mechanical Components,
Technische Universität Chemnitz, Chemnitz, Germany
e-mail: jens.mammitzsch@mb.tu-chemnitz.de

A. Kretschmer
Professorship of Materials Handling and Conveying Engineering,
Technische Universität Chemnitz, Chemnitz, Germany

textile semifinished part, e.g., a fiber rope, into applications with intense competition on the market, economic key figures have to be taken into account, in addition to the mechanical properties. Main goal of the work was to perform competitive investigations with a focus on mechanical properties between leading fiber brands (Dyneema[®] SK75, Spectra[®] S1000) and two HMPE fiber brands that have been manufactured in China (TNX[®], Eosten[®] FT093). These competitive investigations are including tests on the tensile strength of yarns in state of delivery and yarn-on-yarn abrasion tests based on ASTM D 6611 on twisted strands. Tensile tests on semifinished parts, in this case braided fiber ropes with similar rope design, as well as cyclic bend over sheave tests (CBOS tests) on fiber ropes and investigations on the capability of increasing the strength of textile structures (braided fiber ropes) by thermomechanical treatment are completing the investigations on the mechanical properties. In the end, the mechanical parameters are related to the costs of the fiber materials to have a comparison with economical focus.

Tensile Tests on Filament Yarns

The investigations have been started with tensile tests on yarns. All fibers have been provided with a comparable linear density to make sure that effects due to the yarn dimensions can be disregarded. Table 1 is displaying some of the properties of the yarns, as these properties are given in the data sheets for the selected HMPE yarns.

The tensile test on yarns has been performed according to DIN EN ISO 2062 [1], with a free sample length of 500 mm and a testing speed of 500 mm/min [1]. For calculating the tensile strength in N/mm², the material density of all fibers has been determined in accordance with ASTM D 3800 [2].

As shown in Fig. 1, the mean values of the tensile strength did not fit the values given in the data sheet, for all of the tested fibers. Since none of the manufacturers is giving details on the testing procedure and the size of the specimen, used for determining the tensile strength given in the data sheets, a comparison between the measured values and the values given in data sheets is improbable.

Further, it can be seen that the deviation of the values is higher for the Chinese fibers, compared to the fibers from the USA and the Netherlands. For the fiber

Table 1 Properties of the HMPE yarns

Fiber material	Dyneema [®] SK75	Spectra [®] S1000	TNX [®]	Eosten [®] FT093
Tensile strength [N/mm ²]	3400	3040	3250	2700
Country of origin	The Netherlands	USA	China	China
Linear density [dtex]	1760	1778	1780	1760
Price [€/kg]	45.00	approx. 50.00	30.00	22.50

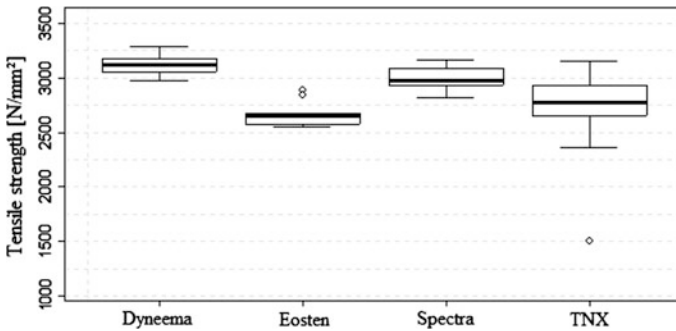


Fig. 1 Tensile strength of HMPE filament yarns

TNX[®], one sample failed at about 55 % of the mean value. These effects might be due to a more stable manufacturing process, in case of the fibers from the USA and the Netherlands.

Yarn-on-Yarn Abrasion Tests

Yarn-on-yarn abrasion tests have been carried out, based on the standard ASTM D 6611 [3], for determining the abrasion resistance of the yarns, and for investigating the possibilities for estimating the lifetime in CBOS tests for fiber ropes. For enabling a load scenario close to the real application, when using a braided fiber rope, it has been chosen to have two changes in the setup, varying from ASTM D 6611:

- Instead of single filament yarns, specimen of the strands, as used for braiding the ropes, have been used in the yarn-on-yarn abrasion test. For this, seven yarns have been twisted at 25.8 TPM to form one strand. The linear density of these strands was about 1230 dtex, what is accepted in ASTM D 661, as long as noted in the testing protocols.
- Instead of one or three full interwraps of the yarns, as specified in ASTM D 6611, only half an interwrap (180 °) has been applied to the strands. This setup has been considered to be closer to the real contact conditions in a fiber rope.

The strands have been loaded at 1 % of their theoretical break load, while performing 67 cycles per minute, what is in full accordance with ASTM D 6611 [3].

As a result, there have not been significant differences between the numbers of cycles to failure within the selected yarns (cf. Figure 2). If these tests can be transferred to estimating the lifetime in CBOS tests, all braided fiber ropes should show comparable lifetime in CBOS tests. This has been investigated later.

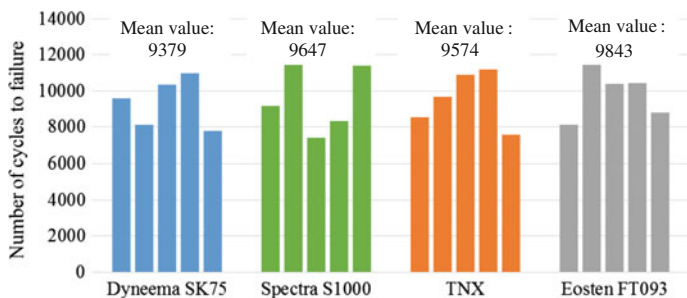


Fig. 2 Yarn-on-yarn abrasion tests based on ASTM D 6611

Tensile Tests on Braided Fiber Ropes

For determining the tensile properties of the selected fibers in textile semifinished parts, fiber ropes have been braided from the filament yarns. In the given case, seven yarns have been twisted to form the strands, which have been used for braiding ropes. The ropes have been braided as 12-strand braided ropes (six strands in S-twist, six strands in Z-twist) in a one-on-two binding (twill braid) with a pitch length of 39 mm. Tensile tests in full accordance with DIN EN ISO 2307 [4] have been performed on the fiber ropes, described above. The results of the tensile tests are shown in Fig. 3.

The textile structure seems to have a big influence on the tensile properties of a semifinished part. Further, it is assumed that the influence is not the same on all HMPE fibers. As can be seen in the results, the ropes made from the fiber Dyneema® SK75, where the highest tensile strength in state of a yarn was found, did not show the highest tensile strength in state of a braided rope, while the strength of the ropes made from Spectra® S1000 was found to be the highest of all fiber ropes, made from the selected fibers.

This is due to the fact that the molecules in the single filaments are aligned with a very high orientation, during fiber manufacturing. This alignment seems to influence the resistance to transversal compressive forces, as they are occurring when a

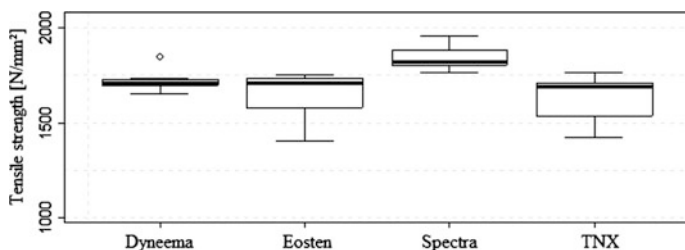


Fig. 3 Tensile tests of braided HMPE fiber ropes according DIN EN ISO 2307

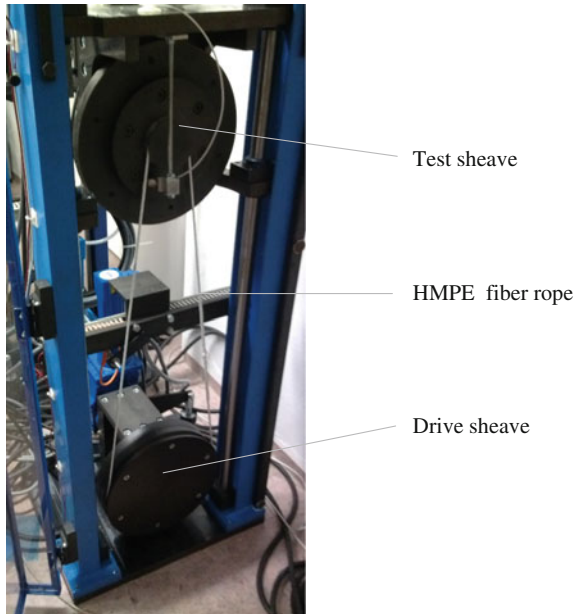
braided fiber rope is loaded with a tensile load. The strength of the ropes made from the Chinese HMPE fibers is very close to the strength of the ropes made from Dyneema® SK75.

It can be stated that it is impossible to competitively estimate the tensile strength of a textile semifinished part, which is usually made from one specified HMPE fiber, using values derived in tensile tests on the basic yarns.

CBOS Tests on Braided Fiber Ropes

Cyclic bend-over-sheave tests (CBOS tests) have been performed to determine the resistance of the selected HMPE fibers against internal abrasion in applications with cyclic loading and deloading. Another challenge was the unavailability of international standards for performing CBOS tests on fiber ropes. Due to this, guideline VDI2358 [5] for performing CBOS tests on steel wire ropes, established by the Society of German Engineers (VDI), has been chosen as a base for performing CBOS tests on braided fiber ropes [5]. In accordance with VDI 2358, a setup as shown in Fig. 4 has been chosen to be appropriate. The rope load is applied via a spindle drive, the cyclic bending movement has been applied by an electrical motor.

Fig. 4 Setup for CBOS tests on braided fiber ropes according VDI 2358



In order to investigate a wide range of parameters, following parameters have been varied:

- Rope tension at constant bending frequency and constant stroke length
- Bending frequency under constant tension and constant stroke length
- Stroke length under constant tension and rope speed (bending frequency adjusted)

The relation between the diameter of the test sheave and the diameter of the rope, called D/d-ratio, has been kept constant at a chosen ratio of $D/d = 12.5$. This value of $D/d = 12.5$ has been chosen to achieve useful results in a reasonable time. The stroke length has been set to a value of $l = 250$ mm, for the cases with constant stroke length.

In Fig. 5, the results of the CBOS tests are displayed. It was found that the fiber ropes with the highest tensile strength also provided the best lifetime in CBOS tests. For most of the fibers, a significant influence of the bending frequency cannot be proven in the investigated interval between 20/min and 40/min. Only in case of the fiber Dyneema® SK75, an increasing bending frequency (from 20/min up to 40/min) led to an improved performance by about 10 % at tensions below 150 N/mm². Due to this reason, only the values for a bending frequency of 40/min are displayed in Fig. 5.

In summary, it was found that the Chinese fibers provided about 85 % of the performance of non-Chinese HMPE fibers, which is a quite good performance when considering the much lower prices (cf. Table 1). Further, it is to be seen that there is no possibility of competitively estimating the lifetime in applications with CBOS loads from the yarn-on-yarn abrasion tests. In the yarn-on-yarn abrasion tests, all fibers provided nearly the same performance. In the CBOS test, the lifetime of the ropes made from the fiber Spectra® S1000 was about 30–80 % higher (depending on tension) than the lifetime of the ropes made from Dyneema® SK75,

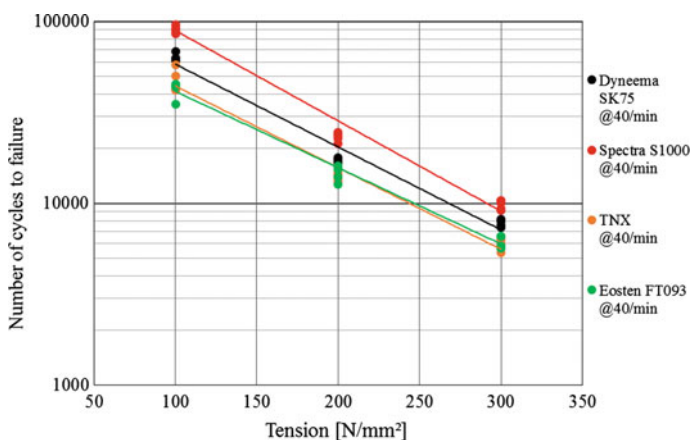


Fig. 5 Results of CBOS tests—influence of the tension

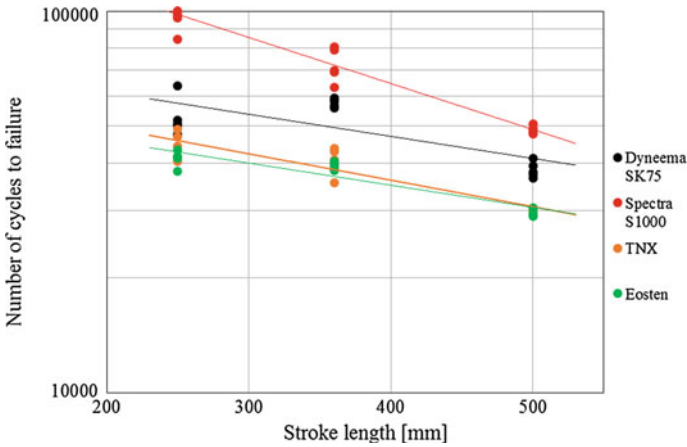


Fig. 6 Results of CBOS tests—influence of the stroke length

while the lifetime of the ropes from Chinese HMPE fibers is about 25 % lower than seen for the fiber Dyneema® SK75. This might be due to the low load, which has been applied on the strands during the tests based on ASTM D 6611.

After investigating the influence of tensions and bending frequencies, the influence of the length of the bending zone has been determined. As shown in Fig. 6, the performance of all fibers is influenced by the length of the bending zone. This influence is caused by the increasing length of the bending zone, what increases the length of rope with introduced thermal energy, due to the relative movement of the strands and the thereby caused frictional heat.

Thermosetting of Braided HMPE Fiber Ropes

Thermosetting is a common production step in modern textile manufacturing. It is mostly used for reducing structural elongation in technical textiles and for reducing thermal shrinkage in polymer fibers. For high-strength fibers, and especially for HMPE fibers, thermosetting can be used for increasing the strength of textile structures and reducing structural elongation in the same time. The textile is loaded with a material-dependent load, heated up to material-dependent temperature, and kept under load and temperature for a certain time. Directly after thermosetting, the textile is cooled down below a critical temperature (material dependent) and the load is released.

For the fiber Dyneema® SK75, data on parameters for optimal thermosetting has already been published (cf., e.g., Heinze/Mammitzsch [6]). A temperature of 130° C and a load of approximately 12 % MBL of the textile are named to be appropriate. During the tests on other HMPE fibers, shown in this chapter, main

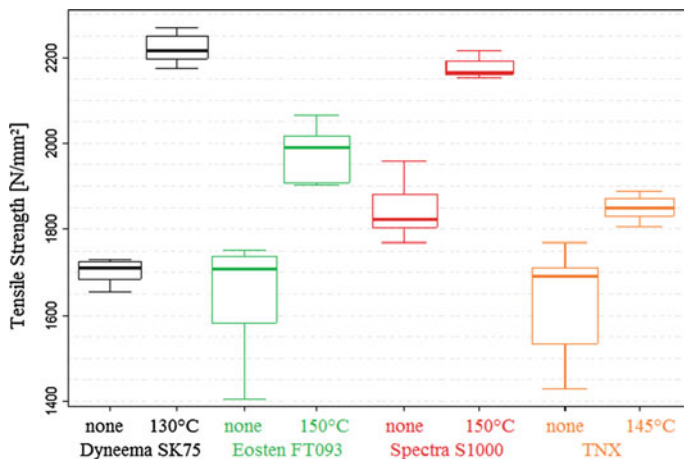


Fig. 7 Increase of strength in HMPE fiber ropes after thermosetting (12 % MBL, optimal temperatures)

goal was to investigate whether the optimal parameters for Dyneema[®] SK75 can directly be transferred to other HMPE fibers or not.

It was found that all fibers are showing an increase in break strength, when using the named parameters for thermosetting. It was further found that better results in thermosetting can be achieved when using higher temperatures, for some of the HMPE fibers, as shown in Fig. 7. The parameters published for Dyneema[®] SK75 have been proven to be optimal parameters. Additionally, it was found that thermosetting also reduces the deviation of the measured values in strength tests.

Summarizing the results of the thermosetting tests, it was found that the highest increase in strength at a thermosetting load of 12 % MBL has been found for the fiber Dyneema[®] SK75, while the gained increase in strength is lower for the Chinese HMPE fibers. Further tests regarding an optimal load have shown that the named 12 % MBL are already displaying the optimum value for all selected fibers.

Price–Performance Analysis

The price of textile semifinished parts is a main decision criterion for purchasing textile parts from various HMPE fibers. In some cases, a cheaper price can effectuate a decision in favor of one special HMPE fiber by outbalancing weaker performance properties. In other cases, a more expensive fiber material can be preferable due to superior mechanical properties. For further estimating these matters, data on the cost distribution during making a fiber rope with a diameter of 6 mm, including thermosetting, has been requested at two rope manufacturers, one

with location in Germany and one with location in a developing nation. In both cases, the costs for the fiber materials came to about 75 % of the total costs for making the rope [7].

Having a look at the prices of the fiber materials (cf. Table 1), it can be calculated that the price of a rope with a special rope design can be reduced by 33 % to 37.5 % using a Chinese fiber. Regarding the weaker performance in the tests described above this also means that the area of cross-section of the rope can be increased by 33 %, what means an increase in diameter of about 6 %, while the price of the rope is the same. This would lead to reduced tensile stresses, when keeping the work load constant, and would therefore, e.g., increase the lifetime in CBOS to values above the values known from the more expensive materials. These effects can be economically reasonable in applications where no strict limitation in installation space is given, or in applications where replacing the textile part is not related to high costs.

In case of the fiber Spectra[®] S1000, showing higher prices than Dyneema[®] SK75, the significantly better performance in CBOS and tensile tests is outbalancing the higher price, and is economically reasonable in all applications where replacing the mechanical component or textile element is related to high costs. The slightly higher deviation in the measured values, compared to Dyneema[®] SK75, is making a critical point regarding safety-related applications, because a higher number of tests for providing a proof of function is needed.

The fiber Dyneema[®] SK75 is showing the most outbalanced profile of properties, regarding price and overall performance. Especially the fact that the deviation in the values is the smallest of all fibers in all of the tests, causes the fact that there is hardly an option for applications where an exact prediction of the lifetime under certain load is needed, e.g. safety-related engineering applications.

Summary

It has been shown that the mechanical properties of Chinese HMPE fibers are not as good as known from market leading fiber brands such as Dyneema[®] and Spectra[®]. It has also been proven that the low price of the Chinese fibers can provide economic advantages in very special fields of application. The capability of increasing the tensile strength by thermosetting has been proven for all fibers. The gain in strength is lower for the Chinese fibers, but might be improved by optimizing the parameters for thermosetting. As shown in the literature, thermosetting for increasing the strength of fiber ropes does not affect the performance in CBOS tests, in case of Dyneema[®] SK75. This has to be further investigated for other HMPE fibers.

References

1. International Organization for Standardization and European Committee for Standardization, DIN EN ISO 2062—Textiles—Yarns from packages—Determination of single-end breaking force and elongation at break using constant rate of extension (CRE) tester, London 2009
2. American Society for Testing and Materials, ASTM D 3800—Standard Test Method for Density of High-modulus Fibers. (West Conshohocken, 1999)
3. American Society for Testing and Materials, ASTM D 6611—Standard Test Method for Wet and Dry Yarn-on-Yarn Abrasion Resistance. (West Conshohocken, 2000)
4. Association Française de Normalisation and European Committee for Standardization, DIN EN ISO 2307—Fibre Ropes—Determination of certain physical and mechanical properties. (Saint-Denis/London, 2011)
5. Verein Deutscher Ingenieure (VDI), VDI 2385—Drahtseile für Fördermittel. (Düsseldorf, 1984)
6. T. Heinze, J. Mammitzsch, Thermofixieren von Seilen aus hochfesten Synthesefasern. (Stuttgart, 2011)
7. J. Mammitzsch, Untersuchungen zum Einsatz von Seilen aus ultrahochmolekularen Polyethylenfasern in Seilen für die Fördertechnik (doctoral thesis). (Chemnitz, 2015)

Natural Materials for Surface Modification of Cellulosic Narrow Woven Fabrics—Strides Towards Fully Bio-based Composites

Thomas Grethe, Hajo Haase and Boris Mahltig

Introduction

Natural fiber-based textile products are increasingly used for composite applications. Fibers like, hemp, flax, or kenaf are interesting materials. For this, new challenges compared to commonly used textile materials are evident. Plant-based fibers can suffer from bio-corrosion by bacteria and fungi. To prevent such corrosion, natural antibacterials such as chitosan, pinene, cinnamaldehyde, eugenol, or camphor can be applied [3, 4]. To get a more continuous release of antibacterial agents, they can be embedded in adsorbent materials like activated carbon or zeolites. A sol gel system can be used to immobilize such systems on fibrous materials. Tannins like Gallic acid and polysaccharides like chitosan also exhibit antibacterial properties. In this study, cinnamaldehyde, eugenol, chitosan, and gallic acid were investigated. The hydrophobic nature of cellulosic fibers leads to additional issues: due to water uptake, the fibers can swell which can weaken the composite structure or can even lead to fatal failures of such composite materials.

Also, most natural fibers show only poor adhesive interactions to the mostly hydrophobic matrices used in composites. To overcome these effects, fibers need a pretreatment with hydrophobic agents. There are lots of products commercially available to achieve excellent hydrophobic fiber properties. For example, different synthetic hydrophobic finishing procedures exist to reduce the water absorbance of

T. Grethe · B. Mahltig (✉)
FTB, Hochschule Niederrhein—University of Applied Sciences,
Mönchengladbach, Germany
e-mail: boris.mahltig@hs-niederrhein.de

T. Grethe
e-mail: thomas.grethe@hs-niederrhein.de

H. Haase
Department of Food Chemistry and Toxicology—Berlin Institute of Technology,
Berlin, Germany

natural fibers. However, fluorocarbon finishing agents are probably the most controversial ones. Additionally, esterifications with hydrophobic substituted carboxylic anhydrides are available [12]. Also, hydrophobic silanes can be utilized to introduce hydrophobic functions in cellulosic materials [5–7]. For example, hexadecyltrimethoxysilane or methacryloxypropyltrimethoxysilane are applied for this purpose [1]. However, these substances are not bio based and also not biodegradable, which is contrary to the idea of fully bio-based composites.

To achieve a higher share of bio components in such materials, other classes of coating agents need to be developed. Natural plant oils are promising agents exhibiting unsaturated carbon bonds that can be oxidatively coupled to create hydrophobic films on surfaces. For example, natural unsaturated oils like tung or linseed oil are known to produce such coatings. Linseed oil consists of approx. 50 % of α -linolenic acid, which is triply unsaturated (Fig. 1).

At the allylic position, one hydrogen atom can be abstracted to form an allyl radical which can react with oxygen to form a hydroperoxide. This hydroperoxide can react further by hydroperoxide decomposition offering the ability for intermolecular cross-linking (Fig. 2) [10].

This polymerization process usually takes several hours under atmospheric conditions. Such a system can act as a finishing agent for cellulosic fibers, if the reaction can be accelerated. A radical starter combined with an oxidative agent is suitable for that purpose. This also offers the ability to introduce a radical function in the cellulosic material, which is also capable to react with the unsaturated bonds of the natural fatty oils [11]. Tung oil is composed primarily of triglycerides of α -eleostearic acid (Fig.3). This polyunsaturated oil is capable of additional reactions; e.g., epoxidations and Diels–Alder type reactions are reported in the literature [2, 9].

A water-based finishing agent for textile substrates can be realized by suspending the oily components in an aqueous system by the use of detergents like sodium oleate or sodium dodecylsulfate. Pre-polymerized materials are often used in common hydrophobization agents. To apply this type of materials for the

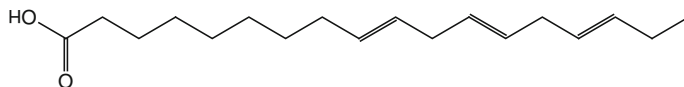


Fig. 1 Structure of α -linolenic acid

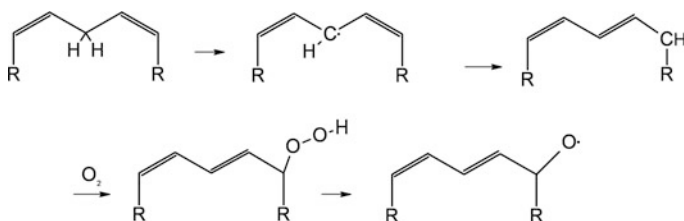


Fig. 2 Oxidative activation of linoleic acid

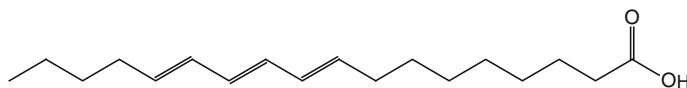


Fig. 3 Structure of α -eleostearic acid

discussed bio-based finishing agents, natural polymers like natural rubber are interesting substances. They can be blended with the oil-based systems to achieve a hybrid coating.

Experimental

(a) Antimicrobial finishing

To immobilize loaded adsorbents, a sol from tetraethyl orthosilicate (TEOS) and glycidyoxypropyltrimethoxysilane (Glymo) was used. These precursors were hydrolyzed by aqueous nitric acid and stirred until a clear solution was obtained. The adsorbent materials were loaded with eugenol and cinnamaldehyde by creating a slurry of the bactericide and the adsorbent. This slurry was then combined with the sol and the resulting coating agent was padded onto linen fabric. Later, the textile samples were dried in an oven at 120 °C for 2 min. Chitosan was solved in acetic acid before adding it to the sol solution. Gallic acid and chitosan solution were added to the sol without any adsorbents.

The antimicrobial properties of the prepared textile samples against *Escherichia coli* are investigated as previously described [8]. Briefly, textile samples (circles of 5 mm diameter) are placed in sterile 96-multiwell cell culture plates together with 200 μ L bacterial suspension (diluted 1:250 in LB medium) per well. After incubation for 3 h at 37 °C in an orbital incubator rotating at 120 rpm, cellular viability is tested by incubation with 0.01 % (w/v) MTT in culture medium followed by lysis in isopropanol and determination of the absorption at 570 nm and a reference wavelength of 700 nm. Data are shown as % viability relative to bacteria in the absence of fabric samples. For each textile sample, three independent measurements are conducted with different cutouts from the same sample.

(b) Hydrophobic finishing

Three types of finishing liquors were prepared. Polyisoprene was dissolved in water with the help of a detergent, for example sodium oleate or SDS. The same procedure was applied with tung oil instead of the polymer. The third liquor was prepared as a solution from tung oil and polyisoprene. Furthermore, sodium peroxodisulfate was applied to initiate the *radical* polymerization reaction. The prepared coating agents were applied on textile surfaces by padding. After padding, the samples were dried for 30 min at about 90°. To investigate the wash fastness, a part of each sample was washed in an aqueous solution of triton X-100 for 30 min and

dried again. The hydrophobicity of all samples was investigated by capillary rise testing.

Results

(a) Antibacterial finishing

Chitosan finished samples showed survival rates of approx. 80 %, which is a rather less sufficient effect. On the other hand, Gallic acid shows survival rates of *E. coli* of approx. 42 % (Fig. 4).

Investigations of samples containing eugenol or cinnamaldehyde in activated carbon and zeolite resulted in different survival rates. The choice of the adsorbent has less influence on the activity, but cinnamaldehyde gives better results than eugenol. A combination of cinnamaldehyde and activated carbon, leading to survival rates of approx. 22 %, gives the best result in this investigation (Fig. 5).

(b) Hydrophobic finishing

Regarding the choice of detergents, the bio-based oleate achieves a more effective and durable hydrophobicity compared to the investigated SDS as shown in Fig. 6.

The height of the capillary rise decreases with increasing tung oil concentration by using oleate as detergent. The wash fastness also increases. The biodegradability of the oleate combined with the natural oil renders the resulting material fully bio based.

As depicted in Fig. 7, the addition of polymers to the tung oil-based agent increases the hydrophilicity while maintaining the washing fastness.

Fig. 4 Antimicrobial effect of chitosan and gallic acid finished fabrics

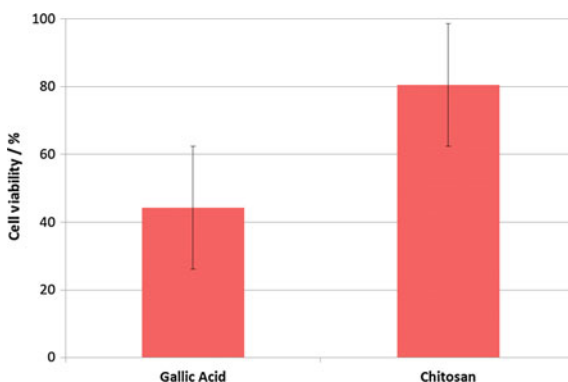


Fig. 5 Antimicrobial effect of eugenol and cinnamaldehyde finished fabrics

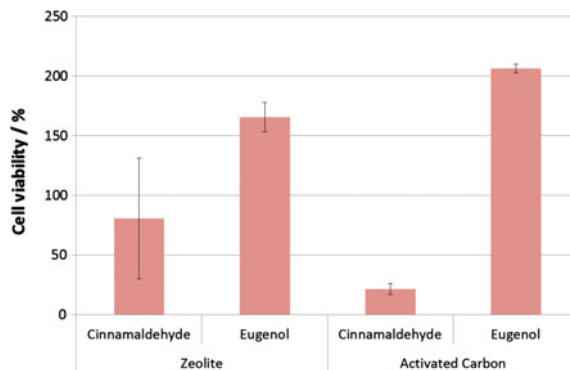


Fig. 6 Height of capillary rise dependent on detergent type and oil concentration in the liquor (untreated reference material: 150 mm)

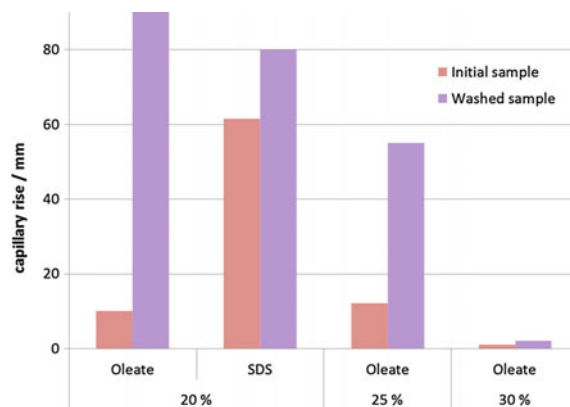
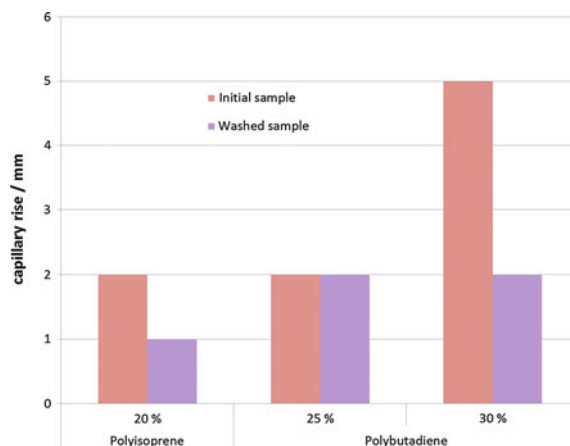


Fig. 7 Height of capillary rise dependent on the addition of different polymers, used detergent was only oleate (untreated reference material: 150 mm)



Conclusion

Antibacterial finishing can be realized on flax fibers using natural biocides. A sol gel system can be utilized to immobilize natural bactericidal substances in a coating on fibrous substrates. However, the antimicrobial effectiveness needs to be enhanced by evaluating further natural substances on their bactericidal properties. Additionally, different adsorber systems can be investigated which potentially are capable to immobilize higher amounts of the mentioned substances. The combination of more than one bactericide may lead to higher antibacterial effects. Permanent hydrophobic effects on natural fibers were demonstrated. Substances like unsaturated fatty oils can act as building blocks to achieve sustainable and effective functionalization of cellulosic fibers. The oxidative cross-linking reactions can be accelerated by initiators, so that an application in textile finishing processes is suitable.

References

1. M. Abdelmouleh, S. Boufi, M.N. Belgacem, A.P. Duarte, A. Ben Salah, A. Gandini, Modification of cellulosic fibres with functionalised silanes: development of surface properties. *Int. J. Adhes. Adhes.* **24**, 43–54 (2004)
2. C. Boelhouwer, Th Knegtel, M. Tels, On the Mechanism of the thermal polymerization of linseed oil. *Fette Seifen Anstrichmittel* **69**, 432–436 (1967)
3. S. Inouye, T. Takizawa, H. Yamaguchi, Antibacterial activity of essential oils and their major constituents against respiratory tract pathogens by gaseous contact. *J. Antimic. Chemother.* **47**, 565–573 (2001)
4. A.K. Johny, M.J. Darre, A.M. Donoghue, D.J. Donoghue, K. Venkitanarayanan, Antibacterial effect of trans-cinnamaldehyde, eugenol, carvacrol, and thymol on *Salmonella* Enteritidis and *Campylobacter jejuni* in chicken cecal contents in vitro. *J. Appl. Poult. Res.* **19**, 237–244 (2010)
5. B. Mahltig, H. Böttcher, Modified silica sol coatings for water-repellent textiles. *J. Sol-Gel. Sci. Technol.* **27**, 43–52 (2003)
6. B. Mahltig, H. Haufe, H. Böttcher, Functionalization of textiles by inorganic sol-gel coatings. *J. Mater. Chem.* **15**, 4385–4398 (2005)
7. B. Mahltig, A. Fischer, Inorganic/organic polymer coatings for textiles to realize water repellent and antimicrobial properties. *J. Polym. Sci. B: Polym. Phys.* **48**, 1562–1568 (2010)
8. B. Mahltig, M. Reibold, E. Gutmann, T. Textor, J. Gutmann, H. Haufe, H. Haase, Preparation of Silver Nanoparticles Suitable for Textile Finishing Processes to Produce Textiles with Strong Antibacterial Properties Against Different Bacteria Types. *Zeitschrift für Naturforschung B* **66B**, 905–919 (2011)
9. J. Malléol, J. Gardette, J. Lemaire, Long-Term Behavior of Oil-Based Varnishes and Paints, I. Spectroscopic Analysis of Curing Drying Oils. *J. Am. Oil Chem. Soc.* **76**, 967–976 (1999)
10. J. Malléol, J. Lemaire, J. Gardette, Drier influence on the curing of linseed oil. *Prog. Org. Coat.* **39**, 107–113 (2000)
11. D. Roy, M. Semsarila, J.T. Guthrie, S. Perrier, Cellulose modification by polymer grafting: a review. *Chem. Soc. Rev.* **38**, 2046–2064 (2009)
12. H. Sehaqui, T. Zimmermann, P. Tingaut, Hydrophobic cellulose nanopaper through a mild esterification procedure. *Cellulose* **21**, 367–382 (2014)

Overview of the Sustainable Materials for Composites and Their Industrial Adaptability

Taraneh Khademi

Abstract Sustainability carries more weight in this century, boosting research and investigations on new environmentally sustainable materials. This paper summarizes some recent literature and developments on the topics of biopolymers, cellulosic fibers, biocomposites and at least their potential as engineering parts and state an overview of natural polymers and the utilization of natural fiber reinforcements to form biodegradable sustainable and on the long view competitive composites. Green Composites are finding adaptability in many fields including automotive industry, construction industry, sporting goods, or consumer products. Main types of bioplastics are listed, defined and considered according to their mechanical performance and market potential. Natural plant fibers are classified by origin, performance and potential for composites as well as compared to traditionally used glass fiber according to mechanical properties and environmental impact. Moreover, advantages of cellulose fibers for composites are listed and compared to their downgrades, with possible modification methods to partially compensate their disadvantages.

Keywords Green · Composites · Biodegrading · Bio polymers · Natural plant fibers reinforcement

Introduction

Composite materials can match a wide variety of applications. By choosing an appropriate combination of matrix and reinforcement material, a new material can be made that exactly meets the requirements of a particular application. Moreover, they provide design flexibility because many of them can be molded into complex shapes. Typical Composite structures made from narrow fabrics include tubular profiles, T-,C-,J section panels, bifurcated beams, connecting rods, rib stiffened panels,

T. Khademi (✉)

Research Institute for Textile and Clothing (FTB), Hochschule Niederrhein—University of Applied Sciences, Mönchengladbach, Germany
e-mail: taraneh.khademi@gmail.com

airframe spars, T-bar profiles, single and double blade joint structures, I beam structures, fillets and other panels [1–3]. Composites are not exclusively used for high-tech industries but they emerge as well in daily life as parts of a car, in bikes, badminton and tennis racket or construction applications, which also incorporate structural parts made of narrow fabrics. Although the resulting product is more efficient, the raw materials are often not environmentally friendly. As a matter of fact, most composite plastics are petroleum-derived, which is the cause for the problematic recycling and waste management of these products [4]. As yet, it has been prevalent to dispose composite waste as landfill, which damages the environment. Driven by a more sustainable thinking society and also by the government, the pressure on companies to recycle materials when they come to their End-Of-Lifecycle increases in the recent years. Biomass-derived materials constitute one of the most sustainable materials, which can also be used for engineering plastics to substitute the traditionally used synthetic polymers. The growing concerns regarding environmental issues have driven an elevated interest in environmentally friendly materials. The primary target is to choose materials, especially matrices, which are biodegradable. Biodegradation means that microorganisms decay an organic matter. Fungi, algae, or bacteria can act in this process as decomposers. Biodegradable polymers, which are utilized for industrial usage, are decayed under controlled humidity and temperature conditions (industrial compost conditions) [5]. Composites based on cellulose reinforcement of petroleum-based polymers are called “Biocomposites”. Composites that are completely biodegradable, because

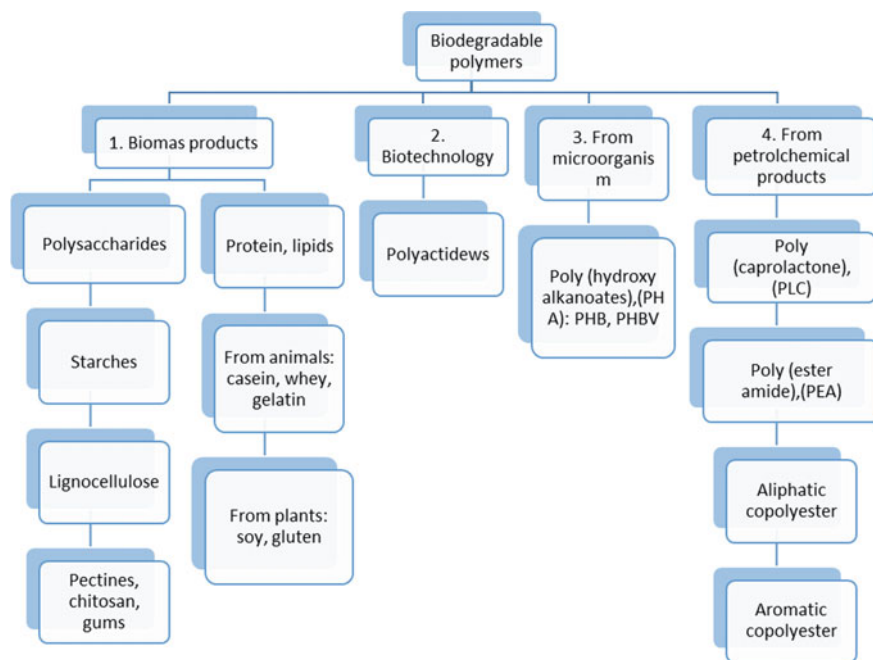


Fig. 1 Classification of biodegradable polymer types [8]

they are produced of biopolymers, which are reinforced entirely by natural derived fibers, are referred as “Green Composites” [6]. In comparison to their synthetic, nondegradable counterparts, “Biopolymers” show deficiency in mechanical and thermophysical properties. Furthermore, one of the main reasons for their marginal usage is the comparably high cost [7]. Nevertheless, these downgrades can be partially overcome by reinforcing these materials with suitable natural fiber reinforcements, which add increased mechanical performance and create an entirely sustainable eco-friendly composite. In the following the materials that refer to the term “Green Composites” are going to be discussed more detailed. Figure 1 shows the classification of the different biodegradable polymers. Suitable fiber reinforcements are going to be discussed in the Chap. 5. Biodegradable polymers can be divided in four different sub-categories based on their raw materials. Except of the last category, which derives from petrochemicals, all the other polymers are actually generated by biomass.

Biodegradable Polymeric Matrix Materials

Starch-Based Biopolymers (TPS)

Due to its high availability and low costs, starch is a widely used raw material for bio-based plastic production. Main sources, which are employed to yield starch, include corn, wheat, rice, or potato [9]. Starch is a polysaccharide, which can be found in plant cells. It consists of amylose and amylopectin, which molar masses vary with the starch source. The former one is a linear and crystalline polymer while the latter one is a branched and amorphous polymer. The relative amount of these two polymers in the starch source exerts influence on the mechanical performance and biodegradability properties of the end-material. Higher amylase content results in better tensile strength, modulus and elongation at break Values [10, 11]. Starch is available in the form of fine white granules, which are insoluble in cold water, but can be processed to a viscous paste with the addition of heat. The intermolecular bonds of the double helix structure in the starch molecules are broken down in hot water, which let the crystalline structure disaggregate. The physical change from solid granulates to viscous state is termed gelatinization [12]. During gelatinization starch can be formed to a thermoplastic material under the influence of mechanical, thermal or thermo-mechanical energy and the presence of a plasticizer like glycerol, sorbitol, xylose, sucrose, or poly ethylene glycol [13]. The procured bioplastic material can be processed to foam, films or molded products by injection molding, foaming, extrusion, film blowing and thermoforming. In Comparison to non-degradable commonly used polymers derived from petrochemicals, starch-based polymers lack in mechanical performance. Moreover, they are highly hydrophilic, have low resistance against solvents and oils and have higher density than commonly used materials. The above listed disadvantages can be managed to some extend by blending starch-based materials with other biodegradable polymers such

as PLA (Polylactid Acid), PHA (Polyhydroxalkanotatesor) PBS (Polybutylene succinate) and by modifying the basic polymer material by adapting the kind and amount of plasticizers (9). For example the “Ales School of Mines” Research center has done about 10 years research on this Topic. One investigation was done on bio-based packaging materials for food in order to substitute currently used polyolefin (such as polyethylene, polypropylene and polystyrene). In cooperation with the Vitembal Company (Remoulins, France) it was possible to invent multi-layered biodegradable composite to replace the expanded polystyrene (EPS). Starch was used as raw material to produce the required foamed structure. In order to overcome the hydrophilic character of starch, natural fibers were incorporated into the basic material, and two external biodegradable and bio-based polyester films were calendered on both sides of the foamed starch sheet to guarantee decreased water absorption and to enhance its overall mechanical properties (Fig. 2). In the course of serious tests, it emerges that cellulose reinforced biocomposite and EPS have similar E/ρ values (E : bending modulus; ρ : density). Additionally the new biocomposite has better impact properties than EPS and it was further detected the water sensitivity is ten times lower for the biocomposite than for EPS because of the intrinsic foamed microstructure.

Subsequently, a serious of degradation tests were done after ISO 14855 composting test under the influence of fungus growth (*Aspergillus*, *Hyphomycetes*) to prove the degradability of the material. As a result about 50 % degradation of the material was measured after 4 months. High strength composites can also be developed by reinforcing the starch-based emulsion-type resins for example with Manila hemp fiber bundles of 100–200 μm diameters, which leads to an increase of tensile strength by raising the volume fraction of fibers (Table 1).

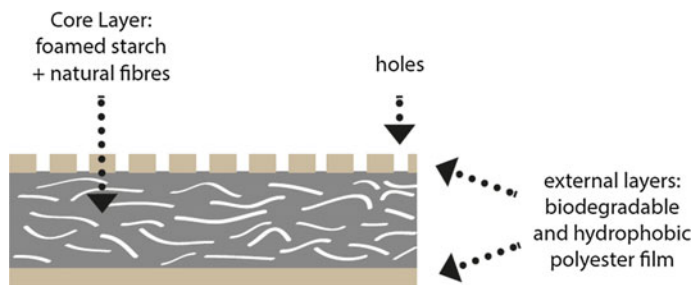


Fig. 2 Multilayered biocomposite structure [14]

Table 1 Correlation of experimental value tensile strength to volume fraction of fibers of Manila reinforced starch based resin [15]

Volume fraction of fibers (%)	Experimental strength (MPa)
30	162.0
50	254.0
70	365.4

Plant Oil-Derived Proteins

Plant proteins are macromolecules, which consist of amino acid polymers. Main sources for plant oil-derived proteins are oilseeds (i.e., soybeans) and grains (i.e., corn, wheat) which are produced as by products from agricultural and biofuel processing activities [16]. Similar to TPS processing, the addition of plasticizer makes the protein processable and formable under appropriate temperatures without degradation. The plant-derived proteins can be manufactured into films using thermoplastic processes such as compression molding and extrusion or can be manufactured to thermoset materials [17, 18]. Therefor as an example presented by Yang, wheat gluten powder was synthesized with rice protein powder and coupled with formaldehyde as crosslinking agent and glycerol as plasticizer at high temperature. Protein-based matrix materials also show low mechanical strength. Like TPS they also have to be strengthened with natural fibers to gain better performance characteristics. Researches have been done to proof that soy-based Polyurethane has 25 % lower total environmental impact compared to petroleum-based Polyurethane. It was shown that the use of soy polyols would result in reductions in net CO₂ turnout, smog production, ecological toxicity, and fossil fuel consumption [19]. Other studies were done [20] in which the bio-based polyurethane from soybean oil-derived polyol and di isocyanate was reinforcement with glass fibers, to reach significantly increased mechanical and thermal properties of the base resin. It was proved that mechanical properties such as tensile and flexural strength as well as tensile and flexural modulus of soypolyol-based composites could compete to composites based on petrochemical polyurethane. They further indicated that because soy-based polyurethanes offer better thermal, oxidative, and hydrolytic stability compared to petrochemical-based polyurethanes, they could become a viable alternative to the petrochemical matrix resins for composites. In this research, soybean oil-based polyol was supplied by Arkema, Inc. under trade name Vikol[®]-1 [21]. Summarized it can be stated that these composites will be more environmental-friendly for the reasons that soybean derived Polyurethane does not produce styrene emission, thereby, resulting in a safer work place and that the monomer Polyol is made from a renewable resource (soybean oil).

From Animal Derived Proteins

Typical proteins that are derived from mammals are elastin, collagen, gelatin and Casein. Elastin can be found in skin, blood vessels and lung tissues of mammal and constitute a basis for biomaterials, which are used for tissue regeneration [22]. Collagen represents the most occupied mammal derived protein material for medical applications. It is used for soft tissue repair and reconstruction. Collagen can be found in mammals' teeth and bones and has to be chemically cross-linked

during processing by the usage of glutaraldehyde for example, to form more stable and stronger matrix structures [23]. The increase in research for collagen in biomaterials is reasoned by its ability to form fibers with high strength and stability through its self-aggregation and crosslinking and moreover for its outstanding cell adhesion and cellular recognition for setting cell attachment and function [24]. For example, there has been investigations done on degradable collagen sponges as scaffold material for tissue repair due to their outstanding biocompatibility to the human body [25].

Polyactid Acid (PLA)

Polyactid acid is manufactured by polymerization of lactide, which can be derived from the fermentation of corn or cane sugar. During the fermentation process the raw materials are converted to lactide through microbial activity under the influence of calcium hydroxide and sulfuric acid [26]. In the next step the yielded lactide can be polymerized without additional solvents by a ring-opening polymerization process [27].

The final properties of the polymer like degree of crystallinity, transition temperature and melting point can be modified by controlling the monomer constellation which leads to two different structures of PLA that are available in the market: Poly-L-lactide(PLLA) which can be amorphous and Poly-D-lactide (PDLA) which is semi [28]. The polymer can then be processed in further steps by using conventional manufacturing routes like injection molding, extrusion, foaming, blending, fiber spinning, blow molding and compounding [29]. PLA is a biodegradable polymer with comparable mechanical properties to PE and polystyrene as well as high melting point (175 °C). These characteristics and the easy processability create a high attention to PLA as a substitute for conventional plastic materials. But the deficits in thermal and mechanical resistance as well as the brittleness and crack sensitivity hamper the application of PLA for engineering parts which diminish the excess to broader industrial markets beyond packaging and agriculture [30]. However, these deficits can be overcome by blending PLA with nanoparticles like Nano clays, which collaterally lead to a better biodegradability of the polymer [31]. Moreover, increasing the crystallization degree of the PLA Polymer can also modify properties. This can be done during thermoforming, extrusion or “heat-aging” treatments while the latter induces additional costs, which on the other hand makes PLA less competitive to other polymers [32]. As another solution, biodegradable plasticizers such as citrate esters can be introduced to increase crystallinity and, moreover, decrease the brittleness [33]. PLA can be fully degraded under temperatures above 60 °C without adding toxins to the environment. Due to its sensitivity to water and temperature, PLA is not suitable for conventional recycling processes, which are used for traditional polymer materials. As a main ecological drawback, the high energy consumption during the conversion from biomass to PLA has to be considered. The total carbon footprint resulting

Table 2 Selected commercial available PLA polymers [9]

Polymer	Manufacturer	Trade name
PLA	Zhejiang Hisun Biomaterials	PLA
	Birmingham Polymers, Inc.	Lactel, absorbable
	Boehringer Ingelheim	Resomer
	Cargill Dow LLC	Nature works
	Galactic SA	Galactic PLA
	Hycall	PLA
	Mitsubishi Plastics, Inc.	Ecolaju
	Purac	Purasorb
	Shimadzu Corporation	Lacty
	Mitsui Chemicals	Lacea
	Chronopol	Heplon
	Dainippon Ink Chem	CPLA
	Teijin	Biofront

from the PLA processing is overall higher than the CO₂ emissions arising from conversion of fossil fuels into resins [34] Table 2 shows some commercial available PLA biodegradable polymers and lists manufacturers and trade names.

Polyhydroxalkanotates (PHA)

PHA is produced via fermentation by bacteria, for example, of carbon compounds from renewable resources like glucose. During the production, different kinds of PHA can be yielded containing different properties according to their chemical structure. Different types of Polyhydroxalkanotates are for example P3HB (poly (3-hydroxybutyrate)) or PHB (poly (hydroxybutanoic acid)). These polymers form more brittle structures with lower elongation due to their high crystallinity. There has been done more investigations to find tougher copolymers with lower melting-biodegradability such as PHBV or PBAT (Poly (butylene adipate-co-terephthalate) to compete with traditional plastics like PVC, HDPE, LDFPE, and PP. PHAs can be applied in packaging, medical, and agriculture industry. It is possible to process PHAs by injection molding, film blowing, film casting, and fiber spinning. Based on its high crystallinity, PHAs are robust against solvents and insoluble in water and consequently resistant to hydrolysis, which induce a great benefit to this material in comparison to other “Green Polymers.” Moreover, it is more biodegradable in normal natural environments without the addition of heat or controlled composting conditions. Testing via ASTM D6691-09 test methods (Standard Test Method for Determining Aerobic Biodegradation of Plastic Materials in the Marine Environment by a Defined Microbial Consortium or

Table 3 Selected commercial available PHA polymers [9]

Polymer	Manufacturer	Trade name
PHA	Biomatera, Inc.	–
	Biomer	PHB, PHBV
	Metabolix, Inc.	PHA, Biopol
	Procter and Gamble	Nodax
	PHB Industrial S/A	–
	Tianan	Enmat
	Copercucar	Biocycle

Natural Sea Water Inoculum) showed that PHPV could be degraded by mineralization to over 75 % within 35 days. It was protocolled that PHAs residues do not harm marine life and soil [35, 36]. Table 3 shows some commercial available PLA biodegradable polymers and lists manufacturers and trade names.

Petroleum-Based Biodegradable Polyesters

It is also possible to manufacture biodegradable polymers by the chemical synthesis of petroleum-based monomers. These polymers are related to the family of Polyesters. This procedure enables a production of polymers with a wide range of physical and mechanical properties by modifying the chemical constitution of polyester and copolyesters. Typical Biodegradable Polyesters are PCL (Poly (E-Caprolactone), PEA (Polyesteramide), aliphatic copolyesters like PBS (Polybutylene succinate), and PBSA (Polybutylene succinate/adipate) as well as aromatic copolyesters like PBST(Poly (butylene succinate terephthalate)) or PBAT (Poly (butylene adipate terephthalate). Among the above-listed biodegradable polyesters, the aliphatic and aromatic copolyesters show superior mechanical and thermal stability up to 200 °C. These polymers can also be blended with bio-based monomers like PLA to create partially bio-based polyesters like Ecoflex/PLA blend by BASF under the name Ecovio[®] [36] (Table 4).

Table 4 Shows some commercial available PBSA/PBAT polymers and lists manufacturers and trade names [9]

Polymer	Manufacturer	Trade name
PBSA	Showa Highpolymer	Bionolle
	Ire Chemical Ltd.	EnPol
	SK Chemicals	Skygreen
	Nippon Shokubay	Lunare Se
PBAT	Eastmann Chemical	Eastar Bio
	BASF	Ecoflex
	Dupont	Biomax
	Novamont	Origo-Bi

Comparison of Biopolymers

As with petrochemical-based polymers, bio-based polymers offer a wide variety of properties from brittle and rigid to tough and flexible. Some of these characteristics for selected Bioplastics are summarized in Table 5.6. Additionally, bio-based polyethylene (Bio-PE) derived from sugar cane, is listed, which has comparable properties to fossil fuel-based PE. HDPE and LDPE can be produced in that way. Certainly these materials are in contrast to TPS, PLA, and PHAs not biodegradable at all, but show good potential for recyclability. The poor recyclability of TPS and limited recyclability of PLA is outweighed by their low to moderate material and manufacturing costs, which circumvent an economic loss due to material loss via waste degeneration. Table 2.1 gives some example of properties of selected bio-based polymers in comparison to some traditionally used synthetic polymers (PS/LDPE/PP). Polyester-type bio-based polymers such as PLA and PHB tend to have the highest tensile modulus and tensile strength, while PCL and PBAT and PBSA copolymers tend to have higher elongation properties. Impact modifiers like DuPont Biomax[®] Strong 100 or 120, which is an ethylene copolymer can be added to improve, for example, the toughness of PLA. Products are also available to improve the thermal stability of PLA such as DuPont Biomax[®] Thermal 300 (Table 5).

All in all, it can be stated that biopolymers have already competitive properties to certain synthetic polymers with a tendency to further improvement. One issue, which still has to be improved, is the adverse higher weight of biopolymers.

Market Overview for Biocomposites

According to the Nova Institute of Ecology and Innovation as well as IFBB, the demand for bioplastics is steadily rising [37]. While Europe shows strong demand for bioplastics, production tends to take place in Asia and America. In 2012, there

Table 5 Comparison of selected biosynthesized polymers with sugarcane-based polyethylene [32]

Material Characteristic	TPS	PLA	PHAs	Bio-PE
Physical Properties				
Density	High	High	High	Low
Strength and stiffness properties	Low	Medium	Low-high	Low-medium
Heat resistance	Poor	Poor	Fair	Fair
Processing consistency	Fair	Improving	TBD	High
Recyclability	Poor	Limited	Possible	High
Material/manufacturing costs	Low	Medium to low	High	Medium to low

was a total production of 1.4 million tons of bioplastics worldwide. From this total amount, 36.2 % were produced in Asia and 50.9 % were produced in South-and North-America. In 2015, Asia became the frontrunner in production of bioplastic, holding an amount of 80.6 % of the world production which was listed with 7.85 million tons in total [38]. This is reasoned by the unfavorable political framework in Europe for the industrial usage of biomass. Figure 3 shows a forecast of the market segments in which several bioplastics can be found until the year 2019.

For automotive and transportation goods as well as textiles, mainly from petroleum-derived Biopolymers or partly other bio-based nonbiodegradable polymers, are going to be used as well as partly PLA and PLA blends while for agriculture mainly starch blends are predicted.

The small-scale bioplastic industries could move rapidly in terms of innovation and commercialization of new technologies correlating to the large-scale available biofuels. It is anticipated that until 2019, there will be 112 producing companies in 129 different places of production and a growing rate of 400 % of a total production until 2018 [40].

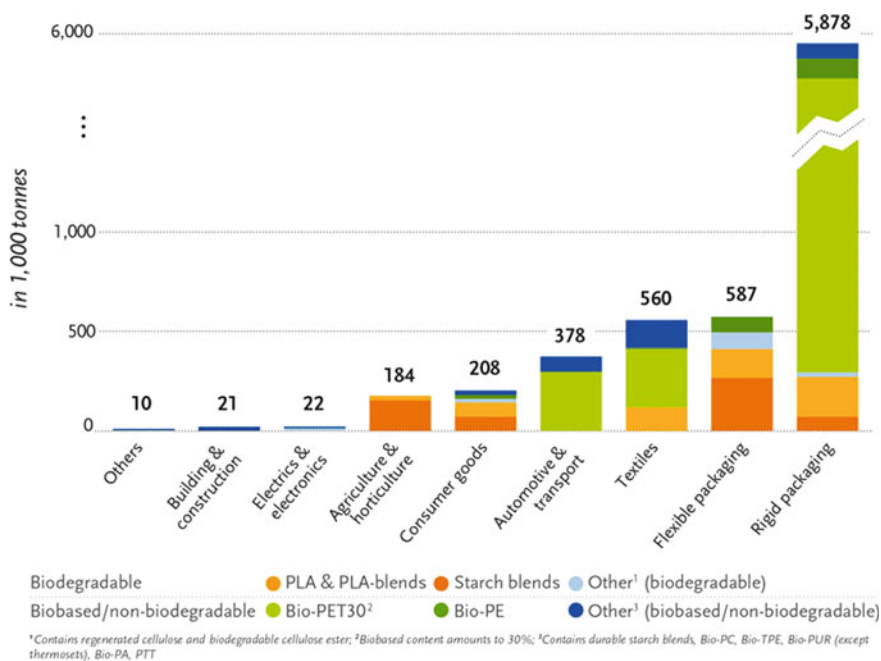


Fig. 3 Global production capacities of bioplastics (by market segment) [39]

Natural Cellulose Fiber Reinforcement Materials

Using reinforcement fibers can add value to properties of biopolymers and traditionally used plastics. When natural fibers are used for reinforcement, a higher bio-based total content can be attached to the composite. For this purpose, various natural fibers were analyzed which could be considered for appropriate utilization and compared against the most commonly used nonbiological and difficult to recycle fiberglass. By adding natural reinforcement fibers to traditional polymers, it is at least possible to create partially bio-based composites. Fibers, which are incorporated in bio-based polymers, represent the most desirable claim on completely ecological and sustainable composites. Reinforcement materials, mainly plant-based fibers, are discussed in this paper. Figure 4 illustrates and classifies all types of natural plant fibers according to their origin. Most investigations in research had been done on the evaluation of flax, hemp, wheat straw, kenaf, jute, coir, abaca, and wood. Latterly there are besides arising new fibers on the market like Isora, Royal- and Oil Palm, Curaua, Date, Hop, and Nettle as well as different kind of grasses and reeds. These new cellulose reinforcing materials offer good properties and have the potential to enlarge the choice for reinforcement materials. In Table 6, some mechanical properties of commonly used and selected alternative plant fibers are summarized and compared to E-glass and Kevlar. Especially, Nettle shows outstanding properties with the highest strength and stiffness amongst the plant fibers at nearly the lowest weight. In the past centuries, the nettle fiber was extensively used to produce narrow textiles like rope, string but also cloth. The forgotten fiber has high potential to enter the market again, offering suitable reinforcing qualities for composite materials [41]. By summarizing all values in the table, it can be seen that the mechanical properties of plant fibers are in general much lower when compared to those of the most widely used competing reinforcing glass fibers. However, because of their low density, the specific properties (property-to-density ratio), strength, and stiffness of plant fibers are comparable to the values of glass fibers.

In a research done by Wambua [44], natural fibers (sisal, kenaf, hemp, jute, and coir) reinforced polypropylene composites were manufactured by compression molding using a film stacking method. Afterwards, the mechanical properties of the single natural fiber composites were tested and evaluated. Additionally, they were compared to corresponding properties of glass mat reinforced polypropylene composites. As a result, kenaf, hemp, and sisal composites showed comparable tensile strength and modulus properties. According the impact properties hemp performs better than kenaf. Moreover, it was explored that with increasing fiber weight fraction the tensile modulus, impact strength and the ultimate tensile stress of kenaf reinforced polypropylene composites increased too. Coir fiber composites displayed the lowest mechanical properties, but their impact strength was higher than that of jute and kenaf composites.

In another research, by Joshi [45], selected life cycle assessment studies of natural fiber and glass fiber composite were analyzed and evaluated toward their



Fig. 4 Classification of natural plant fibers [43, 46–54]

relative environmental performance. The results of Joshi’s study are partly summarized in Table 7 and show that the nonrenewable energy requirements for the production of glass are 5–15 times bigger than those of the two natural fibers counterparts. Hence, the pollutant emissions from Table 5.2 natural fiber production are much lower than from glass fiber production.

Table 8 summarizes the main advantages and disadvantages of natural plant fibers as reinforcement materials. At first glance, it becomes clear that the positive aspects prevail the negative ones. Irrespective of that fact, there are also plenty of

Table 6 Physical properties of selected natural fibers in comparison to E-Glass and Kevlar Partly adapted from [42] further developed with [43]

Fiber	Density (g cm ⁻³)	Tensile strength (MPa)	Young's Modulus (GPa)	Elongation at break (%)
Flax	1.5	345–1,500	27.6	2.7–3.2
Hemp	1.47	690	70	1.6
Ramie	1.55	400–938	61.4–128	1.2–3.8
Jute	1.3–1.49	393–800	13–26.5	1.16–1.5
Sisal	1.45	468–700	9.4–22	3–7
Cotton	1.5–1.6	287–800	5.5–12.6	7–8
Bamboo	0.6–1.5	383–525	22–29	1.4–1.7
Nettle	0.72	900–2200	53–121	1.7–2.1
Elephantgrass	0.82–1.08	226–272	9–10	2.5–2.8
Date stem	0.96–0.99	478	2	24
Coir	1.15–1.5	145–174	3–5	15–46
Banana	1.3–1.35	450	13–15	3.4–4
Isora	1.35	370–440	13–15	5–6
Curaua	1.4	360–1000	8.4–36	3–4.3
Pineapple leaf	1.44	287–1130	24–57	1.6–2
E-Glass	2.55	3,400	73	2.5
Kevlar	1.44	3,000	60	2.5–3.7

Table 7 Nonrenewable energy requirements for production of different fibers in MJ/kg

Nonrenewable energy requirements (MJ/kg)					
Glass fiber mat		Flax fiber mat		China reed fiber	
Raw materials	1.7	Seed production	0.05	Cultivation	2.50
Mixture	1.0	Fertilizers	1.0	Transport plant	0.40
Transport	1.6	Transport	0.9	Fiber extraction	0.08
Melting	21.5	Cultivation	2.0	Fiber grinding	0.40
Spinning	5.9	Fiber separation	2.7	Transport fiber	0.26
Mat production	23.0	Mat production	2.9		
Total	54.7	Total	9.55	Total	3.64

physical or chemical modification methods to outweigh these downgrades. For example, cellulose fibers can be chemically treated with silane or undergo acrylation reaction to minimize moisture uptake, thus leading to better adhesion between fibers and polymer and consequently to improved composite strength [55] which is shown in Table 9 on the sample of oil palm fibers. Another and more common possibility is to treat the fibers with alkali, [56] or using the Duralin process which

Table 8 Advantages and disadvantages of natural plant fiber [45, 58, 59]

Advantages	Disadvantages
Renewable, cheap and worldwide available resource Lower specific weight resulting in comparable specific strength and stiffness to glass reinforced composites Higher required volume fraction of natural plant fibers in composite reduces content of less sustainable polymer matrix High electrical resistance Good acoustic insulating properties Safer handling and working conditions compared to glass fibers Lower environmental impact due to low energy input for production Reduced fuel consumption when used as composite parts in automotive applications due to lower weight of the structural part Superior processing and recycling properties due to no abrasion to mixing and molding equipment Carbon dioxide neutral disposal can be composted, recycled, or combusted	Compounding difficulties due to inherent polar and hydrophilic nature of lignocellulosic fibers and the non-polar characteristics of most matrix materials Broad variance of mechanical properties leading to less reliability compared to standardized synthetic fibers with predictable properties High moisture and chemical absorption can lead to swelling, matrix/fiber decohesion and polymer cracks Processing temperature is limited to 200 °C because of fiber degeneration at higher temperatures Less durable and rot sensitive

Table 9 Mechanical properties of untreated and chemically modified oil palm fiber [60]

Oil palm fiber	Tensile strength (MPa)	Young's Modulus (GPa)	Elongation at break (%)
Untreated	248	6700	14
Silane-treated	273	5250	14
Acrylated	275	11100	26

is working with steam to dissolve the noncellulosic cementing substances and provide a more environmental-friendly solution [57].

Another ecological modification process is the enzyme treatment of natural fibers, inducing an increase of tensile strength of altered abaca reinforced PP Composites up to 45 [61]. Physical methods are linked to plasma, corona, or laser treatment, all resulting in an improved surface of the cellulosic fibers and overall better properties [62].

Natural Cellulose Fiber Disposal

There are three different possibilities to manage the disposal of natural fiber reinforced composites when they decline to End-Of-Life Cycle. The material can simply be recycled by grinding and be re-introduced into a new production cycle.

When natural fibers are mixed with bio compostable matrix materials they can be biodegraded to water, CO₂ and biomass. Also thermal recycling is possible, in which a certain amount of energy can be recovered in relation to their calorific power [63]. When natural reinforced composites have to be disposed, the released amount of CO₂ of the fibers due to combustion process or land fill is neutral relative to the assimilated amount during their growth. All in all, it can be issued that plant-derived reinforcement fibers are environmentally friendly and substantially available. Moreover, they depict a renewable and cheap resource. Plant fibers are light compared to glass, carbon, and aramid fibers. Next to the fact that these fibers comply the approach of sustainability they also fulfill economic approaches due to their low cost at high performance [44].

Industrial Adaptability of Bio- and Green Composites on the Example of Already Established Products

Automobile Industry

Already, in 1929, Henry Ford started to do investigations on the first “Bio-Car”. Twelve years later, he launched a car in which all metal parts, except the steel frame, were replaced by a plastic composite, which consists of 70 % of cellulose fibers from wheat straw, hemp and sisal plus 30 % resin binder. It was reported that the plastic composite was able to “withstand a blow 10 times as great as steel without denting while saving weight up to circa 450 kg in comparison to steel”. Unfortunately the car could never enter the market because governmental regulations at that time on alcohol and hemp forbid further productions possibilities [64]. Recently, SUZUKI exhibited a new sustainable concept for EV model, using banana fiber reinforced epoxy resin for the outer body of the car. For the seat fabrics, the manufacturer also used a mixed yarn consisting of colored banana fiber and cotton. Additionally, the floor mat was prepared by colored banana fiber, which was molded by a binder [65]. Panasonic developed speaker cone, which are made of paper from bamboo fiber. Bamboo has the benefit that it is lighter and harder than wood as well as growing faster [66]. In Freiburg, there was launched a BioMobile project using a technology developed by Bcomp, utilizing a flax-based ampliTex fabric as reinforcement for structural parts like roofs and doors in order to create an overall lighter vehicle [67]. The first 100 % natural automotive product was released in Toyota. The company developed automotive parts from press molded kenaf-PLA non-woven mats, which were applied to the spare wheel cover, door trims, and deck board [68]. EcoTechnilin (UK) has manufactured a composite sandwich panel consisting of non-woven flax/bioresin facings and a paper honeycomb core (“Fibricard”) [69] for a floor panel in the Jaguar F-type. Other potential application areas for Fibricard could be in Trunk load floors (automotive), flooring systems, wall linings (construction), and furniture [70] Lotus Cars uses hemp fiber instead of glass fibers to reduce the weight by 1 kg per panel at the same nominal

wall thickness due to the natural fiber's lower specific density. The hemp-composite is also used to produce the lightweight seats, each 400 g lighter than its same-sized forerunner the *Elise S* roadster. Although the reinforced matrix, which is used in the car bodies of the new "Eco Elise S," is still unsaturated polyester, the company announced that they quest to establish a recyclable (melt-reprocessable thermoplastic) alternative. In an internal testing protocol it was perceived that the hemp-composite seats correspond to conventional used materials which proves hemp's potential adaptability for automotive industry [71]. BMW is doing the next step by currently investing into the concept of the Swedish designer Erik Melldahl who has recently designed an extraordinary Maasaica car which is locally built in Serengeti (Afrika) using 3D printing technology, degradable materials, and traditional handcraft [72].

Constructions

Establishing biocomposite panels in the construction industry is challenging due to some deficits of the cellulose raw material like moisture absorption, microbial attack and UV degeneration. However, these downgrades can be overcome by chemical modifications of the fibers and adding specific polymers to the fiber and matrix [73]. The Danish architecture bureau 3XN designed the "Green Pavilion" which is constructed from biodegradable composite from biological materials such as cork, flax fibers, corn and soybeans. Next to the fact that the sculpture is completely environment-friendly and biodegradable, the exterior skin has a photocatalytic effect of cleaning the surrounding air. The pavilion has been awarded with the JEC Innovation Award 2010 for its design combining sustainability and intelligent materials and is currently exhibit in the Louisiana Museum of Modern Art in Denmark [74]. Another successful example of biocomposites in construction is the Gas Receiving Station by Studio Marco Vermeulen (Fig. 5.14), which is constructed by a full biocomposite facade made from "Nabasco," a composite of bio resin and hemp fiber produced by NPSP Composites [75]. In 2013, the building facade was installed in the Netherlands. Students and professors at Stuttgart University's ITKE (Institute of Building Structures and Structural Design) developed the ArboSkin Pavilion. The facade of the pavilion is made from a bioplastic engineered specifically for the construction industry, which is derived from 90 % renewable materials, like starches, cellulose, and other biopolymers [76].

Sport

Green and biocomposites are already used for plenty sporting goods including for example long boards, skies and boat paddles manufactured by a plant fiber reinforced bioresin matrix system from lingrove and launched under the trade name

“Ekoa” in order to replace carbon [77] Also, Snowboards using ampliTex [78], canoes [79], surfboards, or bike frames by Museeuw using the composite flax/carbon blend material FlaxPreg [80].

Consumer Products

The company Pistol produces in its GREEN LINE Series 8000, cases made of natural fiber composites, using hemp fibers as reinforcement material. The cotton velvet lining cloth and the case and cover materials are pressed together without the use of adhesives in a “one-shot” process [81]. A plastic-like material which is biodegradable, natural and totally environmental-friendly and made of agricultural residues mainly bamboo pulp or rice husks was patented by Enviroarc. This plastic is used to produce biodegradable dishware, pots, packaging and even industrial applications [82]. The Japanese manufacturer Unitika Limited of polymers has developed a highly heat-resistant biodegradable container made of Polylactic acid (PLA). The company was able to develop through polymer modification technology and special fabrication routes, the world’s first biodegradable sheet molded container that is heat-resistant up to 130 °C, which states the temperature specified for heat-resistant materials under the Household Goods Quality Labeling Law. This biodegradable plastic is registered under the trade name “Terramac.” Moreover, the company cooperated with NEC Corporation to form a kenaf fiber reinforced bioplastic derived from corn that is already utilized by NTT DoCoMo Inc. for the entire casing of its FOMA(TM) “N701iECO” mobile phone [83, 84].

Conclusion

In the light of rising environmental concerns, rising petroleum prices, and incalculable future supply of petroleum, renewable sources-derived Green Composites represent the materials of the future. There are already a fair number of bio-based polymers commercially available on the market with rising tendency. Some of these materials are already widely used for mass products like packaging materials. The incorporation of these materials to engineering composite parts can be the next step to establish them stronger in the market. Due to the fact that green polymers are still in their early development stage, there are still some drawbacks like the currently comparably high price and the need for additional plasticizers and chemical modifications in order to match the requirements of the end item. Especially in the case of composite application there is a need for surface treatment of cellulose fibers to make them more reactive and less moisture absorbent, as well as for bioplastic modification in order to guarantee a suitable matrix material with good mechanical and dimensional properties. But it has to be point out that the better performance characteristics and the large-scale applicability of traditionally polymer materials is

reasoned by several years of research and investigations that have already been done on these materials. However, the biodegradable polymers enter the market just recently and are still in the start phase. By initiating mass production of these materials the prices will adjust to the prices of commonly used polymers thus making biopolymers competitive. Plant fiber reinforced biocomposites validate as an alternative to glass reinforced composites to be used as structural parts for cars and other application by showing sufficient mechanical properties and low weight. At the end of their life these composites can be disposed or composted without negative impacts on the environment. All in all, with regard to life cycle evaluation, natural fibers show lower environmental impact than glass fibers due to decreased energy consumption during production and reduced CO₂ emissions. However, establishing these materials in composite man will also boost the access to other markets, building a foundation for a more sustainable economy and society.

References

1. M.A. Islam, B.R. Mills, 3D Woven Structures and Methods of Manufacture. *Woven Textiles: Principles, Developments and Applications*, pp. 267–273 (2012)
2. A.P. Mouritz, M.K. Bannister, Review of applications for advanced three-dimensional fibre textile composites. *Compos. Part A* **30**, 1445–1461 (1999)
3. M. Milwich, Learning from nature: lightweight constructions using the Textiles plant stem. *Polym. Compos. Build.* **304** (2010)
4. S.T. Peters, Introduction, Composite Basics and Road Map. in *Handbook of Composites*, vol. 2 (1998)
5. C. Baley, Matrix polymers. flax and hemp fibres: a natural solution for the composite industry. *JEC Compos.* vol. 85 (2012)
6. K. Goda, M. Sreekala, S. Malhotra, Advances in polymer composites: biocomposites- state of the art, new challenges and opportunities. *Polym. Compos.* vol 3 *Biocompos.* 1–8 (2014)
7. A.K. Mohanty, M. Misra, L.T. Drza, Sustainable bio-composites from renewable resources: opportunities and challenges in the green materials world. *J. Polym. Environ.* **10**, 19–26 (2002)
8. P. Bordes, E. Pollet, Nano-biocomposites: Biodegradable polyester/nanoclaysystems. *Prog. Polym. Sci.* **34**, 125–155 (2009)
9. E.D. Maio, S. Iannace, Biodegradable Composites. *Encycl. Compos.* **1**, 86 (2012)
10. W.S. Ratnayakea, R. Hoovera, Composition, molecular structure, and physicochemical properties of starches from four field pea (*Pisum sativum* L.) cultivars. *Food Chem.* **74**(2), 189–202 (2001)
11. M. Thunwall, A. Boldizar, M. Rigdahl, Compression molding and tensile properties of thermoplastic potato starch materials. *Biomacromolecules.* pp. 981–986 (2006)
12. F.G. Torres, O.H. Arroyo, C. Gomez, Processing and mechanical properties of natural fiber reinforced thermoplastic starch biocomposites. *J. Thermoplast. Compos. Mater.* **20**, 207–223 (2007)
13. A. Vazquez, V.A. Alvarez, Starch- Cellulose Fiber Composite.in *Biodegradable polymer Blends and Composites from renewable Resources*, vol. 245 (2009)
14. A. Bergeret, Environment-friendly protein-/starch-based biodegradable polymers and composites. *JEC Mag.* vol. 39 (2008)
15. S. Ochi, Development of high strength biodegradable composites using Manila hemp fiber and starch-based biodegradable resin. *Compos. Part A Appl. Sci. Manuf.* **37**, 7879–1883(2005)

16. X.S. Sun, Overview of plant polymers: resources, demands, and sustainability. *Bio- Based Polym. Compos.* 382–403 (2005)
17. V.M. Hernandez-Izquierdo, Thermoplastic, processing of proteins for film formation. *J Food Sci* **73**, 30–39 (2008)
18. Y. Wang, G.W. Padua, Tensile properties of extruded zein sheets and extrusion blown films. *Macromol. Mater. Eng.* **288**(11), 886–893 (2003)
19. J.W. Pollack, Soy vs. petro polyols: A life cycle comparison, pp. 1–5 (2004)
20. J.P. Dwan’Isa, Mohanty A.K. Misra, Biobased polyurethane and its composite with glass fiber. *J. Mater. Sci.* **39**, 2081–2087 (2004)
21. S. Husic, I. Javni, Thermal and mechanical properties of glass reinforced soybased polyurethane composites. *Compos. Sci. Technol.* **65**, 19–25 (2005). science direct
22. A. Skopinska-Wisniewska, Surface characterization of collagen/elastin based biomaterials for tissue regeneration. *Appl. Surf. Sci.* **255**(19), 8286–8292 (2009)
23. P.B. Malafaya, G.A. Silva, Natural–origin polymers as carriers and scaffolds for biomolecules and cell delivery in tissue engineering applications. *Adv. Drug Delivery Rev.* **4–5**(59), 207–233 (2007)
24. U. Gruessner, M. Clemens, Improvement of perineal wound healing by local administration of gentamicin-impregnated collagen fleeces after abdominoperineal excision of rectal cancer. *Am. J. Surg.* **182**(5), 502 (2001)
25. C. Yang, M. Bodo, Recombinant collagen and gelatin for drug delivery. *Adv. Drug Delivery Rev.* **55**(12), 1547 (2003)
26. A.C. Albertson, K. Varma, Aliphatic Polyester: synthesis, properties, and applications. *Adv. Polym. Sci.* **2** (2002)
27. C. Jérôme, P. Lecomte, Recent advances in the synthesis of aliphatic polyesters by ring-opening polymerization. *Adv. Drug Delivery Rev.* **60**(9), 1056–1076 (2008)
28. A. Steinbruch, Polyester 3. Applications and commercial products 4. *Biopolymers* **338** (2002)
29. L.T. Lim, R. Auras, Processing technologies for poly (lactide acid) in process. *Polym. sci.* **33**(8), 820–852 (2008)
30. A.B. Nair, P. Sivasubramanian, P. Balakrishnan, Environmental effects biodegradation, and life cycle analysis of fully biodegradable “green” composites. *Polym. Compos. Biocompos.* 515–534 (2012)
31. S.R. Lee, H.M. Park, Microstructure, tensile properties, and biodegradability of aliphatic polyester/clay nanocomposites *Polymer* **43**, 2495–2500 (2002)
32. M. Tolinski, Plastic and sustainability, pp 204–110 (2012)
33. J. Sierra, M. Noriega, E. Cardona, Relationship between properties, citrate content and postproduction time for a plasticized Polylactic acid. in *ANTEC 2010 Society of Plastic Engineers* (2010)
34. M. Tolinski, Plastic and sustainability, pp. 107–110 (2012)
35. S. Medeiros, A.S.F. Santos, A. Dufresne, Bionanocomposites. *Polym. Compos. 3 Biocompos.* **375** (2014)
36. E. DI Maio, S. Iannace, Biodegradable composites. *Encycl. Compos.* **1**, 88 (2012)
37. http://www.bio-based.eu/market_study/media/files/13-07-24PRMarketStudynova.pdf
38. European bioplastics, Institut für Biokunststoffe und Bioverbundwerkstoffe (IFBB)
39. European Bioplastics, Institute for Bioplastics and Biocomposites, nova-Institute (2015)
40. http://news.bio-based.eu/fast-growth-of-based-polymers-production/#_ftn1
41. E. Bodros, C. Baley, Study of the tensile properties of stinging nettle fibres (*Urtica dioica*). *Mater. Lett.* **62**(14), 2143–2145 (2008)
42. A. Bismarck, S. Mishra, Plant Fibers as Reinforcement for Green Composites. in *Natural Fibers, Biopolymers and Biocomposites* (2005)
43. K. Charlet, Natural Fibres as Composite Reinforcement Materials, Description of new source of vegetable Fibers, in *Natural Polymers Volume 1: Composites* (RSC Publishing, UK, 2012) pp. 48–57
44. P. Wambua, U. Ivens, I. Verpoest, Natural fibers: can they replace glass in fiber reinforced plastics. *Compos. Sci. Technol.* **63**, 1259–1264 (2003)

45. S.V. Joshi, L.T. Drzal, A.K. Mohanty, Are natural fiber composites environmentally superior to glass fiber reinforced composites? *Compos. Part A* **35**, 371–376 (2004)
46. R.M. Rowell, Properties and Performance of Natural-Fibre Composites; *Natural Fibres, types and properties*. pp. 4–36 (2008)
47. F.G. Torres, Processing and mechanical properties of natural fiber reinforced thermoplastic starch biocomposites. *J. Thermoplast. Compos. Mater.* **20**(2), 207–223 (2007)
48. I.C. Madufor, M.E. Yibowei, *Physico-Mechanical Properties of Luffa aegyptiaca Fiber Reinforced Polymer Matrix Composite*, vol. 1 (2015)
49. M. Carus, A. Eder, L. Scholz, *BIOVERBUNDWERKSTOFFE Naturfaserverstärkte Kunststoffe (NFK) und Holz-Polymer-Werkstoffe (WPC)*, Fachagentur Nachwachsende Rohstoffe e. V. (FNR) (2015)
50. P. Gaikwad, P. Mahanwar, Surface treated and untreated henequen fiber reinforced polypropylene composites. *Int. J. Chem. Environ. Biol. Sci. (IJCEBS)* **2**(4) (2014)
51. H. Hajiha, M. Sain, The use of sugarcane bagasse fibres as reinforcements in composites. in *Biofiber Reinforcements in Composite Materials* ed by O. Faruk, M. Sain (Woodhead Publishing, UK, 2015) pp. 525–547
52. Zaker Bahreini, Evaluation of calotropis gigantea as a promising raw material for fiber-reinforced composite. *J. Compos. Mater.* June 2009. **43**(11), 1297–1304
53. L. Garzon, L.M. Lopez, J. Fajardo: New Natural Fiber: Toquilla Straw a Potential Reinforcement in Thermoplastic Polymer Composites. in *Conference: ICMS 2014*, <http://icams.ro/index.php>, vol. 5. Available on research gate (2014)
54. R. Mahjoub, J. Bin Mohamad Yatim, A review of structural performance of oil palm empty fruit bunch fiber in polymer composites. *Adv. Mater. Sci. Eng.* **2013** (2013)
55. M. Zimmiewska, J. Mankowski, Cellulosic Bast Fibers, Their Structures and Properties Suitable for Composite Applications. in *Cellulose Fibers: Bio-and Nano- Polymer Composites*, pp. 108–112 (2011)
56. A.K. Mohanty, M. Misra, L.T. Drzal, Surface modifications of natural fibers and performance of the resulting biocomposites: An overview. *Compos. Interfaces* **8**, 313–343 (2001)
57. G.T. Pott, Reduction of Moisture Sensitivity in Natural Fibres. in *Advanced Fibers, Plastics, Laminates and Composites*, pp. 87–98 (2002)
58. J.M. Jacob, T. Sabu, Biofibres and biocomposites. *Carbohydr. Polym.* **71** (2008), p. 344. www.sciencedirect.com (2007)
59. A. Vazquez, V.A. Alvarez, Starch-Cellulose Fiber Composites. in *Biodegradable Polymer Blends and Composites From Renewable Resources*, vol. 250 (2009)
60. M.S. Sreekala, M.G. Kumaran, Effect of chemical modifications on the mechanical performance of oil palm fiber reinforced phenol formaldehyde composites. *Nat. polym. compos.* (2000)
61. A.K. Bledzki, A.A. Mamun, A. Jaszkiwicz, K. Erdmann, Polypropylene composites with enzyme modified abaca fibre. *Compos. Sci. Technol.* **70**, 854–860 (2010)
62. G.K. Satyanarayana, G. Arizaga, F. Wypych, Biodegradable composites based on lignocellulosic fibers: An overview. *Progress Polym. Sci.* **34**, 997 (2009)
63. C. Baley, A.L. Duigou Eco-design, life cycle analysis and recycling. Flax and Hemp fibres: a natural solution for the composite industry. *JEC Compos.* **174** (2012)
64. Popular Mechanics Magazine. in *Auto Body Made of Plastics Resists Denting Under Hard Blows.* **76**(6) (1941)
65. <http://indiacompositesshow.com/bio-composites-in-automotive-applications/>
66. http://news.panasonic.net/archives/2014/0227_26252.htm
67. <http://fribourgnetwork.ch/fnf/2014-online-eng/files/assets/basic-html/page41.html>
68. <http://www.toyota-boshoku.com/global/about/development/eco/kenaf/>
69. http://www.brigit-project.eu/detalle_noticia.php?no_id=2757
70. <http://www.ecotechnilin.com/products.asp>
71. P. Malnati, ECO Elise Concept: Lean, Speedy and Green. <http://www.compositesworld.com/articles/eco-elise-concept-lean-speedy-and-green> (2009)
72. <http://www.uid.umu.se/en/uid-14/projects/td/erik-melldahl/>

73. J.M. Yatim, A.R.M. Sam, *Construct Build Mater* **55**, 103–113 (2014)
74. <http://www.e-architect.co.uk/copenhagen/louisiana-pavilion>
75. <http://trends.archiexpo.com/inspiration/facades-from-decoration-to-innovation/>
76. <http://www.itke.uni-stuttgart.de/entwicklung.php?lang=en&id=58>
77. <http://lingrove.com/applications-2/>
78. <http://www.bcomp.ch/66-0-low-twist-light-fabrics.html>
79. <http://www.flaxland.co.uk/fabric%20boats.html>
80. <http://www.playnaturallysmart.org/2014/05/20/composites-busch-set-up-new-benchmarks-in-ice-hockey-thanks-to-flax/>
81. <http://www.waffenkoffer-winter.de/en/pistol-cases/pistol-case-natural-fibers.php>
82. <http://www.enviroarc.net/products.php>
83. <http://www.nec.co.jp/press/en/0603/2001.html>
84. www.japanfs.org/en/news/archives/news_id025426.html

Erratum to: Influence of Braid Carrier Tension on Carbon Fibre Braided Preforms

Sree Shankhachur Roy, Wentao Zou and Prasad Potluri

Erratum to:
Chapter ‘Influence of Braid Carrier Tension on Carbon Fibre Braided Preforms’ in: Y. Kyosev (ed.),
Recent Developments in Braiding and Narrow Weaving,
DOI [10.1007/978-3-319-29932-7_9](https://doi.org/10.1007/978-3-319-29932-7_9)

The book was inadvertently published with an incorrect surname of the author as “Wentao Zao” in Chapter ‘Influence of Braid Carrier Tension on Carbon Fibre Braided Preforms’ whereas the correct surname is “Wentao Zou”. The erratum chapter and the book has been updated for the same.

The updated original online version for this chapter can be found at
DOI [10.1007/978-3-319-29932-7_9](https://doi.org/10.1007/978-3-319-29932-7_9)

S.S. Roy (✉) · W. Zou · P. Potluri
Textile Composites Group, The University of Manchester, Manchester, UK
e-mail: shankhachur.roy@manchester.ac.uk

© Springer International Publishing Switzerland 2016
Y. Kyosev (ed.), *Recent Developments in Braiding and Narrow Weaving,*
DOI [10.1007/978-3-319-29932-7_17](https://doi.org/10.1007/978-3-319-29932-7_17)